VirginiaTech
Invent the Future

Department of Biomedical Engineering and Mechanics

Virginia Tech
Wake Forest
Biomedical Engineering

2016 STUDENT SYMPOSIUM

sponsored by

ETHICON
a Johnson & Johnson company

Altair

BMES
BIOMEDICAL ENGINEERING SOCIETY

COOK MEDICAL

Medtronic

Wake Forest Innovations

Virginia Tech
Wake Forest University
School of Biomedical Engineering and Sciences

VirginiaTech
Invent the Future®
Department of Biomedical Engineering and Mechanics

A Letter From The Organizers

Dear Attendees,

Welcome to the 15th Annual School of Biomedical Engineering & Sciences Graduate Student Research Symposium hosted by the VT-WFU Biomedical Engineering Society Student Chapter!

The Virginia Tech-Wake Forest University School of Biomedical Engineering & Sciences (SBES) is a joint graduate program formed in 2003 to bring together three prestigious academic institutions: the College of Engineering at Virginia Tech, the Wake Forest University School of Medicine, and the Regional Virginia-Maryland College of Veterinary Medicine. Each university contributes diverse educational and research opportunities to the students, providing a unique graduate experience. On August 11, 2014, Virginia Tech announced a new collaboration between SBES and the Engineering Science and Mechanics department to form the new Department of Biomedical Engineering and Mechanics. This department fosters important networking opportunities across the Virginia Tech campus as well as provides the framework towards an undergraduate biomedical engineering degree and strong vision for the future.

The VT-WFU Biomedical Engineering Society (BMES) Student Chapter was founded to foster communication and collaboration among various research groups. Our mission is to encourage the development, dissemination, integration, and utilization of knowledge in biomedical engineering, as well as interact with the scientific community. The chapter offers unique ways for students to become involved in outreach projects, research collaborations, and social events with other students, faculty, and industry. We are involved in many service opportunities within our local communities, and participate annually in the BMES National meeting.

The SBES Graduate Student Research Symposium was developed to provide students and faculty the opportunity to interact and exchange research ideas with colleagues and industry personnel. The VT-WFU BMES Student Chapter would like to thank our sponsors Ethicon, Cook Medical, Altair, BMES, Medtronic, and Wake Forest Innovations for their generous support. We greatly appreciate your participation and hope that this symposium will promote enhanced discussion and collaboration among researchers. Thank you for your attendance!

The VT-WFU BMES Executive Committee

Brad Hubbard Harleigh Warner *Presidents*	Jackey Chen Jeff Suhey *Vice Presidents*	Marc Thompson Jamie Gaewsky *Treasurers*	Nora Hlavac Kelli Simms *Secretaries*

Scott Verbridge
VT Faculty Advisor

Ashley Weaver
WFU Faculty Advisor

Please visit our website for more information www.sbes.vt.edu/bmes/

8:00	**REGISTRATION, Biotech Place Entrance** **POSTER SET UP, Biotech Place Atrium** **REFRESHMENTS, Biotech Place Atrium**	
9:00-9:10	**WELCOME, VT-WFU BMES PRESIDENTS, Biotech Auditorium**	
9:10-9:40	**ETHICON PRESENTATION, Biotech Auditorium**	
9:45-10:30	**FACULTY AND STAFF ORGANIZATIONAL MEETING, Suite 120**	
9:45-11:15	**ALTAIR SOFTWARE DEMONSTRATION, Room 157**	
	PhD Oral Presentations, Biotech Auditorium **9:45-11:15**	
		Page Number
9:45	**Cumulative Subconcussive Head Impact Exposure in Youth Football Results in Microstructural Changes in Corpus Callosum** *Naeim Bahrami[1], Youngkyoo Jung[1], Joel D. Stitzel[1], Joseph A. Maldjian[2], and Christopher T. Whitlow[1]* *[1] Wake Forest University, Winston-Salem, NC, [2] University of Texas Southwestern Medical Center, Dallas, TX*	2
10:00	**Comparison of Driver Behavior in Crash Events and Normal Driving** *Rong Chen[1] and H. Clay Gabler[1]* *[1] Virginia Tech, Blacksburg, VA*	3
10:15	**Seed-Based Functional Connectivity to Study Motor Function in Children with Cerebral Palsy** *Harshawardhan U. Deshpande[1], Juniper J. LeePark[1], Jonathan M. Lisinski[1], Stephanie C. DeLuca[1], Sharon L. Ramey[1],* *[1] Virginia Tech, Blacksburg, VA*	4
10:30	**Investigation of Blast Polytrauma and Therapeutic Intervention of Hemostatic Nanoparticles** *W. Brad Hubbard[1], Margaret Lashof-Sullivan[2], C. Shaylen Hall[1], Joseph Eck[1], Erin Lavik[2], and Pamela VandeVord[1,3]* *[1] Virginia Tech, Blacksburg, VA, [2] Case Western Reserve University,Cleveland, OH, [3] Research Services, Veterans Affairs,*	5
10:45	**Optical Fiber Based Imaging of Bioengineered Tissue Construct** *Etai Sapoznik[1],Guoguang Niu[1], Peng Lu[2], Yu Zhou[1], Yong Xu[1], and Shay Soker[1]* *[1] Wake Forest University, Winston-Salem, NC, [2] Virginia Tech, Blacksburg, VA*	6
11:00	**Generalized SVD Reconstruction for Interior Tomography** *Rui Liu[1,2] and Hengyong Yu[2]* *[1] Wake Forest University, Winston-Salem, NC, [2] University of Massachusetts, Lowell MA*	7
11:15-11:45	**Poster Session A, Biotech Place Atrium**	
11:45-12:15	**Poster Session B, Biotech Place Atrium**	
12:15 - 1:30	**LUNCH, Biotech Place Atrium**	

	M.S. Oral Presentations, Auditorium 1:30-2:30		M.S. Oral Presentations, Room 155 1:30-2:30	
1:30	**A Biomechanical Comparison of Extrapelvic and Intrapelvic Fixation for Anterior Column with Posterior-Hemitransverse Acetabular Fractures** *Gregory J. Gillispie[1], Sharon N. Babcock[2], Kyle P. McNamara[1,2], Philip J. Brown[1], and Eben Carroll[2]* *[1] Virginia Tech, Blacksburg, VA, [2] Wake Forest University, Winston-Salem, NC*	8	**Investigation of Driver Lane Keeping Behavior in Normal Driving based on Naturalistic Driving Study Data** *Taylor Johnson[1], Rong Chen[1], Rini Sherony[2], and Hampton C. Gabler[1]* *[1] Virginia Tech, Blacksburg, VA, [2] Toyota Motor Engineering & Manufacturing North America*	9
1:45	**Lumbar Vertebrae Fracture Injury Risk in Reconstruction of CIREN and NASS Frontal Motor Vehicle Crashes** *Derek A. Jones[1],James P. Gaewsky[1], Mireille E. Kelley[1], Ashley A. Weaver[1], and Joel D. Stitzel[1]* *[1] Wake Forest University, Winston-Salem, NC*	10	**Head Impact Exposure in Youth Football Practice Drills** *Mireille E. Kelley[1], Jillian E. Urban[1], Logan E. Miller[1], Joeline M. Kane[2], and Joel D. Stitzel[1]* *[1] Wake Forest University, Winston-Salem, NC*	11
2:00	**Development and Validation of a 6 Year-Old Pedestrian Finite Element Model** *Yunzhu Meng[1] and Costin D. Untaroiu[1]* *[1] Virginia Tech, Blacksburg, VA*	12	**Finite Element Analysis of a Novel Design for a Non-Migrating Biliary Stent using Abaqus** *Jared D. Mitchell[1], Clifford Howard Jr.[1], and Philip J. Brown[1]* *[1] Wake Forest University, Winston-Salem, NC*	13
2:15	**Biomechanics of Head Impacts in Soccer** *Jaclyn N. Press[1] and Steven Rowson[1]* *[1] Virginia Tech, Blacksburg, VA*	14	**Quantifying the Effect of Helmet Fit on Helmet Performance** *Jake A. Smith[1] and Steven Rowson[1]* *[1] Virginia Tech, Blacksburg, VA*	15
2:30-2:45	**REFRESHMENT BREAK**			
2:45-4:15	**ALTAIR SOFTWARE DEMONSTRATION, Room 157**			
	PhD Oral Presentations, Biotech Place Auditorium 2:45-4:15			
2:45	**New Arterial Spin Labeling method for Simultaneous Estimation of Arterial Cerebral Blood Volume, Cerebral Blood** *Megan E. Johnston[1], Ho-Ling A. Liu[2], Christopher T. Whitlow[1], and Youngkyoo Jung[1],* *[1] Wake Forest University, Winston-Salem, NC, [2] University of Texas MD Anderson, Houston, TX*	16		
3:00	**Bioprinted Bone Graft for Craniofacial Reconstruction** *Carlos V. Kengla[1], James J. Yoo[1], and Sang Jin Lee[1]* *[1] Wake Forest University, Winston-Salem, NC*	17		
3:15	**Ultrasensitive Microfluidic Assays for Epigenomic Analysis of Neurons from Mammalian Brains** *Sai Ma1, Zhixiong Sun[1], Hehuang Xie[1], M. Margarita Behrens[2], Joseph R. Ecker[2], and Chang Lu[1]* *[1] Virginia Tech, Blacksburg, VA, [2] The Salk Institute for Biological Studies, La Jolla, CA*	18		
3:30	**Hippocampal Dosimetry Predicts for Cancer-Related Cognitive Impairment in Patients who Receive Partial Brain Irradiation** *Catherine Okoukoni[1], Emory McTyre[1], Ann M. Peiffer [1], William H. Hinson[1], Roy E. Strowd[1], Stephen Rapp[1], and Michael D. Chan[1]* *[1] Wake Forest University, Winston-Salem, NC*	19		
3:45	**Assessing the Relative Impact Performance of Hockey Helmets** *Bethany Rowson[1], Abigail M. Tyson[1], Bryan R. Cobb[1], Steven Rowson[1], and Stefan M. Duma[1]* *[1] Virginia Tech, Blacksburg, VA*	20		
4:00	**Fabrication of a Vascularized Renal Construct using Vascular Corrosion Casting** *Jennifer Huling[1], In Kap Ko[1], Anthony Atala[1], and James Yoo[1]* *[1] Wake Forest University, Winston-Salem, NC*	21		
4:45	**ALL - AWARDS AND CLOSING REMARKS, Biotech Place Auditorium**			

ETHICON

PART OF THE Johnson & Johnson FAMILY OF COMPANIES

Better surgery for a better world

Our promise

Better surgery for a better world

At Ethicon, we're working to redefine surgery to change the world for the better. We share an enduring commitment to advance surgical care so more patients live longer, more fulfilling lives. And we are continuously evolving to better serve our customers.

Better Surgery

Creating value for healthcare systems

Ethicon in Australia and New Zealand responded to customers' needs by creating an easy-to-use inventory management solution. This innovative approach allows customers to save time and reduce costs by managing supply orders through an iPhone application.

Better Care

Advancing care around the world

Ethicon's solutions are changing lives around the world – including the life of a small boy in Argentina named Samuel. Using an innovative solution from Ethicon, surgeons in Argentina were able to perform for the first time a revolutionary, life-saving liver transplant on infant Samuel, who is now a healthy, thriving child.

Expanding access to care globally

By collaborating with key stakeholders, Ethicon was able to expand access to innovative surgical care in Brazil, which improved the quality of care, provided a solution with a shorter patient recovery, and helped patients live healthier lives.

Better World

People making a lasting difference

Ethicon associates raise money and volunteer for Operation Smile missions to heal the smiles of children around the world. Meet Armando, an eleven-year-old boy, who now has a new smile and a bright future.

Inspiring the next generation

Ethicon partners with iSPACE, an organization in Cincinnati, Ohio, that encourages children to get excited about science, technology, engineering, and mathematics. Ethicon engineers share real-world applications to instill curiosity in tomorrow's scientists and engineers.

A history of advancing surgery

Thank you Ethicon for their gracious sponsorship of the 2016 SBES Graduate Student Research Symposium. Visit Ethicon's website for more information on how they're revolutionizing surgery.

It all started with a simple question: What if...?

What if there was a better way to help patients heal after surgery? What if we could improve their lives? What if we could change the way surgery was done forever? And in doing so, change the world for the better?

More than 80 years ago, the first group of Ethicon scientists and researchers started to think about healing in a new way. Their questions led to pioneering sutures that advanced surgeons' work and discoveries that enhanced patients' lives.

Today, we produce much more than sutures. Working with our customers and partners, we bring meaningful solutions to every area we touch. To wound closure and general surgery. To women's health and aesthetic medicine. To minimally invasive procedures and metabolic science.

While our world and the field of healthcare have changed, our passion to make a difference for patients remains. As we reach toward every corner of the globe, we remain committed to advancing surgical care and extending patients' access to health care across the globe.

At Ethicon, we continue to take pride in our heritage. We were founded on innovation and will continue exploring ways to improve surgical outcomes. Improving patient care continues to inspire us to work smarter, partner in more meaningful ways, and never be afraid to imagine a better world by asking the one simple question that started it all. What if…?

Our solutions

From leading-edge sutures and endocutters to comprehensive payor and provider solutions, our focus for almost a century has been to deliver innovations that matter to our customers and ultimately make a difference for patients. It means you can continue to depend on us for world-class educational offerings rooted in an unparalleled understanding of the science behind how tissue reacts in surgery. And it means a commitment to quality in all we do.

A career that counts

Want to join our team? We'd love to hear from you. We're always looking for bright, talented people who truly care about improving lives and making a difference. Discover if we have a career opportunity for you today.

Want to learn more? (http://careers.jnj.com/)

DSL 13-0309, DSL 12-9000

Thank you to Altair for their gracious sponsorship of the 2016 SBES Graduate Student Research Symposium. Visit Altair's website to discover how they are innovating in high-end software and consulting services.

A leading global provider of technology that strengthens client innovation, Altair empowers client innovation and decision-making through technology that optimizes the analysis, management and visualization of business and engineering information.

Privately held with more than 2,300 employees, Altair operates 48 offices throughout 20 countries.

With a 30-year-plus track record for product design, advanced engineering software, on-demand computing technologies and enterprise analytics solutions, Altair consistently delivers a competitive advantage to more than 5,000 corporate clients representing the automotive, aerospace, government and defense, heavy equipment and consumer products verticals. Altair also has a growing client presence in the electronics, architecture engineering and construction, and energy markets.

For more information, visit Altair's website at www.altair.com

World Headquarters
1820 East Big Beaver Rd
Troy, MI 48083
USA

Thank you to the Biomedical Engineering Society for their gracious sponsorship of the 2016 SBES Graduate Student Research Symposium. Please visit their website to learn how they have become the leading society of professionals devoted to developing and using engineering to advance human health and well being.

The Biomedical Engineering Society (BMES) is the professional society for biomedical engineering and bioengineering. Founded in early 1968, the Society now boasts over 7,000 members and is growing, rapidly.

BMES serves as the lead society and professional home for biomedical engineering and bioengineering. Our leadership in accreditation, potential licensure, publications, scientific meetings, global programs, and diversity initiatives, as well as our commitment to ethics, all serve our mission to promote and enhance knowledge and education in biomedical engineering and bioengineering worldwide and its utilization for human health and well-being.

The Vision of BMES is to serve as the world's leading society of professionals devoted to developing and using engineering and technology to advance human health and well-being.

The Mission of BMES is to build and support the biomedical engineering community, locally, nationally and internationally, with activities designed to communicate recent advances, discoveries, and inventions; promote education and professional development; and integrate the perspectives of the academic, medical, governmental, and business sectors.

Leading and emerging researchers use BMES as a platform for sharing the latest information and research in the profession. BMES provides industry members exposure to an expanding market. Advertising and sponsorship opportunities can help increase your company's publicity year-round.

For more information, please visit the BMES website at www.bmes.org

BMES
8201 Corporate Drive, Suite 1125
Landover, MD 20785-2224
info@bmes.org

Where ingenuity and integrity converge.

Cook Medical has been working with physicians to create simple solutions to hard problems since 1963. By giving patients better, safer treatment and giving doctors simpler, more effective options, family-owned Cook has grown to more than 12,000 employees worldwide, serving 135 countries and offering more than 16,000 products. Today, the company manufactures and combines medical devices, drugs, biologic grafts and cell therapies to serve more than 41 medical specialties.

Cook's Endoscopy division, located in Winston-Salem, was founded on Cook's core values in 1983. The Endoscopy division creates products that effectively treat those who suffer with problems anywhere in the gastrointestinal tract. Today, the division employs approximately 550 local and regional residents who manufacture a full line of products that help physicians across the globe efficiently care for those patients.

COOK® MEDICAL cookmedical.com

Thank you to Medtronic for their gracious sponsorship of the 2016 SBES Graduate Student Research Symposium. Visit Medtronic's website to discover how they are creating life-changing therapies to help people with chronic diseases.

As a global leader in medical technology, services and solutions, Medtronic improves the health and lives of millions of people each year. We believe our deep clinical, therapeutic and economic expertise can help address the complex challenges — such as rising costs, aging populations and the burden of chronic disease — faced by families and healthcare systems today. But no one can do it alone. That's why we're committed to partnering in new ways and developing powerful solutions that deliver better patient outcomes.

Founded in 1949 as a medical repair company, we're now among the world's largest medical technology, services and solutions companies, employing more than 85,000 people worldwide, serving physicians, hospitals and patients in more than 155 countries. Join us in our commitment to take healthcare Further, Together. Learn more at Medtronic.com.

Medtronic
Vascular Innovations
3576 Unocal Place
Santa Rosa, CA 95403-1774

Wake Forest® Innovations

Thank you to Wake Forest Innovations for their gracious sponsorship of the 2016 SBES Graduate Student Research Symposium.

Wake Forest Innovations improves health through collaborative innovation so that important scientific discoveries can become life-improving realities.

We accomplish this through our three Centers:

- Center for Technology Innovation & Commercialization – accelerates the development and commercialization of inventions.
- Center for Industry Research Collaboration – expedites access to specialized clinical and research capabilities.
- Center for Applied Learning – promotes best clinical practices through experiential training

We believe collaborative innovation between our faculty and staff and with industry is based on sharing expertise, knowledge, risk and reward at all stages of product research and development.

For more information, please visit their website at www.WakeForestInnovations.com.

Wake Forest Innovations
575 North Patterson Avenue, Suite 550
Winston-Salem, NC 27101
innovation@wakehealth.edu

15th Annual Graduate Student Research Symposium

Oral Presentations

Virginia Tech
Wake Forest University
School of Biomedical Engineering and Sciences
15th Annual Graduate Student Research Symposium, May 11, 2016

CUMULATIVE SUBCONCUSSIVE HEAD IMPACT EXPOSURE IN YOUTH FOOTBALL RESULTS IN MICROSTRUCTURAL CHANGES IN CORPUS CALLOSUM

Naeim Bahrami[1], MS; Youngkyoo Jung[1], PhD; Joel D. Stitzel[1], PhD; Joseph A. Maldjian[2], MD; Christopher T. Whitlow[1], MD PhD;
1. Wake Forest School of Medicine,
2. University of Texas Southwestern Medical Center,
Corresponding author: nbahrami@wakehealth.edu

INTRODUCTION

The purpose of this study was to determine the effects of cumulative subconcussive head impact exposure associated with youth football (age<13 years old) on microstructural integrity of the corpus callosum (CC). mTBI[1–3]. We hypothesized that repeated head impacts over a single season of football would lead to diffusion changes in the CC, even in the absence of clinically diagnosed concussion.

METHODOLOGY

Twenty-two male football players (age: 8-13) without a history of concussion participated in this IRB approved study. Head impacts were quantified via the Head Impact Telemetry System (HITS), which uses sensors embedded in each player's football helmet to record kinematic data during all practices and games. The biomechanical metric used was the risk weighted cumulative exposure (RWE_{CP})[4]. All subjects received pre and post-season MRI, including diffusion tensor imaging (DTI). MRI was performed on a 3 Tesla Siemens Skyra Fiber tracking was conducted via automated fiber quantification (AFQ)[5]. Fractional anisotropy (FA), mean diffusivity (MD), linear anisotropy (CL), axial diffusivity (AD), and radial diffusivity (RD) measurements across the fiber were calculated. Percent change in DTI metrics pre- versus post-season was computed per tract for each subject. Linear regression analysis was conducted using age as a covariate to determine the association between RWE_{CP} and DTI change in the CC.

RESULTS

There were statistically significant linear relationships between RWE_{CP} and percent change in FA, MD, RD, and AD within the CC ($p<0.05$) (table 1). There were no statistically significant associations between total RWE_{CP} and CL changes in the CC.

Table 1. Summary of the statistically significant relationships between changes in DTI metrics in corpus callosum (CC) and cumulative head impact (RWE_{CP}).

	R^2	P- value
FA vs RWECP	*0.1507*	*0.0214*
MD vs RWECP	*0.2416*	*0.0032*
RD vs RWECP	*0.1470*	*0.0255*
AD vs RWECP	*0.2237*	*0.0043*

CONCLUSIONS

Our findings suggest that cumulative subconcussive head impact exposure is associated with microstructural changes in the CC. This study adds to the growing body of evidence that a single season of contact sports can result in WM microstructural changes, even in the absence of concussion.

REFERENCES

1. Wilde, E. A. *et al.* Diffusion Tensor Imaging in the Corpus Callosum in Children after Moderate to Severe Traumatic Brain Injury. *J. Neurotrauma* **23,** 1412–1426 (2006).
2. Gorrie, C., Duflou, J., Brown, J., Gibson, T. & Waite, P. M. E. Extent and Distribution of Vascular Brain Injury in Pediatric Road Fatalities. *J. Neurotrauma* **18,** 849–860 (2001).
3. Kim, D. S., Choi, H. J., Yang, J. S., Cho, Y. J. & Kang, S. H. Radiologic Determination of Corpus Callosum Injury in Patients with Mild Traumatic Brain Injury and Associated Clinical Characteristics. *J. Korean Neurosurg. Soc.* **58,** 131–136 (2015).
4. Urban, J. E. *et al.* Head impact exposure in youth football: high school ages 14 to 18 years and cumulative impact analysis. *Ann. Biomed. Eng.* **41,** 2474–2487 (2013).
5. Yeatman, J. D., Dougherty, R. F., Myall, N. J., Wandell, B. A. & Feldman, H. M. Tract Profiles of White Matter Properties: Automating Fiber-Tract Quantification. *PLoS ONE* **7,** e49790 (2012).

Oral, PhD
Auditorium, 9:45

COMPARISON OF DRIVER BEHAVIOR IN CRASH EVENTS AND NORMAL DRIVING

Rong Chen[1], and H. Clay Gabler[1]
1. Virginia Tech (Biomedical Engineering and Mechanics)
Corresponding Author: Rong Chen, Email: rjchen@vt.edu

INTRODUCTION

One of the major challenges in designing effective Forward Collision Warning (FCW) systems is to increase driver acceptance of the systems. Drivers can become annoyed and may disable the system if they feel they are receiving unnecessary warnings. One method of reducing the occurrence of nuisance alarms in FCW systems is to better distinguish driver behavior in crash and normal driving scenarios. The objective of this study is to compare driver behavior during crash events and normal driving.

METHODOLOGY

The overall approach of the study was to compare driver behavior in normal car following events from the 100-Car study against rear-end crash events in the National Automotive Sampling System/Crashworthiness Data System (NASS/CDS). Car following events involving brake application in the 100-Car NDS were extracted using an automated algorithm developed based on data collected from onboard vehicle instrumentation. Similarly, pre-crash data of rear-end crash events were extracted from NASS/CDS's event data recorder (EDR) database. The comparison of driver behavior was quantified based on the time to collision (TTC) and enhanced time to collision (ETTC) at the start of the brake application in both crash events and normal driving.

RESULTS

A total of 95 relevant rear-end crash events from NASS/CDS which contained pre-crash EDR data were extracted from the dataset. After applying the weighting factor, the subset of crash events represents 46,934 nationally representative crash events.

The subset of normal braking events from the 100-Car NDS includes a total of 64 drivers with valid sensor data, resulting in a total of 243,080 braking events extracted from 72,380 trips. All braking events extracted from the 100-Car NDS involved a closing lead vehicle which was stopped in front of the instrumented vehicle.

The average TTC of crash events is approximately 1.4 seconds. All but one crash event had a TTC greater than that of the population median, and only 2 crash events had TTC greater than the population 10th percentile. In addition, unlike normal driving TTC, which generally increases with respect to vehicle speed, TTC of crash events do not show correlation with vehicle speed.

CONCLUSIONS

The current study presents the first study comparing normal driver behavior in car-following to crash events, combining the unique features of both NDS and EDR data. The results from this study can greatly expand our understanding of driver behavior in car-following events, and assist both manufactures in future FCW designs, and regulatory agencies in selecting future FCW test criteria.

The results show that the average TTC and ETTC values of crash events were approximately 1 second, and were comparable to TTC values of crash events in a simulator study [1]. In these crash events, drivers were able to react to the imminent crash scenario but either did not react in time or did not brake sufficiently to prevent the crash. A future system may consider using TTC as an early sign of crash imminent event to ready the FCW or brake-assist system, while simultaneous monitoring the ETTC of the event.

REFERENCES

[1] J. D. Lee, D. V McGehee, T. L. Brown, and M. L. Reyes, "Collision warning timing, driver distraction, and driver response to imminent rear-end collisions in a high-fidelity driving simulator.," *Hum. Factors*, vol. 44, no. 2, pp. 314–334, 2002.

Oral, PhD
Auditorium, 10:00

SEED-BASED FUNCTIONAL CONNECTIVITY TO STUDY MOTOR FUNCTION IN CHILDREN WITH CEREBRAL PALSY

Harshawardhan U. Deshpande[1,2], Juniper J. LeePark[3], Jonathan M. Lisinski[2], Stephanie C. DeLuca[2], PhD, Sharon L. Ramey[2], PhD and Stephen M. LaConte[1,2], PhD.
1. Virginia Tech Department of Biomedical Engineering and Mechanics,
2. Virginia Tech Carilion Research Institute, 3: Virginia Tech Carilion School of Medicine
Corresponding Author: Harshawardhan U. Deshpande Email: harsh87@vt.edu

INTRODUCTION

The majority of seed-based functional connectivity (FC) analyses of functional magnetic resonance imaging (fMRI) data rely on healthy adult anatomy and the participant's ability to perform functional localizer tasks. However, such an analysis for populations such as pediatric cerebral palsy (CP) is challenging due to developmental age, the possibility of focal lesions, and task-coupled motion arising from sensory and motor deficits. Therefore, to study FC of motor networks in children with CP, we have begun a protocol that combines 1) real-time motion feedback [1] during resting state fMRI, rather than a mock scanner, 2) the use of the anatomical precentral 'hand-knob' landmark [2], and 3) alternative normalization methods to register anatomical and functional data.

METHODOLOGY

T1-weighted structural (5 min), resting state fMRI with motion feedback (5 min) and motor task fMRI (6 min) data were collected for two healthy and two CP-affected children on a 3T scanner. fMRI data were pre-processed by performing slice timing correction, motion correction, spatial smoothing (6 mm FWHM) and band-pass filtering (0.01 Hz to 0.08 Hz) with InstaCorr AFNI [3]. Edge detection was applied to the resting state data to aid manual alignment to the anatomical scan. Spherical regions of interest (ROIs) were drawn bilaterally on the hand-knob (6 mm radius), the segment of the precentral gyrus that is associated with hand motor function.

RESULTS

ROIs drawn on the hand-knob region were used as seeds to obtain whole-brain correlation maps (Fig. 1). In the healthy adults, this process showed a mean overlap of 60% (±18) with fMRI maps obtained from the motor task, confirming that the anatomical landmark overlaps with functional motor areas.

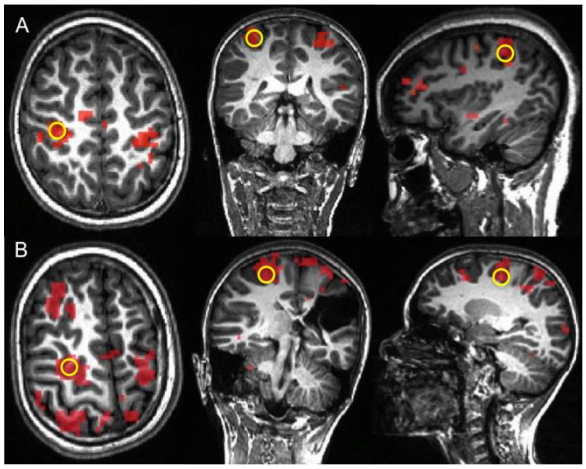

Figure 1: Correlation maps for resting state connectivity at threshold $p < 0.001$ with the seed voxel (denoted by the yellow circle) in the hand knob area of a healthy child (A) and a CP child (B).

CONCLUSIONS

We are developing techniques and protocols that use anatomical landmarks to localize functional activity and do not rely on standard normalization algorithms. We have validated this approach in five healthy adult datasets and have shown here data from healthy and CP children. This method enables FC analyses in a challenging subject population, where age, brain anatomy, and motor function differ from healthy adult studies. In future applications of this approach, we intend to track changes in FC during physical therapy.

REFERENCES

[1] Yang S., et al. *Neuroimage* 27.1 (2005): 153-162. [2] Yousry, T. A., *Brain* 120.1 (1997): 141-157. [3] Cox, R. W. *Comp. and Biomedical research*, *29*.3 (1996): 162-173.

Oral, PhD
Auditorium, 10:15

INVESTIGATION OF BLAST POLYTRAUMA AND THERAPEUTIC INTERVENTION OF HEMOSTATIC NANOPARTICLES

W. Brad Hubbard[1], Margaret Lashof-Sullivan[2], C. Shaylen Hall[1], Joseph Eck[1], Erin Lavik[2] and Pamela VandeVord[1,3]
1. Virginia Tech, Biomedical Engineering and Mechanics
2. Case Western Reserve University, Department of Biomedical Engineering
3. Research Services, Veterans Affairs Salem, VA
Corresponding Author: Dr. Pamela VandeVord, Email: pvord@vt.edu

INTRODUCTION

In response to the lack of therapeutics for internal bleeding following a traumatic event, hemostatic dexamethasone-loaded nanoparticles (hDNP) could be a viable option to help alleviate internal hemorrhaging. Blood loss is the primary cause of death at acute time points post injury in both civilian and battlefield traumas and there is a lack of internal bleeding therapeutics available for in theatre usage. The purpose of this study was to investigate whether a novel nanoparticle configuration could increase survival, reduce cellular injury and reduce anxiety-like disorders in a rodent model of blast polytrauma.

METHODOLOGY

hDNP were conjugated and consist of a block copolymer, poly (lactic-co-glycolic acid) – poly (l-lysine) – poly (ethylene glycol) and a peptide, glycine-arginine-glycine-aspartic acid-serine (GRGDS). These particles were evaluated as treatment in a rodent blast polytrauma model. Rats placed into hDNP and control groups (hNP, cDNP, cNP and Lactated Ringer's) were exposed to blast and given immediate injection. Open field assays were performed on surviving animals to measure levels of anxiety at six days post-blast. At one week post-blast, lungs and brains were extracted. Staining was performed on the lung (H&E; hemorrhage) and sections from the amygdala (glial fibrillary acidic protein (GFAP; activated astrocytes), cleaved caspase-3 (apoptosis), and SMI-71 (blood-brain barrier)). Statistical differences were assessed with analysis of variance (ANOVA) using LSD post-hoc test ($p < 0.05$ - statistically significant).

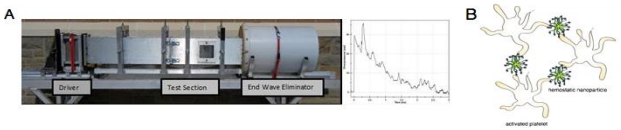

Figure 1: (A) Advanced Blast Simulator at VT and representative blast wave. (B) Schematic of the role of hDNP binding with activated platelets.

RESULTS

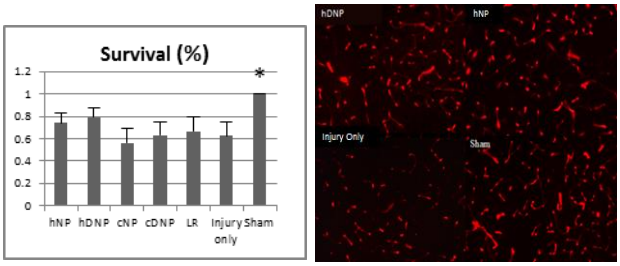

Figure 2: (Left) Survival Data in Treatment Groups after Injury. *p<0.05 (Right) Presence of SMI-71 (BBB integrity) in the amygdala

Survival percentage after injury was significantly different between sham and all control groups (cNP, cDNP, LR, and Injury Only) (Figure 2, Left). Elevated anxiety parameters were found in the Injury Only group compared to the hDNP and hNP groups. GFAP was significantly elevated in the Injury Only group compared to the hNP group in the amygdala. Caspase-3 was significantly elevated in the Injury Only group compared to the hDNP, hNP, and sham groups. SMI-71 (Figure 2, Right) was also significantly reduced in the Injury Only group compared to the hDNP, hNP, and sham groups.

CONCLUSIONS

Our results showed that hemostatic nanoparticles have the ability to reduce hemorrhage and increase survival in blast polytrauma. Through BBB restoration, hDNP are able to mitigate cellular injury and improve cognitive outcomes.

ACKNOWLEDGMENTS

The authors would like to recognize the funding sources: DOD CDMRP Program W81XWH-11-1-0014 and NIH Director's New Innovator Award number DP20D007338.

REFERENCES

Hubbard, W.B., Lashof-Sullivan, M.M., Lavik, E.B., VandeVord, P.J. (2015) Acs Macro Lett, 4(4):387-391.

Oral, PhD
Auditorium, 10:30

OPTICAL FIBER BASED IMAGING OF BIOENGINEERED TISSUE CONSTRUCT

Etai Sapoznik[1,2], Guoguang Niu[2], Peng Lu[3], Yu Zhou[2], Yong Xu[3], Shay Soker[1,2]
1. Virginia Tech-Wake Forest Univ. School of Biomedical Engineering and Sciences
2. Wake Forest Institute for Regenerative Medicine
3. Bradley Department of Electrical and Computer Engineering, Virginia Tech
Corresponding Author: Etai Sapoznik, Email: esapozni@wakehealth.edu

INTRODUCTION

Imaging cells and tissues through opaque and turbid media is challenging and presents a major barrier for monitoring maturation and remodeling of bioengineered tissues. The fiber optics based imaging system described here uses local excitation for fluorescent cell imaging through opaque scaffolds. The objectives of this study included: (1) Assessing the effects of imaging system parameters on image reconstruction outcomes (2) Identifying the impact of physical parameters on image outcome (3) Adapting the system for specific live cell imaging applications

METHODOLOGY

Micro imaging channel (MIC) was embedded in electropsun scaffolds made of Polycaprolactone (PCL) and collagen co-polymers. The MIC was used for insertion of single mode fiber for laser light local excitation (blue-450nm; green-532 nm; red-660). Scaffold were seeded with fluorescent beads and fluorescently labeled cells and placed in an imaging chamber containing cell culture media (DMEM). The sample stage was shifted to allow for multiple excitation points in the scaffold. The emitted signal was detected by EM-CCD detector, which was used to reconstruct an image of fluorescent emission distribution. Images were compared with control image CCD. Initially, fluorescent beads (green and far-red) were used to develop the reconstruction process and to assess image reconstruction outcomes. Image analysis was performed to identify beads location and assessing contrast to noise ratio (CNR) and resolution. Subsequently, fluorescently labeled endothelial and muscle progenitor cells (MPCs) were used to assess coverage of the scaffold's surface and cell differentiation, respectively. . In the third part MS1 cells labeled with FP and muscle progenitor cells from GFP transgenic mouse were seeded on scaffolds and imaged.

RESULTS

Imaging system parameters had a mixed impact on image outcome. While an increase in laser power had a small impact on the beads CNR, the reconstruction window size had a strong influence on the CNR with increased detection region of 1.9 mm^2 best detection compared with smaller window size. Physical parameters had a clear impact on imaging results. Increase in thickness led to decrease in CNR. Far-red beads gave better CNR compared with green beads. Collagen led to slight decrease in CNR for far-red beads, while the background noise was stronger than the green beads signal. When used with labeled cells, the imaging system can identify individual cell nuclei (fig 1a) on scaffold comparable to epifluorescent image (fig 1b). Also, it detected MPC elongation and cell fusion (fig 1c).

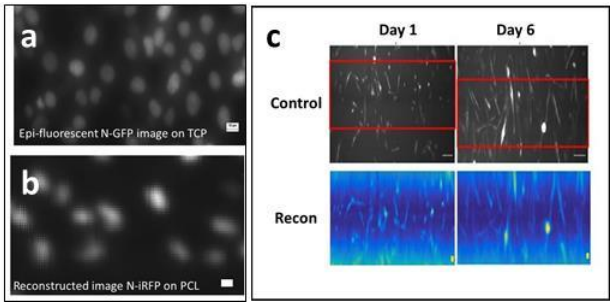

Figure 1: MS1 coverage (a) epifluorescent (b) recon; MPC (c) control and reconstructed images with time

CONCLUSIONS

Imaging system parameters could have an impact of the image outcomes and may need to be adjusted for specific applications. The fiber imaging platform has the potential for imaging through scattering material layers while considering a specific fluorescent spectra. This imaging tool is useful for imaging individual cells in resolution of up to 15 µm, and can identify morphological changes.

GENERALIZED SVD RECONSTRUCTION FOR INTERIOR TOMOGRAPHY

Rui Liu[1,2,3], Hengyong Yu[2]
1. VT-WFU School of Biomedical Engineering and Sciences, Wake Forest University Health Sciences
2. Department of Electrical and Computer Engineering, University of Massachusetts Lowell
3. Department of Biomedical Engineering, Wake Forest University Health Sciences
Corresponding Author: Hengyong Yu, Email: Hengyong_Yu@uml.edu

INTRODUCTION

The interior tomography is a challenging problem in image reconstruction with broad application such as cardiac CT. We proposed a GSVD based image reconstruction method for interior problem.

METHODOLOGY

The system matrix $\mathbf{A}$ and linear transform $\mathbf{\Phi}$ are applied. When $\mathbf{\Phi} = \mathbf{I}$, both TSVD and Tikhonov SVD (HSVD) are applied. The Laplacian operator is applied for GSVD. The objective function $\|\mathbf{Af} - \mathbf{p}\|_{\mathbf{W}}^2 + \xi^2\|\mathbf{\Phi f}\|_2^2$ is solved non-iteratively. $\mathbf{f}$ is the image and $\mathbf{p}$ is the projection data, $\mathbf{W}$ is the weighting factor and ξ is to balance the data fidelity. Iterative reconstruction methods require multiple iterations. However GSVD only need to be performed once. It can be as fast as matrix-vector multiplication procedure.

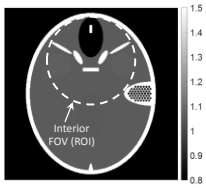

Figure 1: FORBILD head phantom in display window [0.8, 1.5].

RESULTS

GSVD is compared with TSVD, HSVD, FBP, SART and SART-TV. The FORBILD head phantom is employed (Fig. 1) for interior scan. Photon number is modeled as Poisson distribution. The threshold ε for TSVD, ζ for HSVD and ξ for GSVD are selected in a decreasing fashion. The reconstruction results are collected in Fig. 2. The reconstructed results from FBP, SART and SART-TV contain severe truncation artifacts near the boundary of the ROI but much more accurate by the TSVD and HSVD. The TSVD and HSVD contain more high frequency artifact. GSVD cannot reconstruct the high frequency part but the ROI is much smoother compared with TSVD and GSVD with Laplacian transform. GSVD can provide higher image quality at the boundary of the ROI. GSVD method reconstruct the image fast comparable with FBP but more flexible.

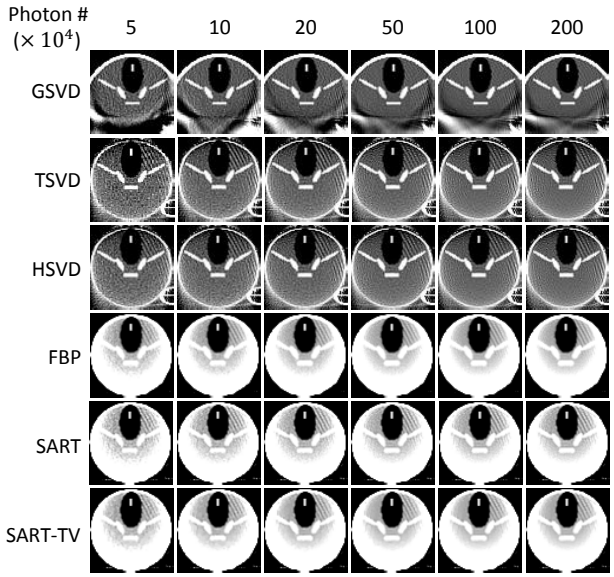

Figure 2: FORBILD head phantom results from six noise levels in display window [0.8, 1.5].

CONCLUSIONS

GSVD is developed for a broad class of inverse problems without an analytic solution. More analysis and experiments will be conducted to further improve the GSVD performance and reconstructed image quality along this direction.

ACKNOWLEDGMENTS

This work was partially supported by the NSF CAREER Award 1540898.

A BIOMECHANICAL COMPARISON OF EXTRAPELVIC AND INTRAPELVIC FIXATION FOR ANTERIOR COLUMN WITH POSTERIOR-HEMITRANSVERSE ACETABULAR FRACTURES

Gregory J. Gillispie[1], Sharon N. Babcock[2], Kyle P. McNamara[1,2], Philip J. Brown[1], and Eben Carroll[2]
1. Virginia Tech – Wake Forest School of Biomedical Engineering
2. Wake Forest University School of Medicine
Corresponding Author: Gregory Gillispie, Email: ggillisp@wakehealth.edu

INTRODUCTION

Acetabular fractures are common among elderly patients with low energy trauma such as falling. Elderly patients represent the fastest growing group in sustaining acetabular fractures[1] and their incidence rate is expected to continue to rise.[2] Anterior column with posterior-hemitransverse (ACPHT) fractures are one of the most common types of acetabular fractures seen in the elderly[3] and have been correlated with early failure after attempted reduction and internal fixation.[4] Typically, ACPHT fractures are treated with an extrapelvic plate along the pelvic brim. An intrapelvic, fixation system is also used where an additional plate is placed on the inner brim. While theoretically this provides a mechanical advantage, it is also more invasive. This study intends to quantify and compare the strength of intrapelvic and extrapelvic fixation.

METHODOLOGY

10 frozen cadaveric pelvises (20 hemipelves) were used in this study. Each specimen was given a standardized fracture, fixated with a plating system according to their group, and potted in polyurethane. Specimens were then loaded at 50% of the donor's body weight[5] (BW) for 3 axial loading cycles. After the final cycle, destructive testing was conducted at a rate of 1 mm/s until the force dropped below 75% of the maximum or displacement reached 30 mm. Force and displacement were recorded for all tests and used to calculate stiffnesses and energies. For the 50% BW test, stiffness and displacement at 50% BW were calculated. For the destructive test, stiffness, elastic energy, and plastic energy were calculated. Yield point, force at clinical failure (defined at 2 mm of displacement), and maximum force were also identified.

RESULTS

A Wilcoxon matched-pairs t-test was used to analyze the data. On average, the intrapelvic group performed better for all test parameters. However, statistical significance ($p < 0.05$) was only reached for yield force, maximum force, and plastic energy. Displacement at 50% of body weight, stiffness during the destructive test, clinical failure force, and elastic energy were all near-significant.

CONCLUSIONS

While intrapelvic fixation did outperform extrapelvic fixation, several measures showed only minor, statistically insignificant differences. There was a high amount of variation between specimens both characteristically and statistically. A low sample size may have contributed. Another possibility is that intrapelvic fixation is not as advantageous as theorized. The most significant differences were seen in measures that were calculated using the highest loads: maximum force, plastic energy, and yield force. From this it might be concluded that the intrapelvic plate does not begin contributing towards the strength of the acetabulum until higher loads are reached. If this is the case, intrapelvic fixation would not likely help prevent early failure of the surgical reduction and the added invasiveness may not necessarily be worth the risks, especially for elderly patients. The data presented in this study suggests that an improved fixation system is still needed for ACPHT acetabular fractures.

ACKNOWLEDGMENTS

DePuy Synthes - funding; Jared Mitchell & Michaela Dimoff

REFERENCES

1. Lonner JH. 1995. **2**. Jeanotte L. 2007. **3**. Ferguson TA. 2010. **4**. Kreder HJ. 2006. **5**. Laing AC. 2010.

INVESTIGATION OF DRIVER LANE KEEPING BEHAVIOR IN NORMAL DRIVING BASED ON NATURALISTIC DRIVING STUDY DATA

Taylor Johnson[1], Rong Chen[1], Rini Sherony[2], Hampton C. Gabler[1]
1. Virginia Tech, Biomedical Engineering and Mechanics
2. Toyota Motor Engineering & Manufacturing North America, Inc.
Corresponding Author: Taylor Johnson, Email: tj916@vt.edu

INTRODUCTION

Road departures are among the deadliest crash modes in the U.S., accounting for only 10% of all crashes but 30% of all fatalities. Lane departure warning (LDW) is an active safety system that alerts drivers when impending departures are detected. This technology has the potential to reduce the number of lane and road departure crashes, but the benefits are expected to be highly dependent on driver acceptance. When warnings are delivered too early and drivers feel there is no risk of departure, they may become annoyed and disable the system. To improve driver acceptance, it is essential to understand normal lane keeping behavior and driver perception of danger in lane departure events. The goal of this study was to investigate lane keeping behavior of drivers in normal driving, including varying lane widths and road curvatures.

METHODOLOGY

This study used a lane departure subset of the Integrated Vehicle-Based Safety Systems (IVBSS) naturalistic study database. The IVBSS study instrumented 108 vehicles to capture normal driving kinematics for 12 days with no LDW intervention. During this time, 5,833 unintentional drift-out-of-lane departure events were detected. To characterize normal lane keeping behavior, a vehicle lateral velocity (LV) – distance to lane boundary (DTLB) distribution was generated. DTLB is the lateral distance between the leading edge of the vehicle and the lane boundary. Negative DTLB indicates a departed vehicle. To investigate lane width and road curvature effects, the distribution was subset by each factor at three levels.

RESULTS

Figure 1 shows the normal driving distribution and an ellipsoid which encloses 99% of driving time points used to visualize normal driving boundaries.

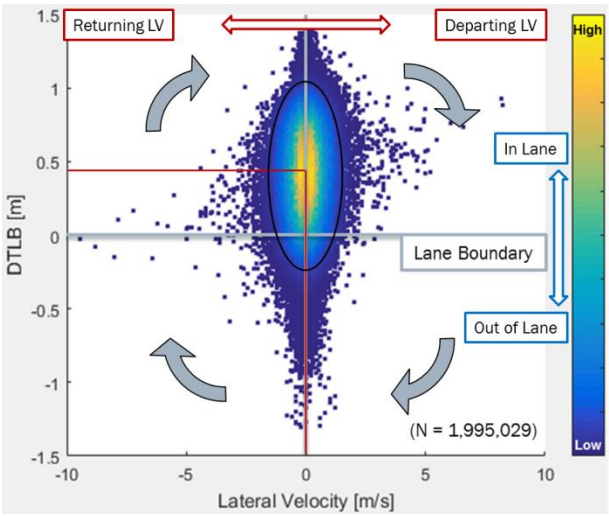

Figure 1: Normal driving distribution.

CONCLUSIONS

This study found normal driving to center around driving straight 0.5 m from the lane boundary. Drivers tend to decrease LV as the lane line approaches. Normal driving was not significantly affected by lane width, but high curvature roads resulted in further departure distances.

ACKNOWLEDGMENTS

The research team would like to thank the Toyota Collaborative Safety Research Center (CSRC) and Toyota Motor Corporation for funding this study.

REFERENCES

[1] Johnson, T., Chen, R., Sherony, R., and Gabler, H., "Investigation of Driver Lane Keeping Behavior in Normal Driving based on Naturalistic Driving Study Data," *SAE Int. J. Trans. Safety* 4(2):2016, doi:10.4271/2016-01-1449.

Oral, M.S.
Room 155, 1:30

LUMBAR VERTEBRAE FRACTURE INJURY RISK IN RECONSTRUCTION OF CIREN AND NASS FRONTAL MOTOR VEHICLE CRASHES

Derek A. Jones[1,2], James P. Gaewsky[1,2], Mireille E. Kelley[1,2], Ashley A. Weaver[1,2], and Joel D. Stitzel[1,2]
1. Virginia Tech-Wake Forest University Center for Injury Biomechanics
2. Wake Forest University School of Medicine
Corresponding Author: Derek A. Jones, Email: derjones@wakehealth.edu

INTRODUCTION

In the United States alone, there are 3.9 million non-fatal injuries attributed to motor vehicle crashes (MVCs) annually, with frontal crashes the most common [1,2]. MVCs are the leading cause of thoracic and lumbar spine injuries, with medical costs up to $124,000 per injury [3]. As injury criteria thresholds have been implemented into regulatory and consumer crash tests, lumbar spinal injury has continued to be neglected [4]. Concurrently, retrospective studies have demonstrated that the incidence of thoracolumbar vertebral body fractures has increased in frontal impacts as a function of model year since 1986 [5,6]. The purpose of this study was to reconstruct four motor vehicle crashes using a Finite Element (FE) Human Body Model (HBM) to elucidate factors that could lead to increased risk of lumbar vertebra injury.

METHODOLOGY

Two real-world frontal motor vehicle crashes with lumbar vertebral fracture and two without were selected from the CIREN and NASS-CDS databases. The Total HUman Model for Safety (THUMS) HBM, capable of predicting lumbar vertebral injury, was used in real-world crash reconstruction for all four cases [7]. On a case-by-case basis, a simplified vehicle buck model was tuned to match the restraint characteristics of the crash vehicle using a FE Hybrid III model [8]. Following the tuning, THUMS was implemented into the model and the crash was driven by the real world event data recorder kinematics. Lumbar vertebrae injury metrics were extracted and analyzed.

RESULTS

Tuning the SVM to specific vehicle models produced close matches between the simulated and experimental crash test responses for head, T6, pelvis resultant acceleration, left and right femur loads, and shoulder and lap belt loads. While vertebral load in the THUMS simulations was highly similar between injury cases and non-injury cases, the amount of bending moment was much higher for the injury cases (Figure 1). Seat back angle had a large effect on both peak vertebral bending moment and compressive force. Both measures increased in severity as seat back angle (measured from vertical) increased.

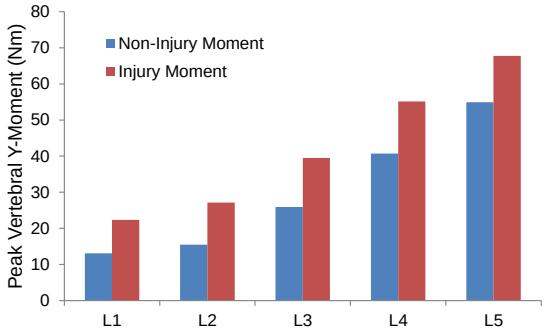

Figure 1: Vertebral body moment as a function of vertebral level for baseline simulations of injury and non-injury cases.

CONCLUSIONS

Motor vehicle crash reconstruction is a valuable tool for elucidating the risk of injury associated with pre-crash factors. In this study, the likelihood of lumbar injury increases with reclining seat-back.

ACKNOWLEDGMENTS

Funding: Toyota's Collaborative Safety Research Center

REFERENCES

[1] Blincoe et al. NHTSA Report No. DOT HS 812 013, 2015 [2] NHTSA *Traffic Safety Facts 2012*, 2014 [3] Rao et al. *Spine J.*, 2014 [4] Hollowell et al. *NHTSA Docket* 1999 [5] Pintar et al. *Ann Adv Automot Med.*, 2012 [6] Doud et al. *Clin Orhop Relat Res.*, 2015 [7] Shigeta et al., *ESV Conference*, 2009 [8] Jones et al. *SAE World Congress*, 2016

HEAD IMPACT EXPOSURE IN YOUTH FOOTBALL PRACTICE DRILLS

Mireille E. Kelley[1], Jillian E. Urban[1], Logan E. Miller[1], Joeline M. Kane[2] and Joel D. Stitzel[1]
1. Virginia Tech- Wake Forest Center for Injury Biomechanics
2. Wake Forest University
Corresponding Author: Mireille E. Kelley, Email: mekelley@wakehealth.edu

INTRODUCTION

Head impact exposure has been studied at the high school, collegiate, and professional levels, however investigations at the youth football level (ages 8-13) has been limited. Although head impact data from youth athletes is scarce, preliminary data suggests that youth football players sustain head impacts approaching the magnitude of collegiate players [1-3]. However, youth football studies have also shown that limiting contact in practice can significantly reduce head impact exposure in youth football athletes [1]. The objective of this study is to evaluate frequency and magnitude of head impacts in practice drills within a youth football team and identify high head impact exposure practice drills.

METHODOLOGY

On-field head impact data were collected from 9 athletes participating in a youth football team for a single season. Head impact data were collected and video was recorded for all practices and games. Head impact data were collected with the Head Impact Telemetry (HIT) System. Video recordings were used to verify recorded head impacts and identify drills during practices. Drills were classified as: 11-on-11, dummy/sled tackling, kickoff practice, Oklahoma, one-on-one, open field tackling, passing drills, position skill work, multi-player tackle, tackling stations, and scrimmage.

RESULTS

A total of 3,761 head impacts were recorded during 36 practices and 11 games. Practices accounted for 2,171 impacts. The median/95th percentile linear acceleration during practices was 20.1/56.1g. Open field tackling drills resulted in the highest magnitude impacts, as can be seen in Figure 2, with a median/95th percentile linear acceleration of 24.6/95.68g. This drill accounted for 2.4% of all practice head impacts, but accounted for 10.2% of all practice head impacts greater than 60g. 11-on-11 had a median/95th percentile linear acceleration of 19.7/51.7g and accounted for 56% of all practice head impacts and 43% of practice head impacts greater than 60g. The drills with frequently lower magnitude impacts were passing drills and dummy/sled tackling.

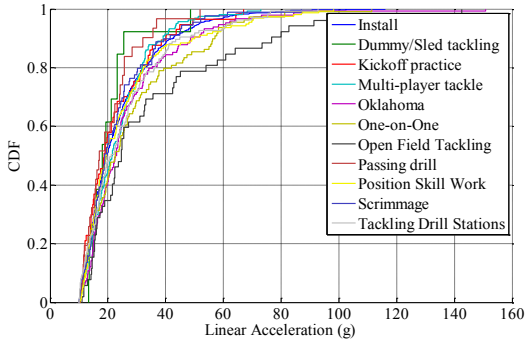

Figure 2: Distribution of linear acceleration of head impacts for each drill.

CONCLUSIONS

This study demonstrates that practice drills can vary greatly in their head impact exposure. Understanding the contributing factors to exposure at the youth level can inform organizations on ways to limit high impact and high frequency drills and, ultimately, keep athletes safe.

ACKNOWLEDGMENTS

Research reported in this publication was supported by the National Institute Of Neurological Disorders And Stroke of the National Institutes of Health under Award Number R01NS094410. The authors would like to thank the South Fork Panthers youth football organization and interns Megan Anderson and Leslie Hoyt.

REFERENCES

[1] Daniel, R.W., et al., 2012. [2] Cobb, B.R., et al., 2013. [3] Urban, J.E., et al., 2013.

Oral, M.S.
Room 155, 1:45

DEVELOPMENT AND VALIDATION OF A 6 YEAR-OLD PEDESTRIAN FINITE ELEMENT MODEL

Yunzhu Meng[1,2], Costin D. Untaroiu[1,2]
1. Virginia Tech
2. Virginia Tech-Wake Forest Center for Injury Biomechanics
Corresponding Author: Yunzhu Meng, Email: mengyz@vt.edu

INTRODUCTION

Child pedestrian protection continues to be an important issue in vehicle crash safety. However, only a child headform impact test is designed for prediction of child pedestrian injuries. The development of a computational child model could be a better alternative that characterizes the whole-body response of vehicle–pedestrian interactions and assesses the pedestrian injuries. In this study, an advanced and computationally efficient finite element (FE) model corresponding to a six-year-old pedestrian child was developed in LS-DYNA.

METHODOLOGY

The model was developed by morphing an existing GHBMC 5th percentile female pedestrian model to a six-year old child geometry reported in literature. Material properties were applied based upon previously published studies. The standing posture has been used as specified in the EuroNCAP testing protocol.

The child model was validated against a very few child component tests identified in literature. Component validations with simple impactor tests were performed in LS-DYNA. Full-body model was validated under lateral loading quantitative and CPC impact was simulated to investigate the injury mechanism (Fig. 1).

Figure 1: Vehicle-to-child pedestrian FE simulation

RESULTS

The results of the model showed a reasonable correlation to the test data in component validations. The child pedestrian model showed also numerical stability under a typical CPC configuration. In addition, the most common injuries observed in pedestrian accidents including fractures of lower limb bones and ruptures of knee ligaments were predicted by the child FE model.

The femur with assumed pediatric properties showed less stiffness and lower fracture force than the similar model with adult material properties [1] (Fig. 2). Although the child stiffness curves were not published, the corresponding simulation curve showed a similar linear shape as that reported in adult tests [2].

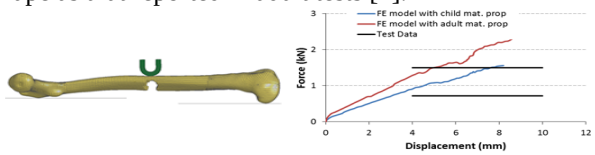

Figure2: Femur Fracture under AP bending loading

In lateral loading simulation, no fractures were predicted during the pelvic region. The time histories of both impact force and the Viscous Criterion (V*C) predicted by the model showed qualitatively the same trend as the corresponding test data [3].

CONCLUSIONS

The child pedestrian model predicted the most common injuries observed in pedestrian accidents. Improvements could be made to the model mesh and especially to material properties.

ACKNOWLEDGMENTS

The authors are grateful for help received from WFU and GHBMC.

REFERENCES

[1] J. Ouyang, et al., "Biomechanical Character of Extremity Long Bones in Children and Its Significance," Chinese Journal of Clinical Anatomy, vol. 21, p. 4, 06.31.2003 2003.
[2] C. D. Untaroiu, et al., "A FE model of the lower limb for simulating automotive impacts," Ann Biomed Eng, vol. 41, pp. 513-26, Mar 2013.
[3] J. Ouyang, et al. "Exp. cadaveric study of lateral impact of the pelvis in children," Acad. J. of 1st med col., vol. 23, pp. 397-401, 2003.

Oral, M.S.
Auditorium, 2:00

FINITE ELEMENT ANALYSIS OF A NOVEL DESIGN FOR A NON-MIGRATING BILIARY STENT USING ABAQUS

Jared D. Mitchell[1], Clifford Howard Jr.[2], and Philip J. Brown[1]
1. Virginia Tech – Wake Forest School of Biomedical Engineering
2. Wake Forest University School of Medicine
Corresponding Author: Jared Mitchell, Email: jmitche@wakehealth.edu

INTRODUCTION

Biliary stenting is most frequently caused by an interruption in the ability to drain bile into the duodenum. This obstructive jaundice is commonly a result of a stricture from a tumor located at the pancreases head, peri-ampulary area, bile duct, or gall bladder. In order to return patency, stenting of the biliary tree is performed by means of endoscopic retrograde cholangiopancreatography (ERCP) [1,2]. There are two main types of stents used to treat this condition each having their respective advantages and disadvantages. Nearly 30% of all biliary stents, however, fail and require removal, exchange, or intervention. One common modes of failure is migration, which occurs 17% of the time with fully covered metallic stents [3].

The main goal of this project was to design a biliary stent that would reduce and prevent stent migration. If stent migration was solved, it would greatly reduce the frequency at which medical practitioners would have to intervene to restore biliary patency.

METHODOLOGY

A biliary stent was modeled in SolidWorks and imported into Abaqus CAE where simulations were performed to analyze stent performance.

RESULTS

We have designed a biliary stent that upon expansion will deploy anti-migration hooks. These hooks displace more than the actual stent body in order to gain more traction from the surrounding biliary and duodenal tissue.

From an initial diameter of 3mm, the stent body deploys to roughly an 8mm diameter while the hook tip deploys to nearly 12mm. This occurs with minimal recoil of 1.76mm (from 19.17mm to 17.41mm).

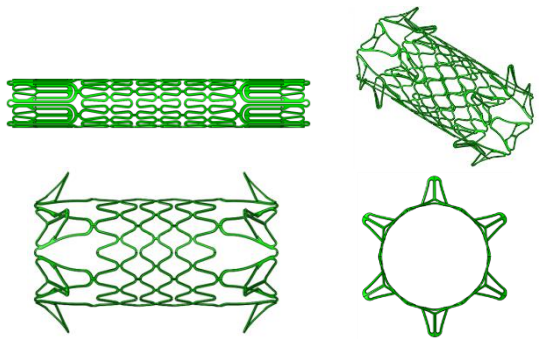

Figure 1: Non-migration Stent

CONCLUSIONS

This design, after alterations, will provide a novel means to solve stent migration. This stent will push future designs to solve stent dysfunction.

ACKNOWLEDGMENTS

The authors would like to thank the effort of Kenneth Russell and Gregory Gillispie and funding provided by Wake Forest Innovations.

REFERENCES

1. Donelli, G., et al., *Plastic biliary stent occlusion: factors involved and possible preventive approaches.* Clin Med Res, 2007. **5**(1): p. 53-60.
2. Dumonceau, J.M., et al., *Biliary stenting: indications, choice of stents and results: ESGE clinical guideline.* Endoscopy, 2012.
3. Leung, J., *Self-Expandable Stents in the Gastrointestinal Tract*, 2013, Springer: New York.

Oral, M.S.
Room 155, 2:00

BIOMECHANICS OF HEAD IMPACTS IN SOCCER

Jaclyn N. Press[1] and Steven Rowson[1]
1. Virginia Tech, Department of Biomedical Engineering and Mechanics
Corresponding Author: Jaclyn Press, Email: jaclynp@vt.edu

INTRODUCTION

Sport-related concussions and their short- and long-term effects are a growing concern across the world for athletes, coaches, and parents alike. Much attention has been focused on women's soccer, as this sport has one of the highest rates of concussion among popular collegiate sports.[1] This multifaceted study aimed to fill knowledge gaps in this population through two objectives: 1) quantifying on-field head impacts, and 2) determining if headgear can reduce concussion risk in soccer impacts.

METHODOLOGY

A total of 26 players from the Virginia Tech Women's Soccer Team consented to participate in this study. Head impact sensors were placed behind the ear of every player before each game and practice to record linear and rotational head accelerations. Results collected were then compared with video recordings of each event.

A JUGS Soccer Machine was used to shoot official NCAA soccer balls at a NOCSAE headform mounted on a Hybrid III 50th percentile neck. The headform was instrumented to measure impact kinematics. Ten different soccer headgears were purchased and tested along with a control (bare headform) condition. A custom head-to-head impactor system was also designed and built to observe how these headgear performed under more severe impact conditions. The struck headform was instrumented to measure impact kinematics.

RESULTS

Video analysis identified a total of 1703 impacts, 89.6% of which were headers. The average number of impacts per player per practice or game was 1.86 ± 1.42. Impact totals varied by position. The sensor's algorithm reported a total number of impacts that was much greater than the number of impacts identified through video analysis (8999 recorded compared with 1703 confirmed).

Select headgears showed a statistically significant decrease in average peak linear head acceleration from the control condition at both ball velocities. Concussion risk for all head-to-ball impacts was below 1%. For head-to-head tests, every headgear showed a statistically significant decrease in average peak linear and rotational head acceleration from the control condition. Concussion risk for all head-to-head impacts was reduced significantly with the use of protective headgear.

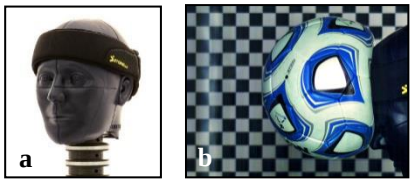

Figure 1: a) Storelli headgear displayed on a NOCSAE headform, b) High speed video of a ball-to-head test.

CONCLUSIONS

This study has quantified head impact exposure for women's soccer players through video analysis of a collegiate women's soccer season. Furthermore, this study illustrated the challenges of using head impact sensors on the field, which are likely not specific to the sensor used. There were statistically significant differences in accelerations with and without the use of protective headgear for both ball-to-head and head-to-head trials. For ball impacts, the differences are small and not clinically relevant. For the head-to-head trials, the differences are meaningful and suggest that the use of protective headgear could reduce concussion risk significantly. These data will help to inform soccer organizations on best practices for player safety in relation to head impacts.

REFERENCES

[1] Hootman, J et al., J Athl Train, 42(2):311-319, 2007.

QUANTIFYING THE EFFECT OF HELMET FIT ON HELMET PERFORMANCE

Jake A. Smith[1] and Steven Rowson[1]
1. Virginia Tech, Biomedical Engineering and Mechanics
Corresponding Author: Jake A. Smith, Email: pghjake@vt.edu

INTRODUCTION

Many clinicians often point to helmet fit as the most important factor in helmet selection. However, there is no published evidence supporting these claims. Helmet manufacturers provide fitting instructions, but there have been no biomechanical studies supporting their definition of fit. From a biomechanical standpoint, it is hypothesized that, given the helmet remains secured atop the head, there will be little variance in the attenuation of the impact amongst differing helmet fit conditions. The goal of this study was to develop a method of quantifying helmet fit and assessing the effect it has on helmet performance.

METHODOLOGY

To develop a method of quantifying helmet fit, a metric was needed to describe fit. It was determined that superficial head pressure was the best way to observe this, so a custom pressure sensor was developed and used to create pressure profiles for helmets fitted to a medium NOCSAE headform (Fig. 1). To evaluate the differences in helmet performance by fit, 2 fitting scenarios were chosen for evaluation on 3 different helmets: Schutt Air XP Pro, Riddell Speed, and Xenith Epic. First, a set of 3 large helmets were fit to meet the helmet manufacturers' fitting guidelines. This was considered our "best" fit condition. Second, a set of 3 extra-large helmets were fit to the headform with no adjustments made. This was considered our "minimum" fit condition. Using pressure profiles generated from the pressure sensor, a metric was developed to quantify helmet fit. This fit metric was designed to account for average pressure, while weighting points of higher pressure in order to take comfort into account.

To evaluate football helmet performance, on-field impact scenarios must be translated to the laboratory. A total of 216 impact tests were performed over a range of impact energies to simulate head impacts ranging in severity from sub-concussive to concussive. A custom pendulum impactor was used to impact the headform mounted on a Hybrid III 50th percentile neck. Each test was performed 3 times to ensure accuracy. The headform was instrumented with 3 linear accelerometers and 3 angular rate sensors. Angular acceleration was calculated by differentiating the angular data. A two-way ANOVA and Tukey HSD were performed to analyze the significance of fit and location within helmets and impact energies.

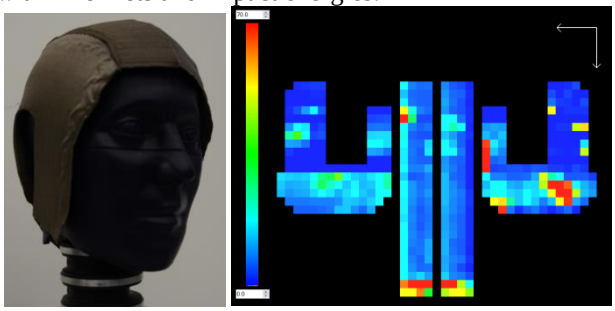

Figure 1: Custom pressure sensor on NOCSAE headform (left) and pressure profile of a large helmet (right)

RESULTS

Both linear and angular acceleration data were analyzed for each helmet at each impact energy level. With regards to fit, each helmet displayed significant differences from the best to the minimum fit conditions. However, they were not uniform across impact energy levels. For the Schutt Air XP Pro, significant differences due to fit were found in all impact velocities for both linear and angular acceleration. The Riddell Speed showed significant differences due to fit in all but the 3.0 m/s tests for angular acceleration. Finally, the Xenith Epic showed significant differences only in the 3.0 m/s and 4.6 m/s tests for linear acceleration.

CONCLUSIONS

Of the tests that showed statistical significance, only the Schutt helmet had substantial differences between the best and minimum fit conditions. This could be due to the contact area between the helmet and head varying with fit, causing the effective stiffness of the foam to vary. In general, the effects of helmet fit are considered small, and further work will investigate the clinical relevance.

Oral, M.S.
Room 155, 2:15

NEW ARTERIAL SPIN LABELING METHOD FOR SIMULTANEOUS ESTIMATION OF ARTERIAL CEREBRAL BLOOD VOLUME, CEREBRAL BLOOD FLOW AND ARTERIAL TRANSIT TIME

Megan E. Johnston[1], Ho-Ling A. Liu[2], Christopher T. Whitlow[3], and Youngkyoo Jung[1,3]
1. Wake Forest School of Medicine, Biomedical Engineering
2. University of Texas MD Anderson Cancer Center, Imaging Physics
3. Wake Forest School of Medicine, Radiology
Corresponding Author: Megan E. Johnston, Email: megjohns@wakehealth.edu

INTRODUCTION

Arterial Spin Labeling (ASL) is a completely non-invasive method of cerebral blood flow (CBF) imaging with MRI. The purpose of this study is to demonstrate the feasibility of a novel ASL method for simultaneously measuring CBF, arterial transit time (ATT), and arterial cerebral blood volume (aCBV) without the use of a contrast agent.

METHODOLOGY

A series of multi-TI ASL images were acquired from one healthy subject on a 3T Siemens Skyra, with the following parameters: PCASL labeling with variable TI [300, 400, 500, 600, 700, 800, 900, 1000, 1500, 2000, 2500, 3000, 3500, 4000] ms, labeling bolus 1400ms when TI allows, otherwise 100ms less than TI, TR was minimized for each TI, two sinc shaped pre-saturation pulses were applied in the imaging plane immediately before 2D EPI acquisition. 64x64x24 voxels, 5mm slice thickness, 1mm gap, full brain coverage, 6 averages per TI, no crusher gradients, 11ms TE, scan time of 4:56. The perfusion weighted time-series was created for each voxel and fit to a novel model. The model has two components: 1) the traditional model developed by Buxton [1], accounting for CBF and ATT, and 2) a box car function characterizing the width of the labeling bolus, with variable timing and height in proportion to the aCBV. All three parameters were fit using a nonlinear fitting routine that constrained all parameters to be positive. The main purpose of the high-temporal resolution TI sampling for the first second of data acquisition was to precisely estimate the blood volume component for better detection of arrival time and magnitude of signal.

RESULTS

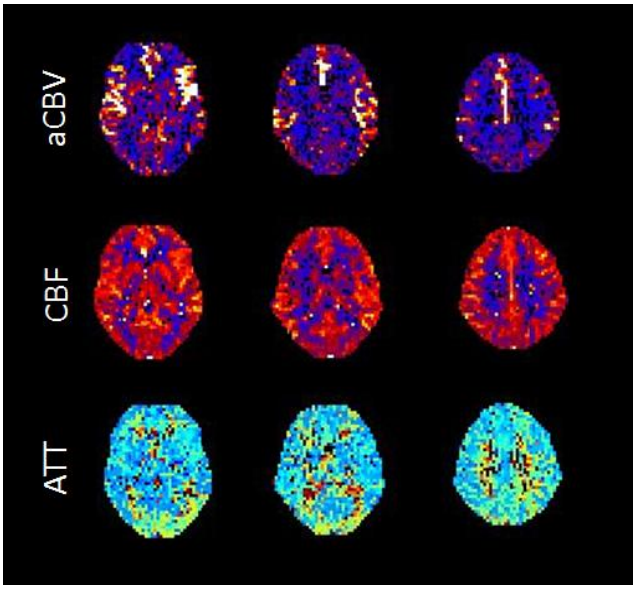

Figure 1: Select slices from one subject's aCBV, CBF, and ATT maps.

Whole brain maps of CBF, ATT, and aCBV were produced, and all three parameters maps are consistent with similar maps described in the literature (see Fig 1).

CONCLUSIONS

Simultaneous mapping of CBF, ATT, and aCBV is feasible with a clinical scan time (under 5 min).

REFERENCES

[1] R. B. Buxton, et al., Magnetic Resonance in Medicine, vol. 40, pp. 383-396, Sep 1998.

BIOPRINTED BONE GRAFT FOR CRANIOFACIAL RECONSTRUCTION

Carlos V. Kengla[1,2], James J. Yoo[1,2], and Sang Jin Lee[1,2]
1. Wake Forest University|Virginia Tech, School of Biomedical Engineering and Sciences
2. Wake Forest University School of Medicine, Institute for Regenerative Medicine
Corresponding Author: Carlos Kengla, Email: ckengla@wakehealth.edu

INTRODUCTION

The CranioMaxilloFacial (CFM) skeleton is composed of many boney structures of complex shape and integration with many other tissues which generate the myriad functions of the head and face. Reconstructive surgical intervention is, therefore, an intricate effort often involving free flaps harvested from other sites of the body. These bone grafts, while improving long-term graft success over other grafting methods, do not have the correct shape and often do not sufficiently repair the CFM anatomy. Our research seeks to improve CFM bone regeneration by enhancing scaffolding material, integrating complex anatomical shapes, leveraging of architecture, and incorporating a stem cell population.

METHODOLOGY

A novel scaffolding biomaterial was produced by mixing polycaprolactone (PCL) (43-50kDa, Polysciences, USA) and tricalcium phosphate nano-powder (Berkeley Advanced Biomaterials, USA) at a 1:1 weight ratio. Scaffold specimen were printed on the Integrated Tissue/Organ Printer (ITOP) platform.[1] Amniotic fluid derived stem (AFS) cells were used for differentiation studies. An Instron universal testing system was used for mechanical analysis. NaOH (Sigma, USA) was used for accelerated degradation. New Zealand white rabbits were used for a mandibular defect surgical model.

RESULTS

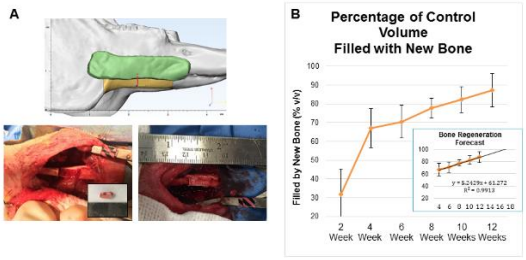

Figure 1: A) Mandibular defect surgical model. B) CT measures within graft show increasing bone volume.

Material properties were found to be within or greater than the range expected for trabecular bone. The compressive properties varied according to printed architecture. The architectures were also confirmed to be anisotropic.

In vitro assessment demonstrates bone-lineage differentiation of AFS cells. *In vivo* experiments show bone regeneration as early as 4 weeks and continuing to 12 weeks.

Table 1: Effect of Architecture on Compressive Modulus

Type	Normal Compression MPa (SD)	Orthogonal Compression MPa (SD)	Percent Difference
Control	20.5(1.3)	25.6 (10.2)	22.0
Core	26.0 (1.7)	32.4 (2.2)	22.1
Shell	76.7 (6.3)	42.5 (7.8)	57.4
Plate	19.6 (7.6)	77.3 (10.9)	118.9

CONCLUSIONS

In vitro and in vivo experiments confirm that the novel PCL/TCP mixture supports bone regeneration. The clinically translational system can produce patient specific grafts. Architectural design supports bone regeneration and appears to limit soft tissue ingrowth.

ACKNOWLEDGMENTS

This work is funded by the Armed Forces Institute for Regenerative Medicine. Many people contributed aid in the animal handling. Greg Gillespie helped with mechanical testing and analysis.

REFERENCES

1. Kang, H.-W. *et al.* A 3D bioprinting system to produce human-scale tissue constructs with structural integrity. *Nat. Biotechnol.* **34,** 312–319 (2016).

Oral, PhD
Auditorium, 3:00

ULTRASENSITIVE MICROFLUIDIC ASSAYS FOR EPIGENOMIC ANALYSIS OF NEURONS FROM MAMMALIAN BRAINS

Sai Ma[1], Zhixiong Sun[2], Hehuang Xie[2], M. Margarita Behrens[3], Joseph R. Ecker[3] and Chang Lu[1,4]
1. School of Biomedical Engineering and Science, Virginia Tech
2. Virginia Bioinformatics Institute, Virginia Tech
3. Genomic Analysis Laboratory, The Salk Institute for Biological Studies
4. Chemical Engineering, Virginia Tech
Corresponding Author: Chang Lu, Email: changlu@vt.edu

INTRODUCTION

Epigenetics refer to any process that alters gene activities without changing the DNA sequence. Previous studies have demonstrated that epigenetic regulation, such as DNA methylation, plays a critical role in many biological procedures, such as brain development underlying memory and learning. Neuronal diversity is essential for brain functions, but leads to a challenge to epigenetic profiling. In mammalian brains, there are more than 200 subtypes of neurons based on morphology, size, connectivity and molecular signature. Each of these subtypes potentially presents distinct epigenomic profile and yields only a tiny amount of neuron samples (< 2,000 neuronal nucleis on average extracted from a mouse cerebellum). Genome-wide study of dynamics of DNA methylation at single-base resolution provides a comprehensive understanding of methylome configuration. However, conventional protocols required more than 300 ng DNA (corresponding to 60,000 cells), which is not applicable for studying subtypes of neurons.

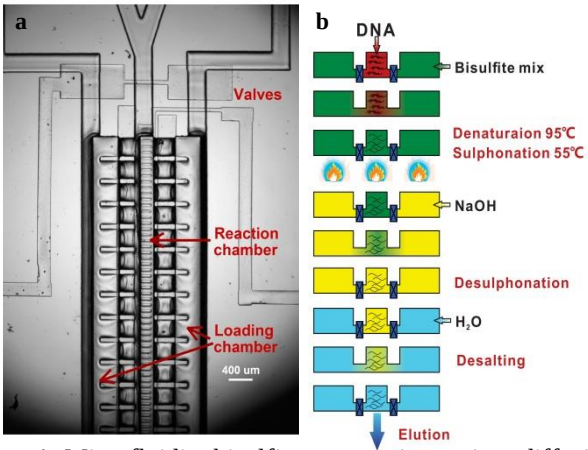

Fig. 1 Microfluidic bisulfite conversion using diffusion based reagent exchange. (a) The microscope image of the chip that contains a reaction chamber connected with two loading chambers on both sides. The connections could be cut off by closing two-layer valves. This scheme allowed the replacement of small molecules inside the reaction chamber by diffusion from/into the loading chambers. (b) The experimental steps of DNA methylation analysis.

RESULTS

We reported the first microfluidic DNA methylation assay (**Fig. 1**) at genome-wide scale and single-base resolution with >3 orders of magnitude higher sensitivity than conventional protocols. We used our microfluidic protocol to perform reduced representative bisulfite sequencing (RRBS) with various amounts of genomic DNA extracted from GM12878 cells or FACS sorted neuron cells. We prepared DNA templates by MspI enzyme digestion, end-repairing and ligation with sequencing adaptors. 300, 10, 1, and 0.3 ng genomic DNA was bisulfite-converted using our device (with > 98% conversion rate). A browser representation of identified cytosine (in CpG content) using RRBS is shown in **Fig. 2**. For all 4 sample sizes, replicate experiments were highly correlated (r = 0.995, 0.992, 0.979 and 0.912 for 300, 10, 1 and 0.3 ng, respectively).

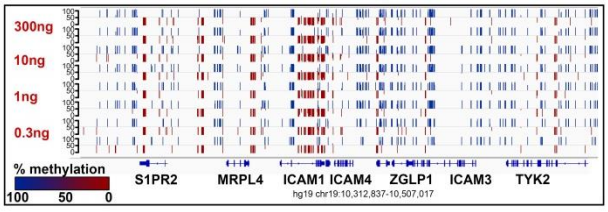

Fig. 2 Genome representation of the RRBS data (CpG methylation status) by microfluidic bisulfite conversion using various starting materials.

ACKNOWLEDGMENTS

We acknowledge support from National Institutes of Health grants CA174577, EB017235, EB019123.

Oral, PhD
Auditorium, 3:15

HIPPOCAMPAL DOSIMETRY PREDICTS FOR CANCER-RELATED COGNITIVE IMPAIRMENT IN PATIENTS WHO RECEIVE PARTIAL BRAIN IRRADIATION: DOSIMETRIC RESULTS OF A PROSPECTIVE CLINICAL TRIAL

Catherine Okoukoni [1,2], Emory McTyre[1], Ann M. Peiffer PhD[1], William H. Hinson, PhD[1], Roy E. Strowd, MD[1], Stephen Rapp PhD[1], Michael D. Chan MD[1],

1. Wake Forest School of Medicine, Department of Radiation Oncology
2. Virginia-Tech Wake Forest University School of Biomedical Engineering,

Corresponding Author: Catherine Okoukoni, Email: cokoukoni@wakehealth.edu

INTRODUCTION

Cancer-related cognitive impairment (CRCI) is relatively common after treatment of primary and metastatic brain tumors, however the temporality of cognitive decline after radiation therapy (RT) is not well defined, with reports of both early (<4 months) and late onset (>12 months) symptoms.[1] Identifying dosimetric parameters predictive of CRCI is difficult due to the heterogeneity of patient characteristics, as well as inadequate documentation of confounding factors. Memory function is especially susceptible to radiation effect after treatment.[1] The objective of this study is to correlate volumetric radiation doses received by critical neuroanatomic structures to post-RT memory impairment.

METHODOLOGY

Between 2008 and 2011, 53 patients with primary brain malignancies were treated with conventionally fractionated RT on a prospectively accrued clinical trial performed at our institution (WFU97100/91105)[3]. Tumor types included glioblastoma (13%), primitive neuroectodermal (21%), and low grade/benign tumors (66%).Ten patients received whole brain RT with region boost, all other patients received partial brain RT. The median radiation dose was 54.0Gy (range 40.0-60.6Gy) delivered in 1.8Gy/fraction (range 1.5-2.5 Gy/fraction).

Dose-volume histogram analysis was performed for the hippocampus, parahippocampus, amygdala, and fusiform gyrus. Hopkins Verbal Learning Test-Revised (HVLT-R) scores were obtained at least 6 months after RT. Impairment was defined as a HVLT-R immediate recall score $\leq$15, based upon studies reporting optimal sensitivity and specificity for detecting impairment using HVLT-R cut-off scores of 14.5-15.5. For each anatomic region, serial regression was performed to correlate volume receiving a given dose ($V_{D(Gy)}$) with memory impairment.

RESULTS

Hippocampal $V_{53.4Gy}$ - $V_{60.9Gy}$ significantly predicted post-RT memory impairment ($p<0.05$). Within this range, the hippocampal V_{55Gy} was the most significant predictor ($p=0.004$). Hippocampal V_{55Gy} of 0%, 25%, and 50% were associated with post-RT impairment rates of 14.9% (95% CI: 7.2% - 28.7%), 45.9% (95% CI: 24.7% - 68.6%) and 80.6% (95% CI: 39.2% - 96.4%), respectively. Dose received by the fusiform gyrus was a significant predictor of impairment, with the most significant relationship at $V_{46.5Gy}$ ($p=0.003$). No statistically significant relationship was observed for the amygdala or parahippocampus.

CONCLUSIONS

Injury to the hippocampus plays a fundamental role in CRCI. This analysis provides dosimetric guidelines to limit cognitive decline after cranial RT. The hippocampal V_{55Gy} is a significant predictor for impairment, and limiting dose below 55Gy may minimize treatment related neuro-cognitive toxicity.

REFERENCES

1. Li J, Bentzen SM, Renschler M, Mehta MP. Regression after whole-brain radiation therapy for brain metastases correlates with survival and improved neurocognitive function. J Clin Oncol. 2007;25(10):1260-1266. doi:10.1200/JCO.2006.09.2536.
2. Rapp SR, Case LD, Peiffer A, et al. Donepezil for Irradiated Brain Tumor Survivors: A Phase III Randomized Placebo-Controlled Clinical Trial. *J Clin Oncol*. 2015;33(15):1653-1659. doi:10.1200/JCO.2014.58.4508.

ASSESSING THE RELATIVE IMPACT PERFORMANCE OF HOCKEY HELMETS

Bethany Rowson[1], Abigail M. Tyson[1], Bryan R. Cobb[1], Steven Rowson[1], Stefan M. Duma[1]
1. Virginia Tech, Department of Biomedical Engineering and Mechanics
Corresponding Author: Bethany Rowson, Email: browson@vt.edu

INTRODUCTION

Ice hockey is a fast-paced sport with a high rate of concussion [1]. Concerns about the potential long-term effects associated with repeated head injuries emphasize the need to mitigate concussions in sports [2]. Although the reduction in concussion risk may vary greatly between different hockey helmets, there were previously no objective resources available to consumers to enable informed decisions. The purpose of this study was to develop and implement a methodology for evaluating the risk of concussion in different hockey helmets.

METHODOLOGY

The Hockey STAR (Summation of Tests for the Analysis of Risk) evaluation system was developed to determine the relative impact performance of different helmet models. A total of 12 impact conditions (4 locations and 3 speeds) were used to evaluate each helmet, with each condition weighted by how often players were exposed to similar impacts on the ice. Concussion risk was calculated for each laboratory impact condition as a function of peak resultant linear and rotational accelerations [3]. Exposure and injury risk for each condition were used in the Hockey STAR equation (Equation 1) to summarize a large number of tests in a single metric that can be compared across helmet models. Higher Hockey STAR values indicate a greater risk of concussion.

$$Hockey\ STAR = \sum_{L=1}^{4}\sum_{\theta=1}^{3} E(L,\theta) * R(a,\alpha) \qquad (1)$$

A total of 1,776 pendulum impact tests were performed to evaluate 37 hockey helmet models. Distributions of concussion risk and Hockey STAR values for all helmet samples were quantified to convey the range of performance in currently available helmets.

RESULTS

Concussion risk varied drastically by helmet type and impact speed (Figure 1). The large variations in concussion risk between helmet models were reflected by a wide range of Hockey STAR values. The median STAR value was 6.12, with an interquartile range of 5.08 to 8.23. The distribution of STAR values was best fit by a log-normal probability density function.

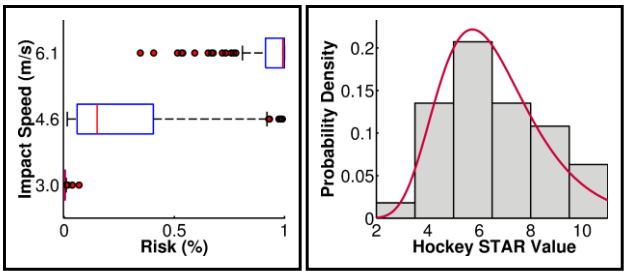

Figure 1: Distributions of concussion risk by impact speed (Left) and Hockey STAR values (Right).

CONCLUSIONS

This work presents a novel methodology for comparing impact performance of hockey helmets, and was used to demonstrate the large differences that exist between helmet models in their ability to reduce concussion risk. The Hockey STAR methodology provides a scientific framework for manufacturers to optimize hockey helmet design for injury risk reduction, while providing consumers with a meaningful metric to assess the relative performance of hockey helmets.

REFERENCES

[1] Hootman, J Athl Train, 2007. 42(2): p. 311-9.
[2] McKee, Brain, 2013. 136(Pt 1): p. 43-64.
[3] Rowson, Ann Biomed Eng, 2013. 41(5): p. 873-82.

FABRICATION OF A VASCULARIZED RENAL CONSTRUCT USING VASCULAR CORROSION CASTING

Jennifer Huling[1], In Kap Ko[1], Anthony Atala[1], and James Yoo[1]
1. Wake Forest School of Medicine, Wake Forest Institute for Regenerative Medicine
Corresponding Author: Jennifer Huling, Email: jhuling@wakehealth.edu

INTRODUCTION

Vascularization is one of the most pressing technical challenges facing tissue engineering of 3D organs. Implanted 3D tissue constructs need to be vascularized, allowing for oxygen and nutrient delivery, in order to survive and mature into functional tissue. Biofabrication techniques have been utilized for pre-vascularization, but limitations exist with respect to the size and complexity of the resulting vessels. We developed a simple and novel fabrication method to create biomimetic microvascular scaffolds for pre-vascularization of engineered tissue constructs.

METHODOLOGY

Vascular corrosion casts were prepared from healthy rat kidneys by perfusion with polycaprolactone (PCL) solution. After the PCL solidified within the renal vasculature, the renal tissue was degraded, leaving a complete PCL corrosion cast. The corrosion cast was then coated with type 1 collagen. Acetone was used to remove the PCL from within the collagen coating, leaving a hollow collagen microvascular scaffold. The fabricated scaffolds were evaluated for vascular preservation with scanning electron microscopy (SEM) and perfusion testing. Also, feasibility of endothelialization was tested with MS1 endothelial cell seeding.

RESULTS

PCL is a novel vascular corrosion casting material, and was able to produce a complete vascular corrosion cast with preservation of the kidney-specific structures (glomerular capillaries). The vascular corrosion cast served as a template for creation of the collagen microvascular scaffold with the same branching architecture as the native vessels (Fig 1A). Perfusion showed that the vascular scaffold retained hollow, connected structures. MS1 cells seeded on the scaffolds formed an endothelial layer with appropriate morphology covering the whole scaffold (Fig 1b-d). To show feasibility as a method of pre-vascularization, these scaffolds were incorporated into a collagen gel-based construct.

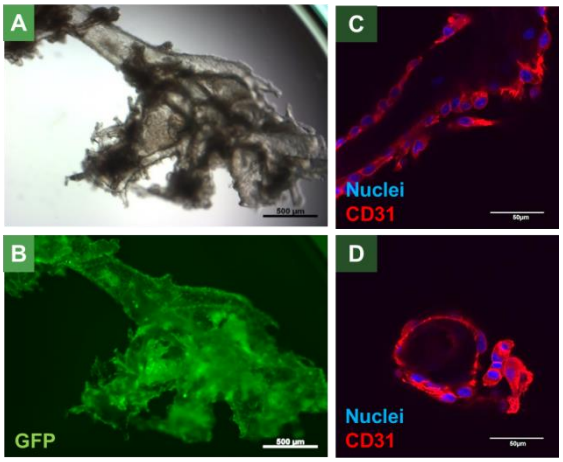

Figure 1: GFP expressing MS1 cells were uniformly seeded on the entire scaffold (a-b). The cells formed a continuous endothelial layer as seen in the confocal images (C-D).

CONCLUSIONS

We have demonstrated the proof of concept for using a vascular corrosion cast as a template for vascular scaffold creation. The collagen vascular scaffolds maintained a network of connected, hollow vessels inside a hydrogel construct. Future work will evaluate the scaffold's ability to promote viability of renal cells and renal structure formation.

REFERENCES

1. Joraku A, Stern KA, Atala A, Yoo JJ. In vitro generation of three-dimensional renal structures. Methods. 2009

Oral, PhD
Auditorium, 4:00

15th Annual Graduate Student Research Symposium

Poster Presentations

MECHANICAL RESPONSE OF THE TRACHEAL SYSTEM TO HEMOLYMPH PRESSURE IN THE BEETLE ZOPHOBAS MORIO

Khaled Adjerid [1], Hodjat Pendar[1], and Jake Socha[1]
1. Virginia Tech (Biomedical Engineering And Mechanics)
Corresponding Author: Khaled Adjerid, Email: adjerid@vt.edu

INTRODUCTION

Insects possess a complex network of tracheal tubes throughout the body used for transport of gases to and from the tissues. In some species, parts of the network are rhythmically compressed, facilitating active ventilation in the insect. Previous work suggests that hemolymph pressure pulses may induce tube collapse, but it is not understood how tracheae respond mechanically to a pressure difference across the wall. In the live animal they observed a collapse pressure range of between 0.56 and 3.56 kPa (1). Tracheal tubes vary in diameter, wall thickness, cross-sectional shape, and taenidial density, which should influence patterns of collapse (1). A simple thin walled-cylinder model predicts that the larger tubes should collapse at lower pressures than the smaller tubes (2).

METHODOLOGY

To study how tracheae respond to hemolymph pressure, we artificially induced pressure rises in the thorax of 7 intact, sacrificed beetles (*Zophobas morio)* by manually compressing the abdomen, creating hemolymph pressures of similar magnitude to those observed in live animals (>2 kPa). Simultaneously, we captured synchrotron X-ray video to monitor tracheal tube diameter in several locations in the body, and measured internal pressure using a Fabry-Pirot pressure sensor (Samba Preclin) inserted into the thorax.

RESULTS

We found that pressure produces collapse patterns that are similar to those found in the live animals. Our analyses found that, as predicted, large tracheal tubes (diameter d>150 μm) begin to collapse at an average pressure of 0.33±0.06 kPa, whereas small tubes (diameter d<150 μm) required nearly twice that pressure (060.59±0.12kPa). The mean pressure at which all tubes began to collapses was 0.48±0.08 kPa . Additionally, the mean pressure at which the tubes fully collapsed was measured at 1.67±0.12 kPa, while that of the live animal is 1.3±0.7 kPa (1).

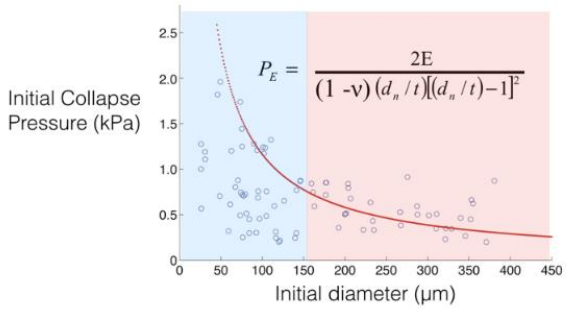

Figure 1: Data of diameter of tracheal tubes vs pressure of initial collapse. Prediction from TWC model equation overlaid in red.

CONCLUSIONS

These results demonstrate that tubes collapse at values that are physiologically relevant. Although the data do not fit the model well, the smaller tubes require collapse pressures that are higher than those of the larger diameter tubes, a general trend predicted by the model.

ACKNOWLEDGMENTS

- Advanced Photon Source at Argonne National Lab
- NSF EFRI (0938047)
- Research Assistants Ngozi Nwoke and Alex Mclean

REFERENCES

1) Pendar, H. The mechanical linkage of abdominal movements and the respiratory system in beetles." Diss.Virginia Polytechnic Institute and State U, 2014. Print.
2) Clinedinst, W. O. A rational expression for the critical collapsing pressure of pipe under external pressure. *Drilling and Production Practice*. American Petroleum Institute, 1939.

EVALUATION OF THORACIC AND LOWER EXTREMITY RESPONSES OF THE HYBRID III AND THOR ATDS UNDER MULTIPLE RESTRAINT CONDITIONS IN FULL SCALE FRONTAL SLED TESTS

Devon Albert[1], Stephanie M. Beeman[1], and Andrew R. Kemper[1]
1. Virginia Tech—Wake Forest University, Center for Injury Biomechanics, BEAM
Corresponding Author: Devon Albert, Email: dla16@vt.edu

INTRODUCTION

To improve the biofidelity of anthropomorphic test devices (ATDs) used in frontal crash testing, the National Highway Traffic Safety Administration developed the Test device for Human Occupant Restraint (THOR-M). The THOR was designed to exhibit more a biofidelic loading response than the Hybrid III (HIII), the current frontal crash test standard. However, matched full scale tests evaluating the responses of the THOR and HIII to different safety restraints have not been performed. Knee bolster airbags (KBABs) may alter the loading responses of the lower extremity and thorax, two of the most frequently injured body regions in frontal motor vehicle crashes. Therefore, the purpose of this research was to evaluate the thoracic and lower extremity responses of the THOR and HIII ATDs under different safety restraint conditions during full scale frontal sled tests.

METHODOLOGY

Full scale frontal sled tests were performed with the THOR-M and HIII for three safety restraint conditions: knee bolster (KB) and no steering wheel airbag (SWAB), KB and SWAB, and KBAB and SWAB. Two tests were performed per condition per ATD. A Toyota Camry three-point seatbelt (with a pretensioner and 4 kN load limiter) was used for each test. The KBs and KBABs were simulated using 65 psi and 19 psi rigid polyurethane foam surrogates, respectively. ATD positions, including KB/KBAB to knee offsets, were matched for consistency. Since each ATD has different internal chest deflection sensors, the ATDs were instrumented with two chest bands (CBs) on the upper and lower thorax to obtain comparable measures of chest deflection. ATD femur forces and moments and CB deflections were sampled at 20 kHz and filtered according to SAE J211.

RESULTS

The HIII and THOR exhibited different thoracic loading trends across the different restraint conditions. Little difference was observed between conditions for the THOR. However, the HIII experienced the largest CB deflections for the KB/no SWAB condition and the smallest deflections for the KBAB/SWAB condition. The lower CB deflection was greater for the THOR than the HIII across all conditions. The THOR also experienced greater upper CB deflections than the HIII for the KBAB/SWAB condition. The HIII only showed greater CB deflection than the THOR for the KB/no SWAB at upper sternum. All other locations and conditions were comparable between ATDs.

The HIII and THOR femurs showed similar trends across restraint conditions, but experienced different peak loads. For both the HIII and THOR, axial femur forces were greatest for the KB/no SWAB condition and least for the KBAB/SWAB condition. The HIII femur experienced a similar bending moment regardless of condition while the THOR experienced similar bending moments for the KB conditions, but a greater moment for the KBAB/SWAB condition. When comparing the THOR to the HIII across all conditions, the THOR had greater axial femur forces, but lower bending moments.

CONCLUSIONS

The HIII and THOR had different thoracic and lower extremity loading responses. The THOR thorax was less sensitive to changes in restraint condition. For all restraint conditions, femur forces and moments differed between the ATDs. Future research will include performing matched PMHS tests to assess ATD biofidelity.

ACKNOWLEDGMENTS

The authors would like to thank Toyota Motor Corporation for sponsoring this research.

Poster,B
Atrium, 11:45

A MIXED EFFECTS MODELING APPROACH TO STUDY THE IMPACT OF PESTICIDES ON FARMWORKERS' BRAIN NETWORKS USING R-FMRI DATA

Mohsen Bahrami[1], Paul J. Laurienti[1], Thomas A. Arcury[2], Sean L. Simpson[3]
1. Wake Forest School of Medicine (Department of Radiology)
2. Wake Forest School of Medicine (Department of Family and Community Medicine)
3. Wake Forest School of Medicine (Department of Biostatistical Sciences)
Corresponding Author: Mohsen Bahrami, Email: mbahrami@wakehealth.edu

INTRODUCTION

Network analysis of the brain has emerged as a powerful method over the last decade to study brain function and its abnormalities. Resting state functional magnetic resonance imaging (R-fMRI) technique measures spontaneous fluctuations of the brain when a subject is not performing an explicit task. Using R-fMRI signals of different brain regions, the functional brain network can be created via computing correlations between these signals. We can study the impact of neurological disorders on the overall network structure of the brain through R-fMRI networks. In this study we use R-fMRI data to study the impact of pesticides on farmworkers' brain networks using a two-part mixed-effects modelling approach (Simpson et al., 2015). We investigate the impact of pesticides on the probability and strength of interregional connections as well as on topological structure.

METHODOLOGY

The adjacency matrix for each participant's network was constructed by computing correlations between all pairs of the 116 regions of the brain according to the AAL template. These matrices served as the outcome variables in our approach. Model covariates included: 1) network features such as clustering coefficient and global efficiency, 2) covariate of interest (pesticide exposure group), 3) physiological parameters such as blood cotinine and cholinesterase, 4) confounders such as age and distance between regions, and 5) interactions between pesticide grouping and network features. The random effects and error term capture within and between network variability.

RESULTS

Table1 shows the estimates of some covariates, along with their standard errors, and their p-values in modeling the strength of connections. Each parameter represents the nodal pairs metrics. $\beta_{S,0}$: intercept, $\beta_{S,C}$: clustering coefficient, $\beta_{S,L}$: leverage centrality, $\beta_{S,d}$: distance, $\beta_{S,COI}$: Covariate of interest (Pesticide exposure group), $\beta_{S,Age}$: Confounder (age), $\beta_{S,COI\times C}$: interaction of COI with clustering coefficient, $\beta_{S,COI\times L}$: interaction of COI with leverage centrality.

Table 1: Summary of Abrasion Test Results

Parameter	Estimate	SE	P-value
$\beta_{S,0}$	0.3489	0.0102	<0.0001
$\beta_{S,C}$	0.1461	0.0046	<0.0001
$\beta_{S,L}$	0.0625	0.0060	<0.0001
$\beta_{S,d}$	-0.1563	0.0026	<0.0001
$\beta_{S,COI}$	0.0146	0.0094	0.1222
$\beta_{S,Age}$	-0.0067	0.0045	0.1384
$\beta_{S,COI\times C}$	-0.0097	0.0084	0.2453
$\beta_{S,COI\times L}$	-0.0307	0.0103	**0.0030**

Results show the significant p-value of interaction of COI and leverage centrality indicating the difference between pesticide exposure group's nodal pairs leverage centralities with normal subjects.

CONCLUSIONS

Our approach allows comprehensively studying the brain network differences between those exposed and unexposed to pesticides

References

Simpson, S.L., Laurienti, P.J. 2015 A two-part mixed-effects modeling framework for analyzing whole-brain network data. NeuroImage. 113, 310-319.

Virginia Tech
Wake Forest University
School of Biomedical Engineering and Sciences
15th Annual Graduate Student Research Symposium, May 11, 2016

ASTROCYTE REACTIVITY FOLLOWING BLAST EXPOSURE INVOLVES ABERRANT HISTONE ACETYLATION

Zachary S. Bailey[1], Michael B. Grinter[1], and Pamela J. VandeVord[1,2]
1. Virginia Tech, Biomedical Engineering and Mechanics
2. Salem Veterans Affairs Medical Center
Corresponding Author: Zachary Bailey: zbailey2@vt.edu

INTRODUCTION

Traumatic brain injury has been deemed the signature injury of current wartime efforts [1]. While several causes for TBI exist, blast wave exposure proved to be the most common cause [1]. Clinical manifestations of blast induced neurotrauma (BINT) include a diverse array of cognitive and behavioral symptoms driven by persistent inflammation at the cellular level. Epigenetics, including modifications to DNA and histone proteins, serve as important mediators of gene expression and cellular function which could underlie inflammation. Histone acetylation is one of the most prevalent modifications which causes chromatin reorganization and can lead to altered gene expression patterns. This study aimed to elucidate changes to histone acetylation occurring following injury and the roles these changes may have in the progression of the BINT pathology.

METHODOLOGY

Animals were subjected to blast overpressure within an Advanced Blast Simulator, as described previously [2]. Sprague Dawley rats were exposed to a blast wave with peak overpressure of 10 psi or 17 psi. Sham animals were anesthetized with no injury. Memory impairments were measured using the Novel Object Recognition (NOR) test at two and seven days following injury. Tissues were collected at seven days for western blot and immunohistochemistry analysis. NOR differences were compared using a repeated measures ANOVA. Western blot and immunohistochemistry comparisons were made using a one-way ANOVA. P-values below 0.05 were considered statistically significant.

RESULTS

Sham animals showed in-tact memory at both time points and showed slight memory improvement. The novel object preference for the 10 and 17 psi groups decreased dramatically between time points. This is indicative the onset of memory impairment following injury.

Glial Fibrillary Acidic Protein (GFAP), a known marker of activated astrocytes, was elevated in the prefrontal cortex (PFC) following blast exposure at both 10 and 17 psi. No changes were observed for Ionized Calcium-Binding Adapter molecule 1 (IBA-1), a marker for microglia. Western blot analysis of histone protein extract, showed no changes in the level of any total histone proteins within the PFC. However, aberrant histone acetylation levels were observed for both injury groups. Acetylation levels of histone H2b, H3, and H4 were decreased in both the 10 and 17 psi groups. Colocalization immunofluorescence was used in order to further investigate any potential correlation between decreased histone acetylation and astrocyte activation. These experiments focused on the anterior cingulate cortex (ACC) within the PFC which plays a role in memory formation [3]. We observed decreased H3 acetylation in astrocytes exposed to 17 psi blast but not in the 10 psi group.

CONCLUSIONS

We have observed decreased histone acetylation within the PFC and within astrocytes in the ACC. The altered histone acetylation patterns correlated with declining recognition memory. Such changes to the epigenome may play an important role in progression of the injury and provide novel therapeutic targets.

ACKNOWLEDGMENTS

This project was supported by the Department of Veterans Affairs RRD contract #RX001104-01.

REFERENCES

1. Elder GA, Cristian A. *The Mount Sinai journal of medicine, New York* 76(2),(2009).
2. Bailey ZS, Grinter MB, De La Torre Campos D, Vandevord PJ. *Neuroscience letters* 604(2015).
3. Lenartowicz A, Mcintosh AR. *Journal of cognitive neuroscience* 17(7),(2005).

Poster,B
Atrium, 11:45

DEVELOPMENT AND VALIDATION OF A FINITE ELEMENT MODEL OF THE WIAMAN LOWER EXTREMITY

Wade A. Baker[1], Costin Untaroiu[1], and Mostafiz Chowhurdy[2]
1. Virginia Tech, BEAM
2. Army Research Laboratory
Corresponding Author: Wade A. Baker, Email: wadeb6@vt.edu

INTRODUCTION

Occupants of military vehicles are likely to be subjected to an underbody explosion resulting from anti-vehicular land mines and improvised explosive devices. During the recent war in Iraq, 26% of all reported combat injuries impacted the lower extremity [1]. Therefore, there is an urgent need to introduce a series of new safety systems and regulations to mitigate lower limb injuries in theatre.

For years the automotive industry has successfully used human anthropomorphic testing devices (ATDs) to quantify the occupant injury risk over a wide range of impact scenarios. However, it has been proven that these ATDs are inadequate when it comes to accurately measuring the response of the human to blast loading. Therefore, a new dummy, called WIAMan (Warrior Injury Assessment Manikin) is under development, led by efforts from the United States Army Research Laboratory (USARL).

METHODOLOGY

A finite element model (FE) model of the lower leg was developed in LS-DYNA software (LSTC) (Fig. 1). Material models in LS-DYNA were assigned based on high and low strain-rate tests to model the viscoelastic behavior of the soft tissue.

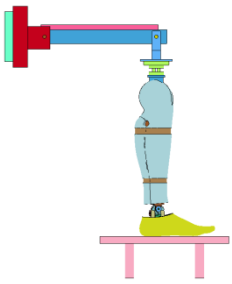

Figure. 1. FE Model of the WIAMan-LX in test rig

The WIAMan FE model was simulated under identical conditions as the experiments done on the physical dummy. Comparisons between the outputs from the simulation and the test data were used to validate the unbooted WIAMan-LX model.

RESULTS

The lower leg FE model shows a good correlation relative to dummy test data (Fig. 2). Average CORA score across all measured signals (knee, tibia, calcaneus, foot) was 0.862.

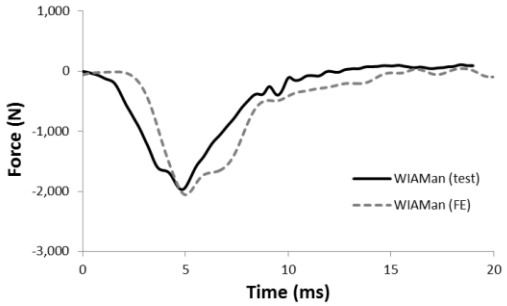

Figure. 2. Comparison of FE to experiment at knee load cell

CONCLUSIONS

The results of FE simulations with the entire WIAMan-LX correlate well to the physical dummy tests. The validated model could be used to improve the design of current dummy.

ACKNOWLEDGMENTS

The author would like to thank ARL for their support.

REFERENCES

[1] A. Ramasamy *et al.*, "In-vehicle extremity injuries from improvised explosive devices: current and future foci," *Philos Trans R Soc Lond B Biol Sci*, vol. 366, pp. 160-70, Jan 27 2011.

SYNERGISTIC REGULATION OF BREAST CANCER VIABILITY BY 3D CULTURE, HYPOXIA, AND BACTERIAL QUORUM-SENSING SIGNALS

Brittany N. Balhouse[1], Scott S. Verbridge[1]
1. Virginia Tech University, Biomedical Engineering and Mechanics
Corresponding Author: Brittany N. Balhouse, Email: bnbalhou@vt.edu

INTRODUCTION

Hypoxia and cell-stroma interactions in the tumor microenvironment (TME) are known to induce resistance to chemotherapy drugs [1, 2]. OdDHL (a bacterial quorum-sensing signal) selectively affects breast cancer cell lines by modulating STAT3 [3]. Because OdDHL is likely present in the TME due to innate bacteria in the breast tissue [4], we sought to understand cell response to OdDHL in the presence of TME stimuli. We hypothesized that the response to OdDHL would be modulated by hypoxia-induced and cell-adhesion mediated resistance. This study underscores the need for physiological disease models for investigating drug response and the need for investigation of bacterial secreted proteins in the TME.

METHODOLOGY

MDA-MB-231 (breast cancer) or MCF-10A (breast epithelial) cells were cultured in either hypoxia (1% O_2) or normoxia (in 2D) or seeded within a collagen hydrogel. The cells were then treated with 25–400 μM of OdDHL. After two days, an alamarBlue® assay was completed to quantify relative differences in viability; increased percent reduction implies increased viability. Significance was determined by ANOVA and Tukey tests.

RESULTS

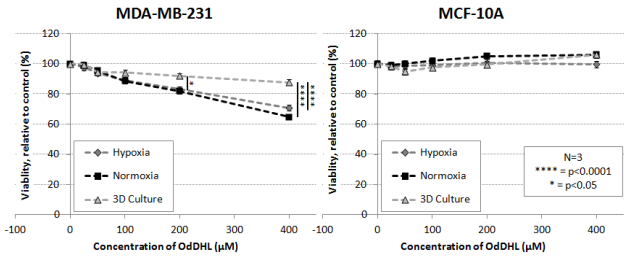

Figure 1: Relative viability with OdDHL

There were significant differences in the cell viability response to OdDHL treatment between the three culture conditions for the breast cancer cells, but not for the breast epithelial cells (Fig. 1). Importantly, there was a significant decrease in breast cancer cell viability at the 400 μM level as compared to the control in all culture conditions (Fig. 2).

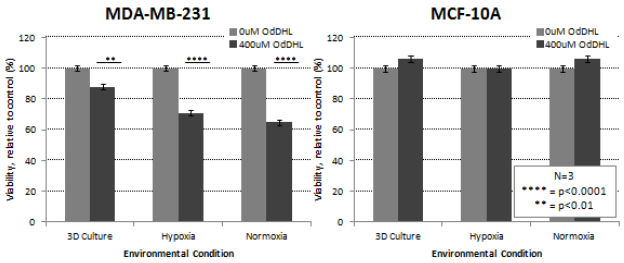

Figure 2: Relative viability with 400 μM OdDHL

CONCLUSIONS

There is a significant reduction in the effect of the OdDHL with TME stimuli. However, because OdDHL had a significant effect in all culture conditions, it merits further investigation of the role of bacterial secreted proteins in the TME.

ACKNOWLEDGMENTS

This work was supported primarily by the Institute for Critical Technology and Applied Science (ICTAS).

REFERENCES

[1]. Sullivan, R. et al. Mol Can Ther 2008. 7(7):1961-73. [2]. Trédan, O. et al. JNCI 2007. 99(19):1441-54. [3]. Li, L. et al. Oncogene 2004. 23(28):4894-902. [4]. Urbaniak, C. et al. Appl Environ Microbiol, 2014. 80(10): 3007-14.

Poster,B
Atrium, 11:45

DIFFERENCES IN THE ABILITY OF BICYCLE HELMETS TO REDUCE RISK OF HEAD INJURY

Megan L. Bland[1] and Steven Rowson[1]
1. Virginia Tech, Biomedical Engineering and Mechanics
Corresponding Author: Megan L. Bland, Email: mbland27@vt.edu

INTRODUCTION

The U.S. Consumer Product Safety Commission (CPSC) reports that cycling accounts for most sports-related head injuries.[1] Bicycle helmets are required by a CPSC standard to prevent accelerations greater than 300 g (skull fracture level[2]) in impact tests. Concussive impacts (100 g[3]) are not tested, which cyclist accident studies show are common.[4] Additionally, common impacts are to the helmet front or side, often at the rim (below the CPSC test area)[4,5]. The standard also does not assess relative impact performance amongst certified helmets.

This study aimed to differentiate abilities of helmets to reduce concussion and skull fracture risks by testing at common impact conditions as well as by the standard.

METHODOLOGY

A twin-wire drop rig and flat anvil were used to replicate the standard. Ten helmets were chosen, with four samples per helmet tested under four conditions: two velocities (3.4 and 6.2 m/s) at two locations mirrored on the helmet (frontal at rim and temporal above test area). The 3.4 m/s and rim reflect common impact conditions,[4,5] while 6.2 m/s is from the standard. Order of test conditions was randomized between samples to avoid bias.

Average peak accelerations were determined per impact condition and helmet. Skull fracture/concussion risks were calculated using published risk curves,[2,3] and results were compared using ANOVA (Tukey's HSD post hoc).

RESULTS

Figure 1 shows risk values for each helmet and location. Concussion risk at the frontal location was minimal and consistent (2.7-17.7%) but varied considerably at the temporal location. Skull fracture risk reflected concussion risk trends at the temporal location, but was less uniform than concussion risk at the frontal location.

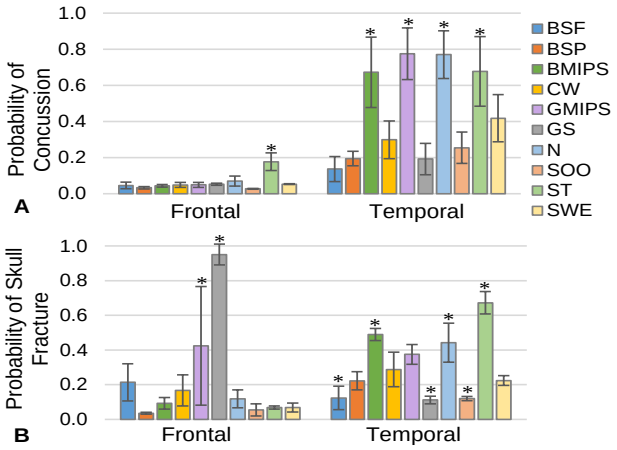

Figure 1: A) Concussion risk at 3.4 m/s and B) skull fracture risk at 6.2 m/s per helmet and location.

CONCLUSIONS

This study shows significant and clinically-relevant differences in the ability of helmets to reduce injury risks. Differences were more consistent at the temporal location. The high skull fracture risks at the frontal location may point to local weak points in helmet design. This location is below the CPSC test area, so it is not considered during the homologation process. Disseminating relative impact performance data such as these would enable consumers to make informed purchasing decisions.

ACKNOWLEDGMENTS

The authors would like to thank the Insurance Institute for Highway Safety for their funding and support.

REFERENCES

[1] AANS, "Sports-related Head Injury," 2014.
[2] Mertz et al., *Stapp Car Crash J*, 47:155-188, 2003.
[3] Rowson et al., *Ann of Biomed Eng*, 41:873-882, 2013.
[4] Williams, *Accid Anal and Prev*, 23:119-131, 1991.
[5] Bourdet, *J Sports Eng & Tech*, 226:282-289, 2012.

DRILL-SPECIFIC HEAD IMPACT EXPOSURE IN YOUTH FOOTBALL PRACTICE

Eamon T. Campolettano[1], Steven Rowson[1], and Stefan M. Duma[1]
1. Biomedical Engineering and Mechanics (Virginia Tech)
Corresponding Author: Steven Rowson Email: rowson@vt.edu

INTRODUCTION

Youth football players represent 70% of all players in the United States, and yet the level of research into head impact exposure within this population is limited [1]. Recently, researchers have begun to instrument youth football players with helmet-mounted accelerometer arrays to quantify head impact exposure and concussion tolerance [1, 2]. These studies looked at practices and games as a whole, with little analysis quantifying the causation of high magnitude impacts. The objective of this study was to analyze youth football practices and determine which drills produced high magnitude impacts.

METHODOLOGY

This study investigated head impact exposure and included 34 players (age 9.9 ± 0.6), who received helmets instrumented with accelerometer arrays associated with the HIT System. Players wore the instrumented helmets at each practice and game throughout the season.

Games and practices were filmed to facilitate video verification of head impacts. Video was used to identify the specific drill associated with each impact greater than 40 g. Each of these impacts was assigned one of nine classifications corresponding to the drill. Impact rates were computed on a per hour basis using Byar's method with 95% confidence intervals for these rates.

RESULTS

For the season, 408 impacts that exceeded the 40g threshold were verified, with 314 (77%) occurring in practice and the remaining 94 (23%) in games. Impacts per hour for each drill were computed with 95% confidence intervals (Fig. 1). The greatest number of impacts greater than 40 g occurred in tackling drills, even though they were only practiced half as often as organized offensive or defensive drills. Overall, game impact rate (14.24-21.57 impacts/hr) did not vary greatly from tackling practice drills (No Blocker: 14.74-21.85 impacts/hr, Blocker: 10.46-23.11 impacts/hr),

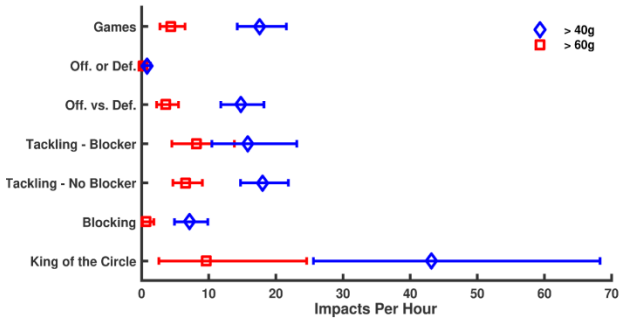

Figure 1: Drills resulting in a tackle were found to lead to higher impact rates.

CONCLUSIONS

Drills without tackling resulted in fewer than 10 impacts above 40 g per practice-hour while drills involving tackling exceeded this (Fig. 1). Drills involving tackling were associated with impact rates similar to game rates, excluding King of the Circle. Even though most practice drills did not result in impact rates greater than games, practices led to a greater number of high magnitude head impacts because there were more practices than games. Coaches and league organizers can use these data to structure practices in ways that mitigate high magnitude impacts. Further research into practice drill impact exposure at all levels of football is necessary to further player safety and characterize exposure on a larger scale.

ACKNOWLEDGMENTS

The authors are grateful to the NIH-NINDS under award number R01NS094410 for supporting this work.

REFERENCES

[1] Daniel, R. et al., Ann. Biomed. Eng., 40(4):976– 981, 2012.
[2] Cobb, B. et al., Ann. Biomed. Eng., 41(12): 2463-2473, 2013.

NOVEL IN VITRO MODEL FOR NEUROMUSCULAR REGENERATION

Jewel M. Cary[1], Nicholas Chartrain[2], Sydney Vaughan[3], Vanessa Brayman[3], Gregorio Valdez[3], and Abby R. Whittington[1, 2, 4]
1. Virginia Tech, School of Biomedical Engineering
2. Virginia Tech, Department of Materials Science and Engineering
3. Virginia Tech Carilion Research Institute
4. Virginia Tech, Department of Chemical Engineering
Corresponding Author: Abby R Whittington, awhit@vt.edu

INTRODUCTION

Peripheral nerve injury has resulted in nearly 5 million disability days per year[1]. The goal of this project was to design and create a dual compartment scaffold that allowed nerve cells to contact muscle cells, thus generating a suitable in vitro model for understanding neuromuscular growth. PEG was chosen as the main material due to its inertness. However, PEG is also known to be nonadhesive for proteins and cells. Previous studies in our laboratory and others have shown fibroblasts seeded on plain PEG are unable to spread while incorporation of RGD peptide with a spacer in PEG hydrogels promoted 70% cell spreading. It was hypothesized that including a minimal essential cell adhesion peptide like RGD within the scaffold would facilitate cell adhesion and cell to cell interaction[2].

METHODOLOGY

An acrylate-PEG-peptide reaction was performed to link the RGD peptide with an acrylate end[2]. The PEG acts as a spacer to allow cells better access to the RGD in the scaffold. The new acrylate-PEG-peptide material will then be polymerized with PEG diacrylate via micro-stereolithography to generate a 3D cell scaffold (Fig 1). Primary culture nerve cells will be placed in one section and muscle cells in the second section with pores connecting the two compartments to allow the cell processes to interact. Cell interaction will be imaged.

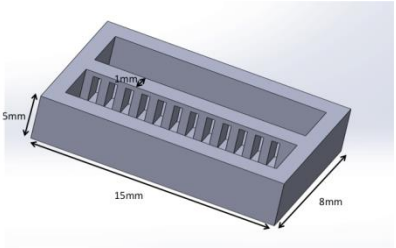

Fig 1: Cell Scaffold CAD Rendition

RESULTS

The primary amine assay reacts fluorescently with primary amines and therefore measures the amount of peptide that did not react and allows the reaction efficiency to be calculated (Table 1). For the acrylate-PEG-peptide reaction, 88% of the peptide reacted while for the acrylate-peptide reaction, 100% reacted.

Table 2: Summary of Primary Amine Assay Results

Sample	Spacer Group	Concentration (μg/mL)	Percentage Peptide Reacted
JC001	PEG	846.15	88%
JC007	None	769.23	100%

NMR was performed but was inconclusive. Initial testing on thin films of UV-cured acrylate-PEG alone with primary neurons also revealed little cellular attachment. Thus, supporting the need for RGD use.

CONCLUSIONS

From these preliminary results, we have determined the reaction efficiency with and without the PEG spacer group is overall greater than 85%. We will characterize the product without the spacer group using NMR and HPLC based on literature precedent before proceeding with 3D printing and cell culture.

ACKNOWLEDGMENTS

Authors would like to thank the Regenerative Medicine Interdisciplinary Graduate Education Program for funding (JMC).

REFERENCES

1. Kehoe S, Zhang XF, Boyd D. *Injury* 43.5 (2012): 553-72.
2. Hern DL, Hubbell JA. *J Biomed Mater Res* 39.2 (1998): 266-76.

IMPLICATIONS OF ULTRA-LOW LEVEL LPS ON VASCULAR DYNAMICS AND TUMOR PROGRESSION

Megan C. Cox[1], Liwu Li[2], and Scott S. Verbridge[1]
1. Virginia Tech-Wake Forest University, Department of Biomedical Engineering and Mechanics
2. Virginia Tech, Department of Biological Sciences
Corresponding Author: Megan C. Cox, Email: meganc4@vt.edu

INTRODUCTION

Lipopolysaccharide (LPS) is a well-known regulator of immune responses and in particular septic shock, where high levels of LPS in the bloodstream trigger the release of damaging pro-inflammatory cytokines. However, it remains challenging to analyze, among a large number of local and systemic factors, the effects of the low levels of circulating LPS that have been found in individuals with chronic inflammatory diseases. While the resulting programming of immune cells has been studied extensively, the impact of low levels of LPS on the vascular phenotypes that have been implicated in diseases such as cancer is not well understood. We hypothesize that the use of a 3D *in vitro* tissue mimic will allow us to model vascular dynamics and analyze the potential of a chronic inflammatory state to initiate the early stages of pathogenic angiogenesis.

METHODOLOGY

Human brain microvascular endothelial cells (HBMECs) were cultured on the surface of 3D collagen hydrogels in the presence of various doses of LPS, with and without vascular endothelial growth factor (VEGF). Advanced imaging and cell characterization assays were used to analyze the cellular phenotypic alterations, including cell proliferation, apoptosis, and metabolism, elicited by LPS exposure and will be presented at a later time.

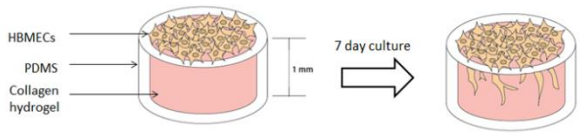

Figure 1: Schematic of *in vitro* angiogenesis assay

RESULTS

When the HBMECs were exposed to subclinical doses of LPS and VEGF, the sprouting density was significantly greater than all other treatment groups, including VEGF only treatment (Fig. 2A). The ultra-low dose LPS with VEGF and the VEGF only treatments were also the only samples that resulted in sprouts that invaded a significantly greater distance than the control (Fig. 2B).

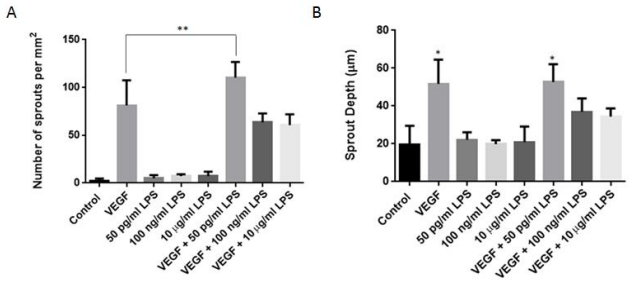

Figure 2: The (A) sprouting density and (B) average sprout depth of the HBMECs as quantified by confocal image analysis. **p < 0.01, *p < 0.05.

CONCLUSIONS

This work helps to elucidate the impact of low-level LPS, and the associated chronic inflammation, on vascular dynamics. The use of a 3D tissue-engineered angiogenesis platform allowed us to model a chronic inflammatory state and analyze early LPS-induced vascular phenotypic alterations. The potential of chronic levels of LPS to promote the development of a microenvironment with an amplified angiogenic potential is of particular significance in the pathogenesis and treatment of cancer, where understanding the implications of the presence of chronic inflammation could be essential to accurately assessing the disease state and administering the most effective therapies.

ACKNOWLEDGMENTS

This work was supported by ICTAS at Virginia Tech and by the NIBIB of the NIH under Award Number R21EB019123.

THE INFLUENCE OF POSTURE ON PMHS AND ATD LOWER EXTREMITY KINEMATIC RESPONSE IN THE UNDER-BODY BLAST ENVIRONMENT

[1]Danielle M. Cristino, [1]Warren N. Hardy
1.Virginia Polytechnic Institute and State University, School of Biomedical Engineering and Sciences
Corresponding Author: Danielle Cristino, Email: cristi07@vt.edu

INTRODUCTION

Improvised explosive devices (IEDs) expose military vehicles to high-rate vertical loading during under-body blast (UBB). In this test series, response and tolerance information was obtained from Post-Mortem Human Surrogates (PMHS) and Anatomical Test Devices (ATDs) that were exposed to UBB in a laboratory setting.

METHODOLOGY

The Accelerative Loading Fixture (ALF), which represents a simplified occupant compartment of a military vehicle, was subjected to vertical acceleration. Instrumented PMHS and ATDs were seated within the ALF with an inside knee angle of either 90 degrees (nominal) or 120 degrees (obtuse). See Figure 1, A.

Kinematics envelopes were produced from video tracking data obtained from markers placed on the lower extremities. Two trials were used for comparison between matched pairs of PMHS and ATD. In trial one, a single PMHS and a single ATD were positioned in the nominal posture. Trial two had identical conditions with the exception of posture, which was obtuse.

RESULTS

Differences in lower extremity kinematics were observed between the PMHS in the two postures. The PMHS with nominal posture experienced initial knee flexion and ankle dorsiflexion. The PMHS with obtuse posture experienced knee extension and ankle plantar flexion followed by dorsiflexion. The nominal posture resulted in greater rotation about the knees than the ankles, while the obtuse posture produced the opposite result. Differences between lower extremity kinematics were also observed between the ATD and PMHS for a given posture. In general, the PMHS lower extremity motion was quicker, more disorderly, and spanned a larger range of motion than that of the ATDs. In contrast to this trend, the ATD ankles in the nominal posture experienced more extreme dorsiflexion than the PMHS (Figure 1, B). When the feet decoupled from the floor, the PMHS experienced plantar flexion, while the ATD continued to dorsiflex.

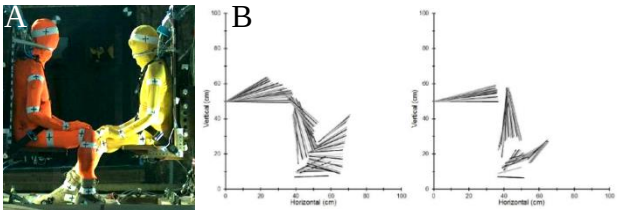

Figure 1: A) Nominal (left) and obtuse (right). **B)** Kinematics Envelopes. PMHS (left); ATD (right)

CONCLUSIONS

The PMHS comparison demonstrates that initial posture influences joint behavior and range of motion. The differences in ankle behavior between the ATD and PMHS suggests that the feet do not transfer forces in the same manner, which could affect forces measured in the tibia. It is unknown whether these differences will affect injury assessment of the lower extremity.

ACKNOWLEDGMENTS

This work was funded by the USAMRMC under Award Number W81XWH-10-2-0165.

REFERENCES

Danelson, K.A., Kemper, A.R., Mason, M.J., Tegtmeyer, M., Swiatkowski, S.A., Bolte, J.H. and Hardy, W.N. (2015) Comparison of ATD to PMHS Response in the Under-Body Blast Environment. Stapp Car Crash J 59: 445-520.

DEVELOPMENT AND FULL BODY VALIDATION OF THE GHBMC 5TH PERCENTILE FEMALE FINITE ELEMENT MODEL

Matthew L. Davis[1,2], Bharath Koya[1,2], Jeremy M. Schap[1,2], and F. Scott Gayzik[1,2]
1. Wake Forest School of Medicine
2. Virginia Tech- Wake Forest Center for Injury Biomechanics
Corresponding Author: F. Scott Gayzik, Email: sgayzik@wakehealth.edu

INTRODUCTION

As part of the Global Human Body Models Consortium (GHBMC) project, comprehensive image and anthropometrical data of the 5th percentile female (F05) were acquired for the specific purpose of finite element model development. The objective of this study is to apply these data to generate an F05 occupant model. Previously developed scaling techniques are used to compare the model to experimental corridors. Furthermore, we hypothesize that the most effective technique for validation will be morphing the F05 model to the M50 body habitus, rather than applying post-hoc scaling methods to the output data.

METHODOLOGY

CAD geometries obtained from a multi-modality medical imaging dataset were utilized for mesh development of the GHBMC F05 occupant (F05-O) model [1]. Structured hexahedral mesh was used in the majority of the body. In general, material definitions were applied based on the GHBMC M50-O v.4.3. The number of contacts in the model was minimized via node-to-node connections and element property assignment based on the underlying CAD data. Full body validation was performed through simulations of the F05 in nine impact conditions: six rigid body loading scenarios one frontal sled, one lateral sled, and one drop test. Results from full body simulations were scaled using a ratio of effective masses. To evaluate the hypothesis, the model was morphed to the average male habitus using the Kriging morphing technique and simulated [2]. Time history data was used for quantitative comparison of the outputs from both the *post-hoc* scaled data and morphed model data using ISO/TS 18571.

RESULTS

The F05-O model consists of 980 parts, 2.5 million elements, 1.3 million nodes, and has a mass of 51.2 kg. For rigid hub impacts, the model achieved a fair total ISO rating with an average score of 0.66. In general, the morphed model and *post-hoc* scaling had similar ISO ratings; however, the morphed model was 0.02 higher on average, supporting the hypothesis (Figure 1). On average, the morphed model predicted peak forces within 17%. The model was also found to predict a higher risk of hard tissue injury compared to the M50-O, reporting more or equal fractures in five of six evaluated rigid impacts reported in the literature. On average, the F05-O model predicted 6 fractures compared to 4.3 for the M50-O.

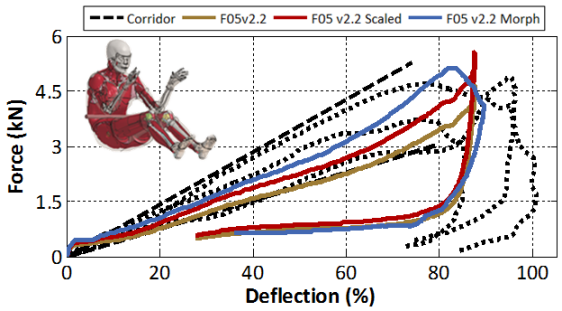

Figure 1: Exemplar F05 model response

CONCLUSIONS

The study addresses a need for an anatomically representative small female finite element model developed via a multi-modality dataset. Quantitative validation against a set of full body simulations indicates good to fair agreement with the data. Furthermore, we quantitatively demonstrate that full body morphing is potentially a more effective means of assessing biofidelity than post-hoc data scaling. The F05-O provides needed insight to the biomechanics of small female occupants as human body modeling is extended to address ever more challenging aspects of injury biomechanics.

REFERENCES

[1] Davis M., IRCOBI, 2014. [2] Beillas P., Stapp, 2015

QUANTITATIVE EVALUATION OF HEAD MOTION KINEMATICS BETWEEN HUMAN BODY MODELS OF VARYING COMPLEXITY

William B. Decker[1,2], Bharath Koya[1], Matthew L. Davis[1,2], F. Scott Gayzik[1,2]
1. Wake Forest University School of Medicine
2. Virginia Tech – Wake Forest University Center for Injury Biomechanics
Corresponding Author: F. Scott Gayzik, Email: sgayzik@wakehealth.edu

INTRODUCTION

Finite element human body models (HBMs) are used to investigate mechanisms and tolerance of the body to various injuries. However, the added complexity to achieve reasonable biofidelity in HBMs can lead to long compute times. To combat this, paired models of distinct levels of complexity have been introduced, with the concept that high biofidelity components of a detailed version can be incorporated into the more simplified model in a modular fashion. Studies have shown significant run time savings by using this method with high-cost deformable components only included in regions of interest (e.g. the brain). However, slight differences in kinematics can lead to differences in strain histories in deformable components between the detailed and simplified models augmented with detailed components, reducing the effectiveness of this approach.

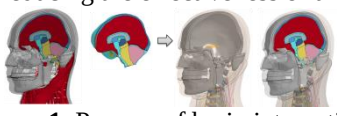

Figure 1. Process of brain integration.

METHODOLOGY

The purpose of this study is to run three matched pair simulations of rigid impacts using the high fidelity GHBMC M50-O (v. 4.4), the computationally efficient GHBMC M50-OS (v. 1.8), and the GHBMC M50-OS_MB (v 1.8), which includes the detailed brain (v. 1.8). A frontal impact (6.7 m/s chest impact), lateral impact (12 m/s plate impact) and one oblique impact (6.7 m/s to the ribs) were simulated. The run time was recorded and head and neck kinematics were output for each run. The comparison of model head kinematic output was done quantitatively through the use of ISO TS 18571.

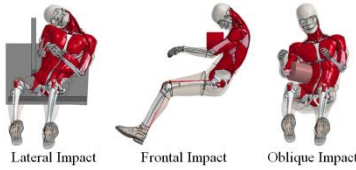

Figure 2. Three impact simulations.

RESULTS

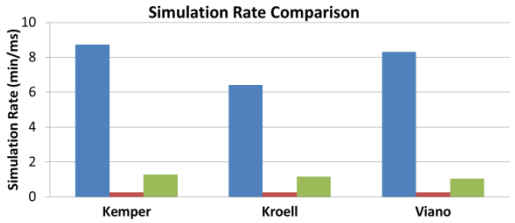

Figure 3. Computational time divided by the length of the simulation. M50-O (B), M50-OS (R), M50-OS_MB (G).

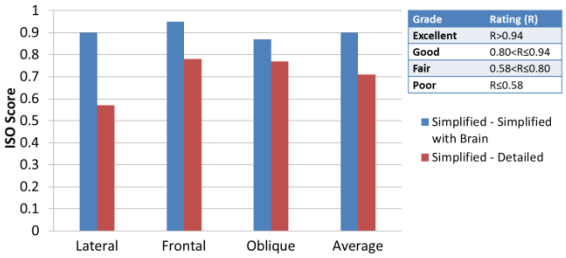

Figure 4. Matched pair comparison ISO scores.

CONCLUSIONS

The incorporation of the detailed brain into the simplified model had negligible effects on head kinematics. With improvements to axial and lateral rotations of the simplified model, the addition of the brain has the ability to yield brain data in the future, while retaining computational advantages of the simplified model.

ACKNOWLEDGMENTS

Funding was provided by the Global Human Body Models Consortium, LLC (GHBMC) which is supported by its member companies, participants and the National Highway Traffic Safety Administration (NHTSA).

REFERENCES

[1]GHBMC, "GHBMC M50 Users Manual ", ed, 2011.

BREAST RECONSTRUCTION: EVALUATION OF PATIENT SPECIFIC IMPLANT RESPONSES

Katherine E. Degen[1,2], Kurtis Moyer,MD[1,2,3], Robert G. Gourdie, PhD[1,2]
1. Virginia Tech, School of Biomedical Engineering
2. Virginia Tech Carilion Research Institute
3. Plastic Surgery, Carilion Clinic
Corresponding Author: Katherine Degen, Email: ked4p@vt.edu

INTRODUCTION

The single most common complication of breast reconstructive surgery is the formation of a dense scar capsule around the silicone implant called capsular contracture. Nearly all patients will experience this complication, though with different degrees of response, ranging from moderate scarring to major disfigurement and pain at the implant site. Presently, there is no way to predict the degree of contraction capsule formation that individual patients will suffer prospectively, nor is there clinical approach to preventing this complication.

METHODOLOGY

Dr. Kurtis Moyer MD, Chief of Plastic Surgery at Carilion, is providing patient samples of scar capsule and de-identified medical information under an active IRB. The standardization of collection is achieved by sampling scar capsule tissue, from around an implanted breast expander device placed by Dr. Moyer, at a precisely defined anatomical location and at a standardized time interval following implantation of the device. Tissue samples are prepared for histology, RNAseq, and patient fibroblast explants.

RESULTS

Ninety-one patients have been analyzed histologically. Image analysis methodologies have been designed to more rigorously quantify all histological variables. Significant differences between capsule grades were found in mean vessel size, as well as collagen maturity density and organization. To build on these findings Collagen subtypes (I, III, and VI) are being evaluated. In addition, fibroblasts appear to be more activated in higher grade capsules. Fibroblasts also distribute differently throughout the tissue, with fibroblast populations existing further from the implant interface in lower grade capsules.

Preliminary RNAseq analysis has been performed on 10 capsules. These results indicate that genes belonging to matrix metabolism, interferon gamma signaling, and immune signaling pathways were significantly enriched in the gene set. Some of these genes of interest include ADAMTS-2, MMPs 1 3 and 8, IL-6 and VEGF-D.

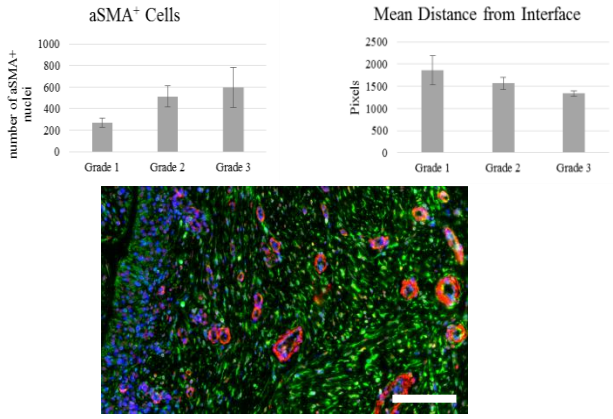

Figure 1: Fibroblasts are more activated and distributed closer to the implant interface in higher grade capsules. The implant interface, shown to the left, and bulk of the capsule tissue both contain a large number of vimentin+ fibroblasts (green). αSMA+ activated fibroblasts (red) are more prevalent in higher grade capsules. Hoescht nuclear stain (blue) Scale bar is 100μm.

CONCLUSIONS

Upon conclusion of this work a quantitative histological and proteomic profile will be developed to better classify capsule grades.

ACKNOWLEDGMENTS

Carilion Rap9 Grant 2013, 2014
VTCRI Medical Scholars Fellowship

Poster,B
Atrium, 11:45

Virginia Tech
Wake Forest University
School of Biomedical Engineering and Sciences
15th Annual Graduate Student Research Symposium, May 11, 2016

A 3D SUBMUCOSAL MICROENVIRONMENT FOR INVESTIGATION OF FIBER ALIGNMENT INDUCED EPITHELIAL-TO-MESENCHYMAL TRANSITION IN COLORECTAL CANCER CELLS

Mahesh Devarasetty[1], Aleksander Skardal[1], and Shay Soker[1]
1. Wake Forest Institute for Regenerative Medicine
Corresponding Author: Mahesh Devarasetty, Email: mdevaras@wakehealth.edu

INTRODUCTION

Recent investigation of colorectal cancer metastasis has identified the tumor microenvironment as a large proponent of metastasis. Factors such as tissue stiffness, fiber alignment and bundling, and cell-cell interactions have been targeted as affecting cancer cell phenotype, proliferation and drug susceptibility. To study these effects in vitro, this study aims to develop a micro-facsimile of colonic submucosal microstructure using cellularized type I collagen (Col I) hydrogels.

METHODOLOGY

Submucosal constructs are fabricated using rabbit colonic smooth muscle cells (RCSMCs) suspended in a Col I hydrogel. Tumor compartments are composed of HCT-116 colorectal carcinoma cells (ATCC) that are cultured using hanging drop methodology at 10,000 cells/spheroid. Once spheroids are formed, they are embedded into submucosal constructs during initial collagen deposition.

RESULTS

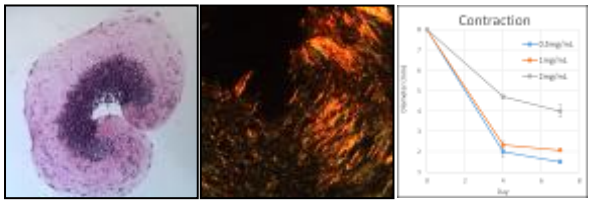

Figure 1: Submucosal Construct

Submucosal constructs were imaged after seven days in culture to assess the extent of remodeling performed by the RCSMCs. Our results are outlined in figure 1. Figure 1, left is H&E staining demonstrating the gross contraction and organization of the cells after culture. Smooth muscle cells aligned and elongated while contracting the collagen gel. Figure 1, middle shows the degree of collagen bundling with a picrosirius red stain: orange signal represents highly bundled collagen. Figure 1, right outlines construct contraction over 7 days and across a range of collagen concentrations.

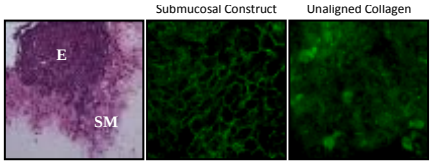

Figure 2: Tumor morphology and phenotype

Once the tumor compartment was integrated into the submucosal construct, we verified that the RCSMCs were interacting on a proximal level through H&E staining, figure 2, left. We then assessed tumor phenotype using immunohistochemistry against the WNT pathway marker B-Catenin. When B-Catenin is localized to the nucleus, it indicates a mesenchymal transformation. In figure 2, middle and right, the B-Catenin staining shows nuclear localization in unaligned collagen (mesenchymal pattern) and membranal localization within the submucosal construct (epithelial pattern).

CONCLUSIONS

Our results indicate that RCSMCs remodel the extracellular matrix into a "normal" or healthy environment that induces "normal" or epithelial expression from HCT-116 cells. Future directions include probing the biomolecular effects of fiber alignment as well as the integration of cancer-associated fibroblasts into the model to replicate the cellular content found in in vivo tumors.

ACKNOWLEDGMENTS

XCEL, Golfer's Against Cancer, and WFIRM

TUMOR ENGINEERING TO ELUCIDATE THE EFFECT OF MILD HYPERTHERMIA ON TRANSPORT OF SWNHS IN THE TUMOR MICROENVIRONMENT

Matthew R DeWitt1, and M. Nichole Rylander[2]
1. Virginia Tech-Wake Forest School of Biomedical Engineering
2. University of Texas at Austin – Mechanical Engineering)
Corresponding Author: Matthew DeWitt, Email: mttdwtt@vt.edu

INTRODUCTION

Therapeutic use of mild hyperthermia (41-43°C) has extensively been studied for enhancement of a wide range of chemotherapeutic drugs. While in vitro and in vivo studies have shown enhancement with mild hyperthermia, the practicality of simultaneous application of the two modalities in the tumor environment can be difficult to achieve, limiting the overall utility of the combination. Current studies to evaluate nanoparticle mediated thermal enhancement therapies are primarily executed in a traditional 2D cell culture system in which the particles are applied directly over seeded cells resulting in possibly exaggerated effects of synergy.

We have developed a novel perfusable tissue engineered model of the tumor microenvironment of collagen tissue containing human breast cancer cells and vessels with endothelial cells and we validated and characterized nanoparticle transport within and determined the effect of mild hyperthermia in the tissue level transport of SWNHs.

METHODOLOGY

The 3D culture system described in Figure 1B was utilized to study uptake by the MDA-MB-231 cells in a co-culture setup with a monolayer of TIME cells, elucidating the effect of mild hyperthermia on diffusion and uptake by the cells. The temperature was varied between 42°C and 37°C and a nanoparticle solution was administered in the endothelial media cavity for up to 6h. FACs was used to quantify uptake.

Figure 1: A) Depiction of setup B) Nanoparticles in central vessel

RESULTS

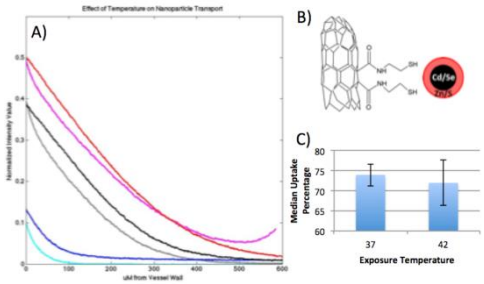

Figure 2: A) Radial intensity values of QD-SWNH fluorescence at 37 and 42°C at 30m, 3h, 6h. B) Depiction of SWNH-QD. C) FACS median uptake of MDA-MB-231 within matrix at 37 and 42°C.

Following characterization of the 3D microfluidic model, SWNH-QD (Figure 2B) were created and tested in the system under normothermia and mild hyperthermia (Figure 2A). Radial fluorescent intensity from the vessel wall is plotted. A significant change in fluorescent intensity can be seen for the approximately 100nm particles at the 3 h time point, highlighting the effect of mild hyperthermia on extravasation and diffusion within the matrix. FACs data additionally supports that more uptake of particles is seen at hyperthermia.

CONCLUSIONS

We have demonstrated that tumor engineering models can be utilized to study the transport of SWNHs within the tumor microenvironment. Two tissue engineered models, were developed and validated to understand the effect of hyperthermia on nanoparticle transport which is crucial when developing novel photothermal therapies.

ACKNOWLEDGMENTS

Funding: NSF Early CAREER Award and the NSF-GRFP

EFFECT OF EXCITATION BEAM ON DOSE EFFICIENCY FOR X-RAY FLUORESCENCE COMPUTED TOMOGRAPHY (XFCT)

Xu Dong[1], Guohua Cao[1]
1. School of Biomedical Engineering and Sciences, Virginia Tech
Corresponding Author: Xu Dong, Email: xu14@vt.edu

INTRODUCTION

X-ray fluorescence Computed tomography (XFCT) has been proposed as a molecular modality for specific element 3-D imaging of a subject. In this method, X-ray are used to produce characteristic X-ray signals through interaction with the high atomic number elements in the imaged object. And the element distribution information could be quantified by the internal characteristic x-ray signal.

The signal could be extracted from interfering background because the characteristic x-ray fluorescence has a certain energy for a specific element. This property guarantees the high concentration sensitivity of this XFCT imaging modality. However, the sensitivity of a XFCT system depends on many factors such as dose level and detection efficiency. To optimize XFCT system design, the relationship between excitation beam and concentration sensitivity need further to be investigated.

METHODOLOGY

Three groups of excitation beam were applied to a XFCT system for different concentration. A linear relationship can be obtained from the concentration information and collected fluorescence signal. We can define the minimal detectable concentration (MDC) under each excitation beam group by taking signal to noise ratio to be 4 as the standard for signal that is significant enough to be detected. The concentration sensitivity is characterized by the MDC for different excitation beam.

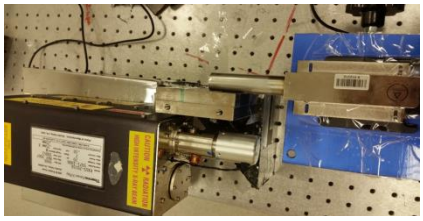

Figure 1: Photo of experimental system.

RESULTS

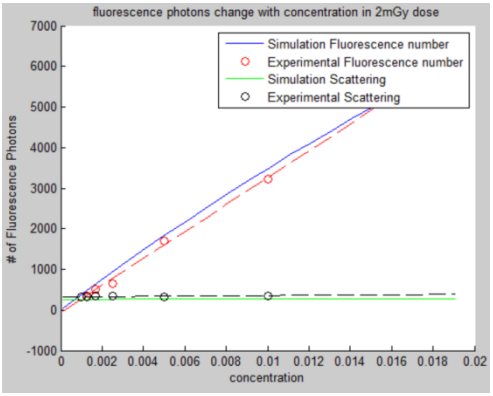

Figure 2: Comparison of experimental and simulated data.

Table 3: Summary of MDC over excitation beam

Group	Excitation beam	MDC(weight percentage)	MDC(mg/mL)
1	40KVp, 1.02mm Cu	0.0182%	0.182
2	40KVp, 5.20mm Al	0.0893%	0.893
3	40KVp, 2.08mm Al	0.135%	1.35

CONCLUSIONS

The concentration sensitivity change with different input excitation beam. From my experiment, 40KVp with 1.02mm Cu as filter excitation beam gives best concentration sensitivity.

ACKNOWLEDGMENTS

Thanks all the members in X-ray system lab.

REFERENCES

[1] Poludniowski, G.G., and Evans P.M. Medical physics 34.6 (2007): 2164-2174.

CONTACTLESS DIELECTROPHORESIS AS A METHOD OF SEPARATING HIGHLY SIMILAR MOUSE OVARIAN SURFACE EPITHELIAL CELLS AT DIFFERENT STAGES OF MALIGNANCY

Temple A. Douglas[1], Jaka Cemazar[1], Eva M. Schmelz[2], and Rafael V. Davalos[1]
1. School of Biomedical Engineering and Sciences, Virginia Tech – Wake Forest University
2. Human Nutrition, Foods and Exercise, Virginia Tech
Corresponding Author: Temple A. Douglas, Email: tadougla@vt.edu

INTRODUCTION

A common problem in the treatment of tumors is drug resistance and disease recurrence. When a tumor is treated, the majority of the cells treated die, leaving behind cancer stem cells, macromolecules and space for the tumor to repopulate. Those cells that remain are often resistant to the drug and can be more malignant, making further treatment of the tumor difficult and leading to treatment failure. We demonstrate a diagnostic modality that uses contactless dielectrophoresis (cDEP) to separate tumor cells based on their malignancy by detecting differences in their intrinsic bioelectrical properties[1].

METHODOLOGY

In cDEP, we flow the cells through a microfluidic chip and apply an electric force across the channel. As the cells flow through the chip, they encounter an array of posts. The gradient of the electric field increases in the area near the posts, causing the cells to experience a force attracting them to the posts and trapping them. The polarizability of the cells in the device determines the capacity of the cells to trap on posts. Cells of different malignancies often have different polarizabilities and exhibit different trapping behaviors in certain electric field frequency ranges, with malignant cells having a higher trapping probability[2]. We studied mouse ovarian surface epithelial (MOSE) cells with increasingly malignant potential by flowing them through the device and trapping them[3].

RESULTS

MOSE cells (highly malignant MOSE-L_{FFL} and intermediate malignancy MOSE-L cells) passed through the device while using different flow rates and applying different voltage and frequency combinations. Cell viability after flowing through the device was found to be high for most voltage/frequency combinations[4]. Cell separability was found to be enhanced at higher flow rates, possibly due to improved force balancing precision.

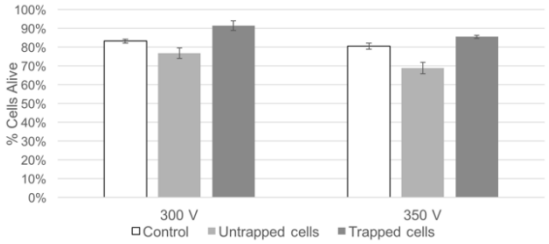

Figure 1: MOSE cell viability at different flow rates and voltage/frequency combinations.

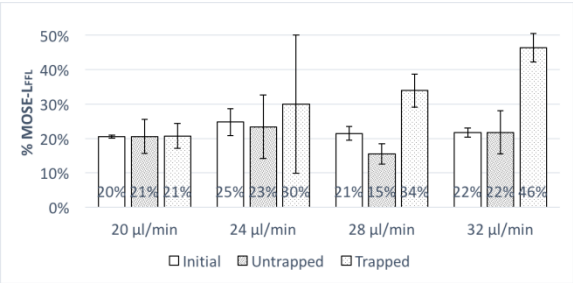

Figure 2: Separability of populations at different flow rates, 30kHz and 350Vrms. Percentage MOSE-L_{FFL} cells in a mixture of MOSE-L and MOSE-L_{FFL} cells.

CONCLUSIONS

Separability and Viability of the output cell population can be improved by optimizing flow rate, voltage and frequency applied to cells in cDEP.

ACKNOWLEDGMENTS

This work was supported by NIH 5R21 CA173092-01, and NSF IGERT DGE-0966125 MultiSTEPS.

REFERENCES

[1]Pethig, R., Advanced Drug Delivery Reviews, 2013.
[2]Salmanzadeh, A. Biomicrofluidics, 2013.
[3]Roberts, P.C. et al, Neoplasia, 2005.
[4]Čemažar, J. et al., Biomicrofluidics, 2015.

Poster,B
Atrium, 11:45

EFFECT OF POST MORTEM DEGRADATION ON THE MATERIAL PROPERTIES OF BOVINE LIVER PARENCHYMA

Kristin M. Dunford[1], Andrew R. Kemper[1]
1. Affiliation (Virginia Tech-Wake Forest University, Center for Injury Biomechanics)
Corresponding Author: Kristin M. Dunford, Email: kmcamp@vt.edu

INTRODUCTION

The liver is one of the most frequently injured organs in motor vehicle collisions. Anthropomorphic test devices (ATDs) are used to assess the risk of sustaining an injury from motor vehicle collisions using internal sensors and corresponding risk functions. However, none of the current ATDs are equipped to represent solid abdominal organs in the human abdomen and therefore cannot be used to predict abdominal organ injury. Consequently, finite element models (FEMs) are becoming an integral tool for assessing abdominal organ injury risk. Although FEMs predict injury based on the calculation of physical variables related to injury such as stress and strain, they must be validated based on biomechanical data in order to accurately assess injury risk.

Previous studies have conducted tension and compression coupon tests on human and bovine liver parenchyma to determine the material properties of the liver. However, the effect of post mortem degradation on the material properties has not been fully characterized. Specifically, the effects of degradation occurring within 24 hours of death have not been taken into account while evaluating test data used to quantify tissue level-tolerance values for FEMs.

The purpose of this study is to quantify the effects of post mortem degradation on the material properties of bovine liver parenchyma using tension and compression testing at various time points after death, specifically focusing on less than 24 hours to 48 hours post mortem.

METHODOLOGY

Uniaxial tension and compression testing will be conducted on the parenchyma of 5 bovine livers. Bovine livers will be used since their material properties are similar to human livers (Kemper et al. 2010). Livers will be acquired from local slaughterhouses immediately after death. A custom blade assembly and slicing jig will be used to obtain samples of constant thickness of the liver (Kemper et al. 2010). A custom stamp will be used to obtain "dog-bone" shaped parenchyma specimens for tension testing while a circular cutting tool will be used to obtain cylindrical coupons for compression testing. Three samples of each liver will be tested at three different time points. The three time points are: as soon as possible after death (~4 hours), 24 hours after death, and 48 hours after death.

Each coupon will be tested once to failure at the same loading rate. Load and acceleration data will be obtained from each of the specimens. Optical markers will be placed on the coupons and tracked using high speed video to measure the local displacement during testing. Failure stress and strain will be calculated for each coupon. Data will be analyzed using a paired t-test to determine if there are significant changes in the material properties in respect to post mortem time.

RESULTS

There are currently no results. Local slaughterhouses are being contacted to determine the feasibility of obtaining bovine livers immediately following death. A detailed protocol is being developed for tension and compression testing.

CONCLUSIONS

It has not yet been determined how liver parenchyma material properties change over time after death. This study will provide novel data that can be used to understand the effects of post mortem degradation on the material properties of liver parenchyma.

REFERENCES

Kemper, A. R., Santago, A. C., Stitzel, J. D., Sparks, J. L., & Duma, S. M. (2010). Biomechanical Response of Human Liver in Tensile Loading. *Annals of Advances in Automotive Medicine*, *54*, 15-26.

Virginia Tech
Wake Forest University
School of Biomedical Engineering and Sciences
15th Annual Graduate Student Research Symposium, May 11, 2016

ASSESSMENT OF LATERALIZATION DURING MOTOR ACTIVITY USING FNIRS

Amnah M. Eltahir[1], Stephen M. LaConte[1,2]
1. Virginia Tech/Wake Forest School of Biomedical Engineering and Sciences
2. Virginia Tech Carilion Research Institute
Corresponding Author: Amnah Eltahir, Email: amnah@vt.edu

INTRODUCTION

Functional near infrared spectroscopy (fNIRS) is an emergent non-invasive neuroimaging modality. Similar to functional magnetic resonance imaging (fMRI), fNIRS measures hemodynamic correlates (oxy- and deoxy-hemoglobin concentrations) of neurological activity. On application of fNIRS is to study motor cortex during manual tasks [1]. A common metric evaluated during motor tasks is laterality, or the extent of activation in ipsilateral and contralateral hemispheres to the active limb. Our goal is to develop fNIRS as a tool for assessing laterality in motor tasks.

METHODOLOGY

Healthy adult subjects were recruited for fNIRS scanning sessions. Eight emitter and eight detector optodes (20 channels) were placed over the motor cortex. A block paradigm of alternating 30 s resting and 30 s active hand motion (for a total of six blocks) was recorded. The participants were prompted to perform either a bimanual task, or a unimanual task (left/right hand).

RESULTS

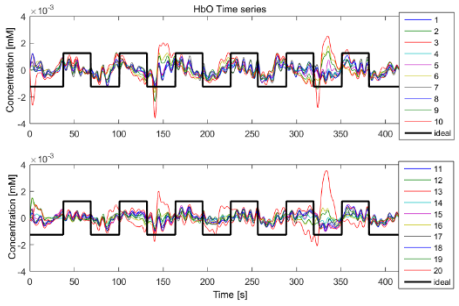

Figure 1: HbO time series for left (top) and right (bottom) time series during right manual task.

Correlation values were taken with the "ideal" task paradigm (Fig.1 1 in black). The mean correlation coefficients in each hemisphere (C_L and C_R) were used to calculate the left laterality index ($LI = C_L - C_R$).

Table 4: Subject averages of laterality indices for each concentration for bimanual task, right hand task and left hand task.

Concentration	Bimanual	Right	Left
HbO	-0.098	-0.080	0.040
Hb	0.113	0.123	-0.037
HbT	-0.085	-0.024	-0.053

Preliminary data are reported in Table 1 for average LI's during each task. The change in LI's for HbO are opposite to what we expect, while the change in LI's for Hb seems more consistent with our assumption.

CONCLUSIONS

The differences in LI across the tasks are not significant and are inconsistent with the literature [1]. Adjustments to our current approach may yield more consistent results.

ACKNOWLEDGMENTS

We would like to acknowledge Allison McKinnon, Chris Anzalone, and Aaron Whitehurst for providing assistance during data collection.

REFERENCES

[1] Leff, Daniel Richard, et al. "Assessment of the cerebral cortex during motor task behaviours in adults: a systematic review of functional near infrared spectroscopy (fNIRS) studies." NeuroImage 54, no. 4 (2011): 2922-2936.

Poster,B
Atrium, 11:45

NON-ENZYMATIC SELECTIVE OSMOTIC SHOCK FOR THE ISOLATION OF HUMAN ISLETS

Kevin Enck[1,2], JP McQuilling[1,2], Sivanandane Sittadjody[1], and Emmanuel C Opara[1,2]
1. Wake Forest University, School of Biomedical Engineering
2. Wake Forest Institute for Regenerative Medicine
Corresponding Author: Kevin Enck, Email: kenck@wakehealth.edu

INTRODUCTION

Islet transplantation (IT) is a promising technique that is an alternative to whole pancreas transplantation for the treatment of Type 1 diabetes. IT requires the isolation of the islets from the pancreas, and enzymatic digestion of pancreatic tissue is the current gold standard procedure for islet isolation. However, enzyme-based islet isolation is a non-selective tissue digestion that is prone to islet cell damage with consequence to long-term islet transplant function. Therefore, developing a non-enzymatic method may greatly improve the quality of isolated islets. Atwater et al. have recently developed a selective osmotic shock (SOS)-based procedure that utilizes Glut-2 proteins that are only present on pancreatic islet β cells to protect these cells while destroying other cell types in the pig pancreas. However, this procedure has not yet been applied to human islet isolation.

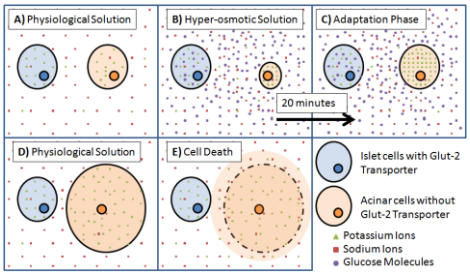

Figure 2: Step-by-step process of SOS as cells adapt to rapidly changing concentrations.

METHOD

Cadaveric pancreas obtained with consent is finely minced and placed in a high glucose concentration RPMI 1640 media (300-600 mM) for 20 minutes. This enables islet β cells to take up glucose via Glut-2 transporters in the membrane in order to equilibrate the osmotic strength of the external solution, whereas acinar cells rapidly lose water and take up potassium in order to adapt to the extracellular osmotic strength, and this causes these cells to shrink. When the incubation media is aspirated and fresh media containing no glucose is added to the tissue, a process repeated 3 times, β cells quickly release the glucose while acinar cells take up water to recover cell volume causing swelling and cell lysis. (Figure 1)

RESULTS

Using this physiological technique we have isolated human islets with intact pericapsular membrane, the extracellular matrix (ECM) that surrounds the islets (Figure 2 A-C) in contrast to the amorphous islets isolated with enzymatic digestion (Figure 2 D-F). Figure 2 presents comparisons between the SOS and enzymatic isolation methods based on Dithizone staining (DTZ) and live/dead staining (CFDA/PI). We have also assessed the function of these islets using the dynamic perifusion procedure with low and high glucose levels to assess insulin secretion, and found that SOS-isolated islets were more responsive to high glucose stimulation than Collagenase isolated islets.

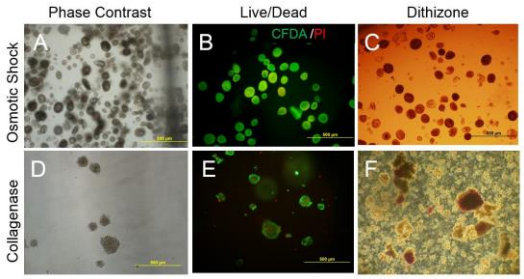

Figure 3: SOS and enzymatic isolation comparison

CONCLUSION

Using a less harsh and more physiological isolation technique for pancreatic islets can help solve some of the current issues with islet transplantation. By preserving the ECM and pericapsular membrane, islets will be surrounded by their natural environment which will allow them to function properly and survive longer *in vivo* once transplanted.

REFERENCE

Atwater, I, et al. *Trans Proceed* 42, 1 (Jan 2010): 381–86.

HEART RATE AND EXTRACELLULAR SODIUM AND POTASSIUM MODULATION OF GAP JUNCTION MEDIATED CONDUCTION IN GUINEA PIGS

Michael W. Entz II[1], Sharon A. Geoge[1], Michael Zeitz[2], James W. Smyth[2], and Steven Poelzing[1]
1. Virginia Polytechnic Institute and State University, School of Biomedical Engineering and Sciences
2. Virginia Tech Carillion Research Institute
Corresponding Author: Michael W. Entz II, Email: mentz2@vt.edu

INTRODUCTION

Recent studies suggest that ephaptic coupling (EpC) modulates cardiac conduction velocity dependence on gap junctions (CV-GJ relationship)[1,2]. However, it remains unknown whether GJ can modulate the CV-EpC relationship. EpC is modulated by extracellular sodium and potassium, sodium channel availability, and perinxal width as shown in experimental work as well as mathematical models[3].

HYPOTHESIS

Pharmacological uncoupling of GJs will unmask conduction sensitivity to $[K^+]_o$ and $[Na^+]_o$ in guinea pigs with narrow perinexi.

METHODOLOGY

$[K^+]_o$ and $[Na^+]_o$ were varied in Langendorff perfused guinea pig ventricles (Solution A: $[K^+]_o$=4.56 and $[Na^+]_o$=153.3 mM. Solution B: $[K^+]_o$=6.95 and $[Na^+]_o$=145.5 mM). Gap junctions were inhibited with carbenoxolone (CBX) (15 and 30 µM). Epicardial CV was quantified by optical mapping. Perinexal width was measured with transmission electron microscopy. Total and phosphorylated Cx43 were evaluated by western blotting.

RESULTS

Solution composition did not alter CV under control conditions or with 15µM CBX. Decreasing the basic cycle length (BCL) of pacing from 300 to 160ms uniformly decreased CV in both solutions. At 30 µM CBX, a change in solution did not alter CV either longitudinally or transversely at BCL=300ms. However, decreasing BCL to 160ms caused CV to decrease in hearts perfused with Solution B in the transverse direction. Solution composition did not alter perinexal width, nor did it change total or phosphorylate Serine 368 Cx43 expression. These data suggest that the solution dependent CV changes were independent of altered perinexal width or GJ coupling. Solution B shortened action potential duration more than A in reference to control, while decreasing BCL decreased APD similarly.

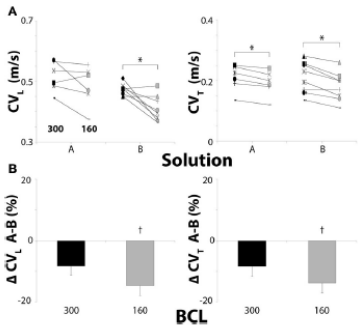

Figure 4 – Conduction measurements for hearts perfused with 30µM CBX. Black: Solution A, Gray: Solution B. (A) Effects of BCL on CVL and CVT. (B) Relative percent changes in CVL and CVT between Solutions A and B show CV slowing at 160ms BCL. *, p<0.025 between pacing rates. †, p<0.025 between Solutions A and B.

CONCLUSIONS

Increased heart rate and GJ uncoupling can unmask small CV differences caused by changing [K+]o and [Na+]o. These data suggest that modulating extracellular ionic composition may be a novel anti-arrhythmic target in diseases with abnormal GJ coupling, particularly when heart rate cannot be controlled.

ACKNOWLEDGMENTS

This work was supported in part by grants from the National Institutes of Health (R01 HL102298-01A1 to SP) and Virginia Tech Carilion Research Institute Medical Research Scholars Award to ME.

REFERENCES

1. Veeraraghavan et al. Pflugers Arch, 2015
2. George et al. Pflugers Arch, 2015.
3. Lin et al. IEEE Trans Biomed Eng, 2013.

Poster,B
Atrium, 11:45

BONY AND SOFT TISSUE INJURY RISK SENSITIVITY OF DRIVERS IN SIMULATED MOTOR VEHICLE CRASHES

James P. Gaewsky[1,2], Ashley A. Weaver[1,2], Bharath Koya[1,2], and Joel D. Stitzel[1,2]
1. Wake Forest School of Medicine
2. VT-WFU Biomedical Engineering
Corresponding Author: James P. Gaewsky, Email: jgaewsky@wakehealth.edu

INTRODUCTION

Human body finite element models are a valuable tool to computationally evaluate injury metrics and risks in MVCs and ultimately reduce the risk of injury and mortality. The risk of injury is influenced by crash severity, vehicle restraint systems, occupant demographics and health, as well as the occupant's pre-crash posture and position within the occupant compartment. This study used dynamic finite element models to quantify the sensitivity of several specific injury risks due to variance in driver and vehicle restraint positions immediately prior to real world crash events. Injury mechanisms evaluated included vertebral burst fractures, bimalleolar fracture, and pulmonary contusion (PC).

METHODOLOGY

Two real world MVCs from the Crash Injury Research and Engineering Network (CIREN) were computationally reconstructed. For each case, a simplified vehicle model was tuned to respond in frontal MVC tests similar to the real world vehicle model. Kinematic boundary conditions from the CIREN database were applied to the vehicle model and the Total HUman Model for Safety (THUMS) to reconstruct the crash environment and occupant (Figure 1).

Figure 5: THUMS in MVC environment.

A design of experiments variation study was performed to vary the longitudinal seat track position, seat back angle, seatbelt D-ring anchor height, and steering column angular and linear positions across 120 simulations per case reconstruction. Dynamic forces, stresses and strains were evaluated in bony structures and soft tissue organs and subsequently injury threshold values and risks were estimated. Several injury metrics were assessed, including injuries to the spine, lower leg, and chest. To assess PC, maximum principal strain in each lung element was evaluated. The volume fraction exceeding 0.34 maximum principal strain at any time during the simulation indicated the probable fraction of contused lung tissue [2].

RESULTS

Reconstruction of a real world MVC occupant who sustained multiple vertebral body burst fractures, revealed the anteroinferior portion of the lumbar vertebrae exhibited strain concentrations of up to 2.5%. This strain level (>1.5%) can lead to vertebra fracture, especially in older MVC occupants such as the 80 year old in this CIREN case [3]. The most likely pre-crash occupant position for this MVC reconstruction resulted in 46.7% of the left lung being contused, compared to 49% measured in the case occupant's CT.

CONCLUSIONS

Fractures and organ injuries in two MVC finite element reconstructions were predicted across 120 pre-crash occupant position simulations. Injury risk increased in more reclined and rearward seated occupants.

REFERENCES

[1] Wilcox RK, *European Spine J. 2004* [2] Gayzik FS, *Stapp Car Crash J.* 2007. [3] Kayanja MM, *The Spine J.* 2004.

Virginia Tech
Wake Forest University
School of Biomedical Engineering and Sciences
15th Annual Graduate Student Research Symposium, May 11, 2016

A FLUID DYNAMICS SIMULATION AS A MODEL TO EXPLORE THE INSECT RESPIRATORY SYSTEM

Joel Garrett[1], Rafael Davalos[1], John J. Socha[1]
1. Virginia Tech, Biomedical Engineering and Sciences
Corresponding Author: Joel Garrett, Email: jfg@vt.edu

INTRODUCTION

Like all animals, insects depend on the internal movement of fluids to sustain life. Despite their small size, they use complex internal networks to effectively transport gases, liquids, and food through their bodies. Previously, we studied respiratory patterns in the Madagascar hissing cockroach (*G. portentosa*) to understand how abdominal pumping, tracheal compression, and spiracular valving are coordinated to produce airflows. We found that the animal is able to control abdominal pumping and spiraclular valving to compensate for changes in oxygen availability, such as increasing the abdominal pump frequency when exposed to hypoxic conditions.

Here we explore how these behaviors are used to regulate internal flows using a computational fluid dynamics simulation. In addition to improving our knowledge about how the insect respiratory system coordinates flow production and valving, we aim to apply the results of this study toward developing low-power, small-footprint microfluidic systems for new engineered devices.

METHODOLOGY

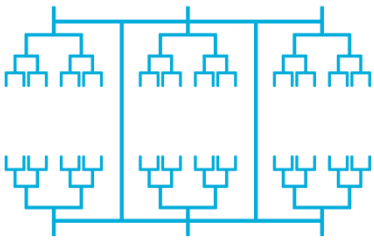

Figure 1: Schematic of the fluid dynamics system used in this study in its most basic form, featuring three channel generations, three sections corresponding to the insect body segments, six inlets and outlets, and fluid uptake at the tips of the innermost channels.

We used COMSOL computational fluid dynamics software to investigate the following parameters: branching schema, channel width, channel length ratio, pump frequency, pump amplitude, valve phasing, valve duty cycle, and valve locations. We varied these parameters through a range of values determined from previous animal experiments, as well as purely theoretical states not seen *in vivo*, and identified their effects on flow rate, flow direction, and shear stress on channel walls.

RESULTS

Numerical analysis of the simulation outputs revealed several basic relationships between the system parameters and its performance. The maximum shear stress on the walls generally correlates with the factor relating daughter channel width to the parents'. However, the average stress in on the walls was a function of simple geometry; narrower channels overall experienced greater hydraulic resistance and thus more shear stress on the channel walls.

We also found that controlling hydraulic resistance alone could not create unidirectional flow from the anterior channels to the posterior channels, but by incorporating a valve with a phase offset from the pump, we could reliably drive unidirectional flow. Modulating the duty cycle of the valve gives further control over flow direction.

CONCLUSIONS

Our preliminary results suggest a variety of parameter combinations that can be combined to optimize for flow rate, shear stress on the channel walls, interior mixing, or interior diffusion. This model provides a new platform for studying a generalized insect respiratory system incorporating the core components of abdominal compression, tracheal tube collapse, and spiracular valving.

In addition to improving our knowledge about how the insect respiratory system coordinates flow production and valving, we aim to apply the results of this study toward developing low-power, small-footprint microfluidic systems for new engineered devices.

Funded by NSF EFRI 0938047

Poster,B
Atrium, 11:45

ULTRA-FAST MULTI-SOURCE INTERIOR TOMOGRAPHY

Hao Gong[1], Guohua Cao[1]
1. School of Biomedical Engineering and Sciences, Virginia Tech
Corresponding Author: Guohua Cao, Email: ghcao@vt.edu

INTRODUCTION

Computed tomography (CT) has been widely utilized in the diagnosis, treatment, and scientific research of cardiovascular diseases (CVD). However, current cardiac CT technology is still limited by motion blurring, x-ray scatter artifact, and accumulative radiation dose. We recently proposed a conceptual multi-source interior CT architecture for cardiac imaging [1]. This system architecture utilizes stationary distributed carbon nanotube (CNT) x-ray source arrays and simultaneously operates multiple imaging chains for faster CT data acquisition, to improve the temporal resolution. It also integrates collimator based interior tomography to reduce the radiation dose. Despite the improved temporal resolution, the additional x-ray beams could induce non-negligible cross scattering that degrades image quality in terms of contrast-noise-ratio (CNR) and scatter-induced artifacts. The objective of this study is to evaluate and demonstrate the feasibility of this novel multi-source strategy.

METHODOLOGY

Our conceptual CNT source array based multi-source interior CT is illustrated in Figure 1. The construction of a prototype system can be very expensive and time-consuming. Therefore, a bench-top single-source imaging platform was set up to physically simulate this architecture. In addition, the dedicated scatter correction methods were developed to improve image quality.

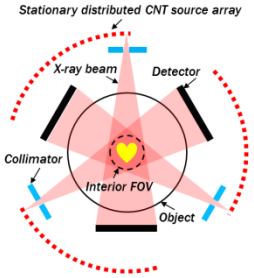

Figure 6: Schematics of multi-source interior CT

RESULTS

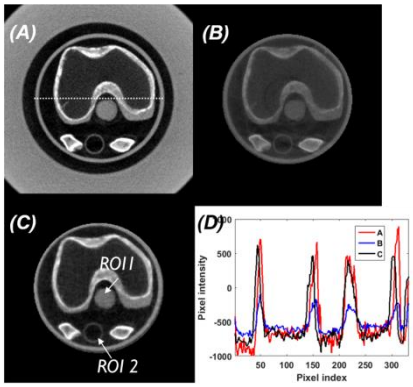

Figure 2: (A) The zoom-in reference image. (B) Interior ROI image w/o scatter correction. (C) Interior ROI image after scatter correction. (D) The line profiles (dash line).

Table 5: CNR and mean pixel value

Image type	CNR	Mean HU of ROI 1
Reference	10.32	0
w/o scatter correction	7.56	-350
w. scatter correction	10.27	42.6

CONCLUSIONS

Proper scatter correction methods can help promote the advantages of multi-source interior CT.

ACKNOWLEDGMENTS

This work was partially supported by Dr. Cao's seed grant from ICTAS and NSF career award.

REFERENCES

G. Cao, et al, "A Stationary-Sources and Rotating-Detectors Computed Tomography Architecture for Higher Temporal Resolution and Lower Radiation Dose", IEEE access, 2014

THE EFFECTS OF PRE-CRASH VELOCITY REDUCTION ON RIB FRACTURE IN A COMPUTATIONAL HUMAN BODY MODEL

Berkan Guleyupoglu[1,2], Jeremy Schap[1,2], Matt Davis[1,2], F. Scott Gayzik[1,2]
1. Wake Forest University School of Medicine
2. Virginia Tech – Wake Forest Center for Injury Biomechanics
Corresponding Author: F. Scott Gayzik, Email: sgayzik@wakehealth.edu

INTRODUCTION

Road traffic injuries are a leading contributor of DALYs (Disability Adjusted Life Years) lost [1]. Active safety systems will play a large role in reducing the likelihood of occupant injury but, such systems need to function in concert with passive safety countermeasures, underscoring the need for a method to evaluate the two simultaneously. Human body models are ideally situated to serve as this link. The purpose of this study is to evaluate the effects of pre-crash braking systems on the ribcage of a human body model.

METHODOLOGY

The Global Human Body Models Consortium (GHBMC) 50th percentile male occupant was gravity settled into a generic interior equipped with a three point belt and airbag. Fifteen simulations were conducted, including four scenarios at three severity levels: median (17 kph), severe (34 kph) and NCAP (56.4 kph) plus three additional at the highest severity. The four scenarios were: No pre-crash system (baseline), forward collision warning (FCW), FCW with pre-braking assist (FCW+PBA) and FCW and PBA with autonomous pre-crash braking (FCW+PBA+PB). The final three cases, had a constant ΔV (37.5 kph) with 1.0 g's, 1.2 g's and 1.4 g's of pre-crash braking. The generic pulse were taken from the literature and the pulse was scaled to match target ΔV values. Fracture prediction is achieved through a piecewise linear plasticity material model with element deletion for cortical rib fractures above 0.018 strain.

RESULTS

Reduction of ΔV's during the pre-crash phase reduced rib fractures across all severities. Median cases had the lowest amount of fractures predicted. Fracture predictions in the severe cases were more evenly spread between rib 7 and 8 but more focused on rib 8 in NCAP cases. In NCAP cases, while the addition of pre-crash braking systems does reduce the overall fracture prediction, higher intensity braking caused an increase in fracture predictions (Figure 7). Most of the cases had greater interaction with the seatbelt prior to a load limit being reached however this was not true for the NCAP FCW+PBA+PB case.

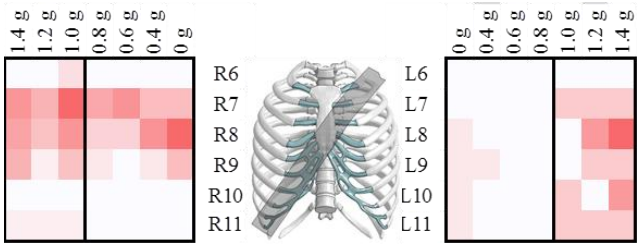

Figure 7 Predicted rib fractures in NCAP cases. Heat map separated by rib number and G's of pre-crash braking. Solid black line in delineates change to the higher intensity pre-crash braking cases.

CONCLUSIONS

The reduction of ΔV's through forward collision avoidance systems (FCAS) can reduce local injury to the occupant. With a higher ΔV, greater benefit was observed with the addition of FCAS.

ACKNOWLEDGMENTS

Work was supported by the Global Human Body Models Consortium, LLC and NHSTA under GHBMC Project No.: WFU-005. All simulations were run on the DEAC cluster at Wake Forest University, with support provided by Drs. David Chin and Timothy Miller.

REFERENCES

[1] Peden M. World Health Organization; 2014

DETERMINING *IN VITRO* MIGRATION AND DIFFERENTIATION OF NEURAL PROGENITOR CELLS IN BIOENGINEERED SMOOTH MUSCLE TISSUE ENGINEERED CONSTRUCTS

Matthew D. Hartman[1,2], Elie Zakhem[2], and Khalil N. Bitar[1,2]
1. VT-WFU School of Biomedical Engineering and Sciences
2. Wake Forest Institute for Regenerative Medicine
Corresponding Author: Khalil Bitar, Email: kbitar@wakehealth.edu

INTRODUCTION

Neuro-degenerative diseases of the gut result in motility disorders. Tissue engineering provides an approach to restore innervation of smooth muscle tissues. Our lab has previously established a technique to engineer intrinsically innervated smooth muscle tissue constructs using a co-culturing system of smooth muscle cells and neural progenitor cells. These constructs have demonstrated *in vitro* functionality. Following *in vivo* implantation, retrieved constructs maintained their cellular morphology, phenotype and functionality. This study hopes to provide evidence of migration of tagged NPCs and their differentiation in a simple assay made of one innervated smooth muscle cell construct and two non-innervated constructs, to provide evidence of migration of NPCs and their differentiation.

METHODOLOGY

(1) Neural progenitor cells (NPCs) were isolated from rabbit small intestine.
(2) Smooth muscle cells (SMCs) were isolated from rabbit internal anal sphincters.
(3) NPCs were tagged with green fluorescent protein via lentiviral transduction and maintained in culture.
(4) Two types of constructs were engineered:
    i. SMC construct only
    ii. SMC construct innervated using tagged NPCs.
(5) The innervated SMC construct was placed between two SMC only constructs after 3 days of culture and remained in the assay for 11 days.
(6) Force generation was measured from physiological stimulation of SMC only constructs and innervated SMC constructs.
(7) Fluorescence microscopy of *in vitro* migration assay maintained during culture.
(8) Immunohistochemistry was performed on constructions after the assays and following physiology testing.

RESULTS

(1) Microscopic analysis confirmed tagged NPCs in culture.
(2) Force generation showed that the smooth muscle constructs engineered with tagged NPCs maintained their function, indicating that the tagged NPCs have the ability to differentiate into functional neurons.
(3) Microscopic analysis of the engineered constructs following the assay indicates the possibility of migration and differentiation of tagged NPCs.

CONCLUSIONS

This study provides preliminary evidence of the feasibility of tagging NPCs and their ability to maintain their differentiation and function after 3D co-culture with SMCs. Tracking the migration of tagged NPCs *in vitro* provides a basis for *in vivo* tracking of the cells following their transplantation into animals. This method provides a way to study and confirm the migration and differentiation of neural progenitor cells following their contact with SMC only constructs *in vitro*.

ACKNOWLEDGMENTS

This study was supported by Wake Forest Institutional Funds.

REFERENCES

Rego, S. L., Zakhem, E., Orlando, G., & Bitar, K. (2015). Bioengineered human pyloric sphincters using autologous smooth muscle and neural progenitor cells. Tissue Engineering Part A, doi:10.1089/ten.TEA.2015.0194

OVERPRESSURE EXPOSURE INDUCES ACUTE STRUCTURAL REACTIVITY IN GLIA

Nora Hlavac[1] and Pamela J. VandeVord[1,2]
1. Virginia Tech, Biomedical Engineering and Mechanics
2. Salem Veterans Affairs Medical Center
Corresponding Author: Nora Hlavac, Email: nhlavac@vt.edu

INTRODUCTION

Blast-induced neurotrauma is a growing concern in both military and civilian populations. Exposure to primary blast induces acute cellular changes in the brain as well as chronic deficits in memory and behavior.[1-2] However, the injury sequelae remain largely unknown. Glial cells, particularly astrocytes, become reactive in acute stages of injury. They are integral in both protective and disruptive processes after traumatic injury to the brain.[3] Definitive mechanistic links between glial cell response and the pathology of traumatic brain injury remain to be fully elucidated. This study aims to characterize glial reactivity to shock wave exposure through the use of *in vitro* models. We are interested in acute alterations in cellular structure as a result of mechanical perturbation and secondary injury mechanisms.

METHODOLOGY

Primary astrocytes were isolated from Sprague-Dawley rat pups. Dissociated cells were cultured in 6-well plates at $2x10^5$ cells/well and exposed to overpressure in a fluid-filled shock wave generator.[4] Sham groups were treated equivalently, with the exception of exposure to overpressure. Viability was assessed at 24 hours post-exposure by MTT assay. Structural injury was investigated through alterations in membrane and cytoskeletal protein expression. Protein samples were collected at 24, 48 and 72 hours post-exposure to measure levels of glial fibrillary acidic protein (GFAP), β-actin and vinculin using Western blot analysis.

RESULTS

Astrocytes were exposed to a peak overpressure of approximately 20 psi (Figure 1), previously identified as a mild injury threshold in animals.[5] At this overpressure, cells remained viable at 24 hours post-exposure with no significant changes from the sham.

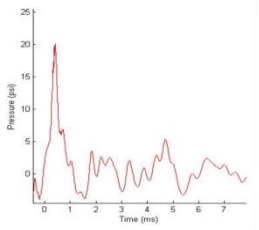

Figure 1: Representative shock wave produced by the shock wave generator.

Because both mechanical perturbation and secondary injury can induce cytoskeletal alterations, expression of β-actin and vinculin were assessed. Additionally, GFAP is an intermediate filament protein that is upregulated by reactive astrocytes. Glial reactivity was observed by 48 hours post-exposure as measured by structural protein alterations compared to sham. These results were in agreement with previous results from cellular models of primary blast exposure.

CONCLUSIONS

Overpressure insult induced transient structural changes in astrocytes. Additionally, the cells became reactive by the 48 hour time point. This work prompts further research into the molecular secondary injury mechanisms that drive these early alterations.

ACKNOWLEDGMENTS

We would like to thank Dr. Rzigalinski (VCOM) for providing cell preps.

REFERENCES

1. Cho, HJ, et al. 2013. Neurosci, 253(3): 9-20.
2. Sajja, VSSS, et al. 2015. *Sci Reports*, 5: 15075.
3. Sajja, VSSS, et al. 2016. *Front Integr Neurosci*, 10: 7.
4. Hlavac, N, et al. 2015. *Biomed Sci Inst*, 51: 439-445.
5. Hubbard, WB, et al. 2014. *Biomed Sci Inst*, 50: 92-99.

Poster,B
Atrium, 11:45

ELECTROPORATION AND MOLECULAR THERAPY FOR TARGETED CELLULAR ABLATION

Jill W. Ivey[1], Eduardo L. Latouche[1], Glenn J. Lesser[2], Waldemar Debinski[2], Rafael V. Davalos[1], Scott S. Verbridge[1]
1. Virginia Tech-Wake Forest University, Department of Biomedical Engineering and Mechanics
2. Wake Forest Baptist Medical Center, Comprehensive Cancer Center
Corresponding Author: Jill Ivey, Email: jivey@vt.edu

INTRODUCTION

Glioblastoma multiforme (GBM) is an extremely lethal brain cancer, with a grim prognosis. The nearly universal recurrence of GBM tumors is attributable to the failure of current therapies to selectively target malignant cells without destroying healthy brain tissue. We hypothesize that malignant GBM cells exhibit distinct physical characteristics that can provide targets for selective killing using irreversible electroporation (IRE). We have developed 3D tissue models, with tunable tissue microenvironment, to study cell responses to IRE and how these responses correlate to cell morphology.

METHODOLOGY

3D tissue mimics of type 1 collagen were created. Scaffolds were seeded with glioblastoma cells (U87, C6, DBTRG, U251) or healthy brain cells (NHA, D1TNC1, PC12). Cells were treated with ephrinA1 (eA1) to induce a morphology change. Cells were exposed to 1µs pulse high-frequency irreversible electroporation (HFIRE) pulses. Live/dead staining and finite element modeling was used to determine lethal thresholds. The morphology of the cells are analyzed by confocal microscopy.

RESULTS

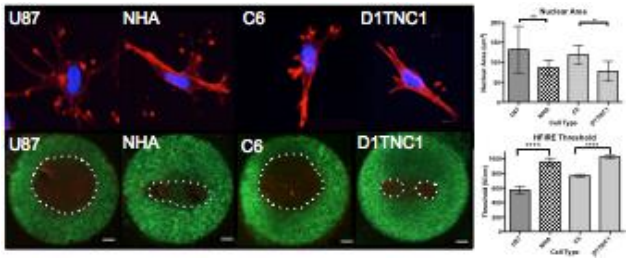

Figure 1. HFIRE threshold correlation with nuclear area

HFIRE was shown to exhibit intracellular effects with nuclear size a predictor of HFIRE lethal thresholds. The glioma cell lines exhibited increased nuclear area and lower HFIRE lethal thresholds compared to healthy cells (Fig 1). This allows for a margin of selectively treating malignant cells while sparing healthy cells. The selectivity achieved by HFIRE can be enhanced by molecular targeted eA1 due to a morphology change that increases nuclear to cytoplasm ratio (NCR) for malignant cells but leaves healthy cells unchanged (Fig 2).

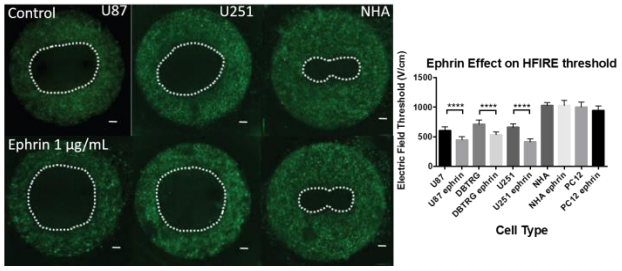

Figure 2. Margin of selectivity enhanced with ephrinA1

CONCLUSIONS

The HFIRE killing mechanism is such that an increased NCR correlates with a lower electric field lethal threshold. This allows for the selective targeting of these cells using a range of electric field distributions that induce no damage to the healthy cells studied but elicit a death response in malignant cells. This range for selective targeting can be enhanced using targeted eA1 therapy which selectively changes the NCR of only malignant cells. This selectivity may present therapeutic opportunities for treating therapy-resistant GBM cells.

ACKNOWLEDGEMENTS

This work was supported by the R21 Award from the NCI and funding from ICTAS at Virginia Tech.

REFERENCES

Davalos RV, Mir LM, Rubinsky B. Tissue ablation with irreversible electroporation. Ann Biomed Eng. 2005; 33(2):223-31.

DEVELOPMENT OF A 3D MODEL OF THE BEETLE HEART TO UNDERSTAND FLOW PRODUCTION

Melissa C. Kenny[1], Pam Tegelman-Malabad[2], Laura Miller[3], Garrett P. League[4], Julián F. Hillyer, and John J. Socha[1]
1. Dpt. Biomedical Engineering and Mechanics, Virginia Tech
2. Giles High School, Pearisburg, VA
3. Dpt. Mathematics, University of North Carolina
4. Dpt. Biological Sciences, Vanderbilt University
Corresponding Author: Melissa C. Kenny, Email: mck66@vt.edu

INTRODUCTION

The insect circulatory system is open, meaning that hemolymph (insect blood) flows freely throughout the body. The pulsatile dorsal vessel (DV) is the principal hemolymph-pumping organ and is functionally divided into a posterior muscularized heart and an anterior aorta [1]. Previous studies have examined the DV in several species, but few examine it in beetles [2]. Our research aims to understand flow production in the DV. Here, we measure the basic anatomical features of the heart of the beetle, *Zophobas morio*. These results will be used to generate a 3D model of the DV for computational studies.

METHODOLOGY

Male and female adult *Z. morio* were obtained from Carolina Biological and housed in a colony with *ad libitum* food and water. To visualize the DV, we dissected sacrificed beetles for direct viewing as well as fixing, dehydrating, and sputter coating portions of the DV for SEM imaging. We also used fluorescent staining, which involved dissection followed by fixing and staining with I-1 phalloidin-Alexa Fluor 488 before imaging with a Nikon 90i compound scope.

RESULTS

Table 6: Anatomical measurements on dissection.

Measurement	Value
Weight	0.433 ± 0.056 g (n=26)
DV Length	21.5 ± 1.2 mm (n=26)
DV Diameter	147 ± 30.3 μm (n=3)
Heart Length	12.4 ± 0.7 mm (n=26)
Aorta Length	9.2 ± 0.7 mm (n=26)

These values were used to generate a 3D model of the heart as an elastic tube with peristaltic contractions. Applying the immersed boundary method [3] to the 3D model showed significant net flow only for compression ratios of ≥50%. This suggests that large-amplitude tube contractions are needed to overcome viscous resistance.

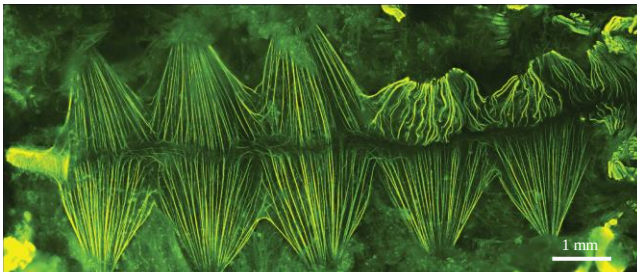

Figure 1: The entire heart of *Z.morio*, obtained from phalloidin staining. Anterior is to the left.

CONCLUSIONS

We measured anatomical features of the DV using bright field imaging, SEM, and fluorescence imaging. While these techniques were helpful, we found that the heart is easily damaged and obstructed by musculature. Future studies should address improved methods of viewing the heart for refined measurements. Initial attempts at a 3D model of the DV are able to generate flow using peristaltic contractions of the heart wall without full occlusion of the tube; however, it is not yet a complete view of what is actually occurring. Further development of this model with refined parameter measurements is a step towards developing a full, novel biomechanical model to study the function of the DV in *Z. morio*.

ACKNOWLEDGMENTS

Supported by NSF 0938047 (J.J.S), RET 1301037 (J.J.S), NSF CAREER 1151478 (L.A.M.), IOS-1257936 (J.F.H.).

REFERENCES

[1] Glenn et al., 2010. J. Exp. Biol. 213: 541-550.
[2] Morgan and Morgan, 1980. Geoscience. 7: 22-28.
[3] Peskin, 2002. Acta Numerica. 1-39.

Poster,B
Atrium, 11:45

ROLE OF INTERSTITIAL CELLS OF CAJAL (ICCS) ON SPHINCTERIC TONE IN THE PYLORUS

Dylan Knutson[1,2], Elie Zakhem[2], and Khalil N. Bitar[1,2]
1. Virginia Tech-Wake Forest School of Biomedical Engineering and Sciences
2. Wake Forest Institute for Regenerative Medicine
Corresponding Authors: Dylan Knutson, Khalil Bitar
Email: Dknutson@wakehealth.edu, kbitar@wakehealth.edu

INTRODUCTION

Interstitial Cells of Cajal (ICC) operate as smooth muscle pacemakers throughout the Gastrointestinal (GI) tract. Recent work has shown that they might affect sphincteric tone. Their absence (ICC-opathy) has been associated with several diseases including Gastroparesis and Chronic Unexplained Vomiting and Nausea.

Progress has been made on understanding their contribution to overall GI function, however their role in several functions is still unclear. The aim of this experiment is to measure ICC contribution to sphincteric tone when stretched, using tissue engineered pylorus.

METHODOLOGY

(1) Smooth muscle cells were isolated from human pyloric sphincter tissues.
(2) ICCs were isolated from GFP murine small intestine.
(3) Two groups of 3D pyloric sphincter constructs were engineered:
    a. Smooth muscle only (SMC)
    b. Co-culture of smooth muscle with ICCs (SMC+ICC).
(4) The presence of ICCs in the constructs was confirmed using immunohistochemistry.
(5) Constructs were evaluated for their ability to generate basal tone using a force transducer.

RESULTS

(1) Primary GFP-ICCs were visualized under microscopy and exhibited morphological characteristics of ICCs.
(2) Live microscopy on the engineered pyloric constructs showed fluorescence GFP ICCs within the smooth muscle of the construct indicating the successful co-culture in the constructs.
(3) Immunohistochemistry analysis of the engineered SMC+ICC tissues showed positive stain for TMEM16 (Ano1 channels) confirming the presence of ICCs.
(4) Engineered tissues were evaluated using organ bath. A 10% stretch was applied to all tissues (Figure 1 – dashed line). Following stretch, the basal tone increased in both types of constructs. There was no significant change in tone generated by either type of constructs.

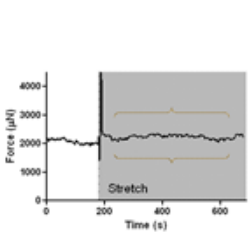

Figure 1: Representation of tone measurement.

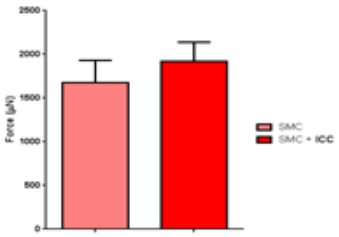

Figure 2: bar graph of basal tone between construct types.

CONCLUSIONS

ICCs were successfully incorporated in the engineered pyloric smooth muscle constructs. There was no significant change in basal tone between constructs engineered using SMC only and SMC co-cultured with ICCs indicating that the tone generated was purely myogenic. Additional studies will look at the contribution of ICCs to the relaxation of the smooth muscle.

ACKNOWLEDGMENTS

This work was supported by Wake Forest Institutional Funds and NIH/NIDDK R42DK105593.

AN INTEGRATED ORGANOTYPIC LIVER-INTESTINE SYSTEM FOR EVALUATION OF DRUG TOXICITY *IN VITRO*

Anjaney Kothari[1], Rebekah Less[1], and Padma Rajagopalan[1, 2, 3]
1. School of Biomedical Engineering and Sciences, Virginia Tech, Blacksburg, VA 24061, United States
2. Department of Chemical Engineering, Virginia Tech, Blacksburg, VA 24061, United States
3. ICTAS Center for Systems Biology of Engineered Tissues, Virginia Tech, Blacksburg, VA 24061, United States
Corresponding Author: Anjaney Kothari, Email: anjaney@vt.edu

INTRODUCTION

Hepatic toxicity is a major concern associated with drugs and pharmaceuticals. To evaluate drug toxicity, there has been a push towards use of *in vitro* organotypic liver models over animal models. While these *in vitro* models are relevant, they exclude an important participant in drug metabolism– the intestine. *In vivo*, liver and intestine cross-talk via two routes: (1) the portal vein, which carries metabolites and drugs from the intestine to the liver; and (2) the bile duct, which brings the drugs and toxins metabolized in the liver back to the intestine. This enterohepatic circulation affects the absorption and bioavailability of drugs. Peristaltic flow in the intestine also affects drug absorption. Additionally, intestinal microbiota is known to influence drug metabolism. It is, thus, important to design an integrated liver-intestine platform that mimics organ-specific microenvironments and flow features to better understand first-pass metabolism and toxicity of drugs *in vitro*.

The objective of this work is to integrate (1) multicellular organotypic liver models that include non-parenchymal hepatic cell types like liver sinusoidal endothelial cells and Kupffer cells, with (2) an intestinal culture system that includes the intestinal microbiota and peristaltic flow to closely emulate the intestinal microenvironment. As the first step towards this objective, we are integrating intestinal explants with the widely used collagen sandwich model of hepatocyte culture to evaluate toxicity of acetaminophen (APAP), a widely used drug.

METHODOLOGY

Intestinal tubes extracted from rat jejunum segments will be inverted and mounted on PDMS rods inserted through two diametrically opposite holes in a Transwell® insert. These Transwell® systems will be integrated with collagen sandwich cultures of primary rat hepatocytes as depicted in figure 1 (not to scale).

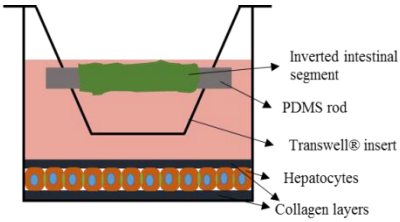

Figure 1: Integrating intestinal explants with collagen sandwich model

These integrated cultures will be treated with acetaminophen and hepatic function markers such as albumin, urea and AST/ALT and enzymes involved in APAP metabolism such as CYP2E1 will be quantified.

EXPECTED RESULTS

We expect that toxicity data from the integrated liver-small intestine models would better correlate with *in vivo* toxicity data from animal models. This would validate the efficacy of our integrated platform that closely mimics the microenvironment of both liver and intestine and recapitulates the cross-talk between these two organs.

ACKNOWLEDGMENTS

AK would like to acknowledge Computational Tissue Engineering Interdisciplinary Graduate Education Program, Virginia Tech for research fellowship.

REFERENCES

Vu, L. T., Less, R. R., & Rajagopalan, P. (2014). The promise of organotypic hepatic and gastrointestinal models. Trends in biotechnology, 32(8), 406-413.

Poster,B
Atrium, 11:45

NOVEL INTEGRATED IN VITRO GASTROINTESTINAL AND HEPATIC MODEL FOR INVESTIGATING DRUG TOXICITY

Rebekah Less[1] and Padma Rajagopalan[1,2,3]
1. School of Biomedical Engineering and Sciences, Virginia Tech, Blacksburg, VA
2. Department of Chemical Engineering, Virginia Tech, Blacksburg, VA
3. ICTAS Center for Systems Biology of Engineered Tissues, Virginia Tech, Blacksburg, VA
Corresponding Author: Padma Rajagopalan, Email: padmar@vt.edu

INTRODUCTION

To date, in vitro models of both the liver and the gastrointestinal (GI) tract have been developed individually with very limited efforts to integrate them into a single system. These models provide limited information on the complementary actions of the GI and liver. There is a surprising lack of in vitro models that can simulate how the liver and GI complement each other's role in vivo. In an attempt to bridge this gap, our goal is to design and assemble an in vitro model of the GI tract and liver using either Caco-2 cells or a GI sheet integrated with a 3D multi-cellular organotypic liver model.

METHODOLOGY

Caco-2 (human colon adenocarcinoma) cells were purchased from ATCC (Manassas, VA). Primary intestinal epithelial cells and hepatocyte cells were obtained through the surgical excision of rat intestines and livers, respectively. Caco-2 and primary intestinal cells were cultured on Millipore Transwell inserts. Primary hepatocytes were cultured as collagen sandwiches (CS). Acetaminophen (APAP) was used as model toxins to study absorption, metabolism, and toxicity in this integrated organ system. Transepithelial electrical resistance (TEER) measurements were conducted to measure tight junction integrity of intestinal monolayers.

RESULTS

APAP, a prototypic hepatotoxicant, was administered over a 5-20mM concentration range. When 5mM of APAP was administered, Caco-2 cells exhibited 24±1.3% decrease in their trans-epithelial electrical resistance only in the integrated model. This loss in the gap junction integrity of Caco-2 cells was accompanied by a 41±8.0% decrease in albumin production, a 59±10% decrease in urea production, a 92±3% decrease in glutathione, and an AST/ALT ratio of 1.62±0.27 in hepatocytes. The decrease in hepatocyte function was attributed to the generation of reactive oxygen species in Caco-2 cells upon APAP administration. Interestingly, loss in gap junction integrity was not observed in Caco-2 cells cultured individually. Similarly, hepatocytes cultured individually did not exhibit markers of toxicity until a high concentration of APAP was administered.

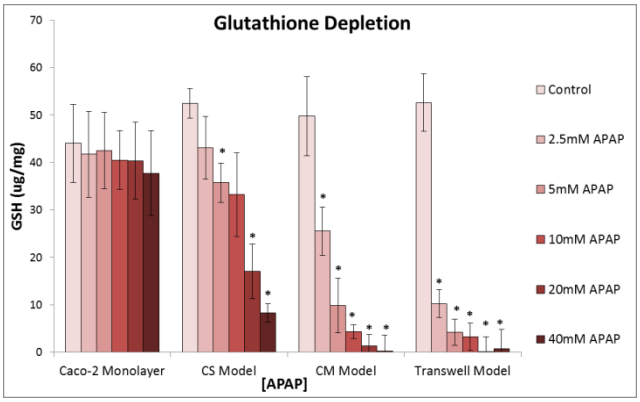

Figure 1: Glutathione depletion after Acetaminophen

CONCLUSIONS

Results suggest the integration of GI tract and liver models can increase sensitivity of drug toxicity models in vitro, creating a need for more complete drug absorption, metabolism, and toxicity assessment system. By integrating both organ models (GI tract and liver) in toxicity testing, a more complete evaluation of drug absorption and metabolism can be generated. Ongoing efforts are focused on integrating a GI cell sheet with a 3D multi-cellular organotypic liver model. The changes in hepatocyte function such as functional markers and expression of cytochrome P450 proteins will be monitored. Additionally, changes to the structure of the GI cell sheet are also being investigated. Recreating the organ-to-organ interaction between the GI and the liver will serve as a powerful platform to systematically decipher the effects of drugs and chemicals.

MOVEMENT AND LOADING SYMMETRY CHANGES WHEN WEARING A FUNCTIONAL KNEE BRACE FOLLOWING ACL RECONSTRUCTION

Evan McConnell[1], Robin Queen, FACSM[1]
1. Kevin Granata Lab, Department of Biomedical Engineering and Mechanics, Virginia Tech, Blacksburg, VA
Corresponding Author: Evan McConnell, Email: mevan6@vt.edu

INTRODUCTION

Movement and loading asymmetry have been reported following anterior cruciate ligament (ACL) reconstruction during landing[1]. Previous work has examined these asymmetric movement patterns using discrete measures, and these asymmetries have been reported to be risk factors for secondary ACL injuries[2]. The purpose of this project was to examine the impact of functional brace wear on frontal and sagittal plane kinematic and kinetic inter-limb movement symmetry during landing in ACL reconstruction (ACL-R) patients.

METHODOLOGY

20 adolescent athletes (15.8 ± 1.2 years) (7 male, 13 female) 6 months following ACL-R performed 5 trials of a stop-jump task in both a braced (B) and non-braced (NB) condition, with the first landing being analyzed. A custom fit functional knee brace (DJO, Vista, CA) was worn on the ACL reconstructed limb (AL) during the B trials. Mean curves were created for each limb (AL and unaffected limb (UL)) for the vertical (vGRF) and anterior-posterior ground reaction forces (apGRF), as well as knee angles and moments in the frontal and sagittal planes. Inter-limb symmetry was analyzed by calculating the coefficient of multiple determination (CMD) between the AL and UL mean curves. Students' t-tests were utilized to compare CMD values between B and NB conditions ($p \leq 0.05$).

RESULTS

No significant differences existed for inter-limb movement and loading symmetry between B and NB conditions among all subjects. Secondary analysis revealed significant differences in apGRF ($p=0.014$), vGRF ($p=0.011$) and sagittal knee angles ($p=0.003$) in subjects with improved sagittal knee angle symmetry in the B condition (responders). No differences existed in subjects with decreased symmetry in the B condition (non-responders).

Table 1: CMD Values Among All Subjects

	NB	B	p-value
apGRF	0.721	0.755	0.130
vGRF	0.656	0.694	0.056
Knee Flexion Angles	0.951	0.959	0.294

CONCLUSIONS

Brace wear improves loading symmetry in adolescent patients that also exhibit improved sagittal knee angle symmetry while braced 6 months following ACL-R. These results indicate that there are both responders and non-responders to brace wear following ACL-R. Future work to identify responders and non-responders to brace wear will allow for targeted brace wear interventions in ACL-R patients.

ACKNOWLEDGMENTS

The authors would like to thank DonJoy Orthopedics for funding this study. We would also like to thank Boyi Dai for initial collection of biomechanical data and the orthopedic surgeons for patient referrals for this study.

REFERENCES

1. Pappas, E., and F.P. Carpes. "Lower Extremity Kinematic Asymmetry in Male and Female Athletes Performing Jump-landing Tasks." *Journal of Science and Medicine in Sport* 15.1 (2012): 87-92.
2. Paterno, M.V., et al. "Biomechanical Measures During Landing and Postural Stability Predict Second Anterior Cruciate Ligament Injury After Anterior Cruciate Ligament Reconstruction and Return to Sport." *The American Journal of Sports Medicine* 38.10 (2010): 1968-978.

Poster,B
Atrium, 11:45

EVALUATION OF DIRECTIONAL DEPENDENCE OF BRAIN RESPONSE IN YOUTH ATHLETES USING AN ANATOMICALLY ACCURATE FINITE ELEMENT MODEL

Logan E. Miller[1], Jillian E. Urban[1], Mireille E. Kelley[1], and Joel D. Stitzel[1]
1. Virginia Tech- Wake Forest Center for Injury Biomechanics
2. Wake Forest University
Corresponding Author: Logan E. Miller, Email: logmille@wakehealth.edu

INTRODUCTION

There are approximately 5 million athletes playing organized football in the US; 2,000 HS players, and 3.5 million youth players [1]. Although head impact exposure has been studied at the professional, college and high school levels, studies at the youth level have been limited.

METHODOLOGY

On-field head impact data has been collected for practices and games over the course of four football seasons (2012-2015) with the Head Impact Telemetry (HIT) System. We have collected approximately 40,000 impacts from 150 individual athlete seasons of youth football. Each head impact has an associated azimuth (Figure 8B) and elevation (Figure 8A) angle which will be used to categorize impacts by location (Figure 8C). Representative impacts at each location will be simulated using the atlas-based brain model (ABM), an anatomically accurate brain model developed by our lab [2]. The variation in strain response and location of maximum strain will be analyzed for each impact interval.

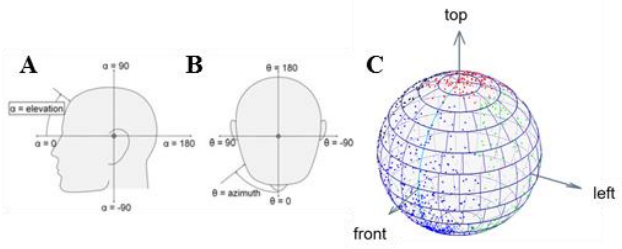

Figure 8: Azimuth (A) and elevation (B) measurements, and a plotted subset of the HITS data (C).

RESULTS

The strain for a simulated lateral impact with a peak linear acceleration of 56 g's and a maximum angular acceleration of 3,000 rad/s^2 is shown in Figure 9.

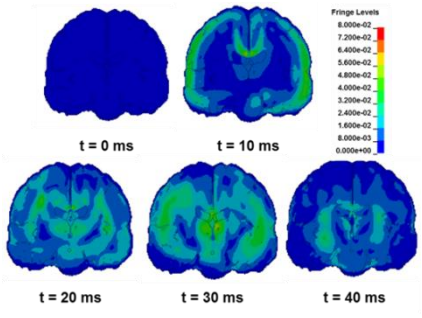

Figure 9: Maximum principal strain response of the ABM during a lateral impact.

Through simulation of impacts at various locations, we observed variations in strain response and locations of peak strain. Also, rotational loading had a significant effect on the development of strain in the brain.

CONCLUSIONS

This study demonstrates that there is a directional dependence of the strain response in the brain. Quantifying the connection between impact location, impact magnitude and brain deformation will aid researchers, clinicians, and equipment manufacturers in head injury prevention.

ACKNOWLEDGMENTS

Research reported in this publication was supported by the National Institute Of Neurological Disorders And Stroke of the National Institutes of Health under Award Number R01NS094410. The authors would like to thank the South Fork Panthers youth football organization.

REFERENCES

[1] Daniel, R.W., et al., 2012. [2] Miller et al., 2016

PREDICTING SUCCESS OF A WEIGHT LOSS INTERVENTION USING GRAY MATTER AND WHITE MATTER VOLUMES

Fatemeh Mokhtari[1,2], Jonathan Burdette[1], Jack Rejeski[3], and Paul Laurienti[1,2]
1. Laboratory for Complex Brain Networks, Department of Radiology, Wake Forest School of Medicine
2. VT-WFU School of Biomedical Engineering and Sciences, Wake Forest University
3. Department of Health and Exercise Science, Wake Forest University
Corresponding Author: Fatemeh Mokhtari, Email: fmokhtar@wakehealth.edu

INTRODUCTION

Obesity is considered as a leading cause of decreased life expectancy, as obesity is associated with various physical and mental impairments [1]. Prediction of weight loss success and maintenance before treatment prescription would allow for a tailored intervention to be prescribed for each individual.

METHODOLOGY

The n=58 obese older adults were randomly assigned to three 18-months lifestyle interventions: 1) only diet-induced weight loss (WL); 2) WL in association with aerobic exercise training; and 3) WL in association with resistance exercise training. All participants completed a baseline magnetic resonance imaging session. Participants were categorized into the bottom and top halves of body mass index loss after intervention. Voxel-based morphometric analysis was performed to obtain maps of gray matter (GM) and white matter (WM), and the resulting maps were used in a machine-learning algorithm (support vector machine) to classify participants in the bottom half and top half of weight loss performance. A repeated random sub-sampling validation approach (with 100 permutations) was used to estimate the generalizability of our model.

RESULTS

Table 1 summarizes the average of classification performance across all 100 permutations, obtained using the GM, WM, and combined classifiers (GM + WM).

Figure 1 shows average ROC curves across 100 permutations for the 3 classifiers. Three paired 2-sample t-tests showed that combined classifier significantly outperforms GM and WM classifiers.

Table 1. Average classification performance within all permutations

Classifiers	Accuracy	Sensitivity	Specificity
GM	74.64	78.43	70.86
WM	71.36	74.43	68.29
Combined	75.39	79.00	71.79

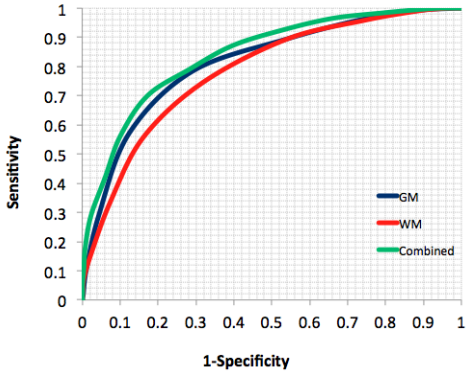

Figure 1: ROC curves; area under the curve 80.56, 77.87, 83.77% was resulted from GM, WM, and combined classifiers.

CONCLUSIONS

There is a discriminant spatial pattern in the gray matter and white matter volume, which predicts weight loss success following a 6-month weight loss intervention. The combination of weight loss and weight regain predictions could be used in individual patient during the development of personalized treatment plans.

REFERENCES

1. Initiative, N.O.E. and N.A.A.f.t.S.o. Obesity, The practical guide: identification, evaluation, and treatment of overweight and obesity in adults. 2011: National Heart, Lung, and Blood Institute.

Virginia Tech
Wake Forest University
School of Biomedical Engineering and Sciences
15th Annual Graduate Student Research Symposium, May 11, 2016

MICROSCOPE MODIFICATION FOR SLIDE SCANNING AT MULTIPLE POLARIZATION ANGLES

Jade Montgomery[1], and Robert G. Gourdie[1]
1. Virginia Tech, School of Biomedical Engineering and Sciences
Corresponding Author: Jade Montgomery, Email: jmont@vt.edu

INTRODUCTION

The natural birefringence of collagen is often exploited in order to image collagen within tissue samples[1]. This natural birefringence is typically enhanced by stains such as Picrosirius Red and then viewed under a confocal microscope equipped with polarization filters. There are two kinds of polarization that can be used: circularly polarized and linearly polarized[1]. Circular polarization allows the imaging of collagen fibers in all angles, which is good for general imaging of the extracellular matrix but makes fiber angle quantification more difficult, especially in thick tissue sections. Linearly polarized light meanwhile only allows imaging of two narrow bands of angles directly perpendicular to one another, allowing collagen fiber angles in even thicker tissue sections to be viewed and their angles quantified. In order to image all fiber angles with linearly polarized light, images must be taken at multiple quenched rotations of both the analyzer and condenser polarization filters.

Preliminary data collected at a single fiber angle in anti-scarring drug clinical trial histological sections suggested a novel matrix realignment, and required confirmation by imaging at multiple fiber angles. Doing this manually with the equipment possessed by our lab would have been extremely time consuming and difficult. In order to streamline and improve the accuracy of the process, a mechanical microscope addition was built.

METHODOLOGY

Stepper motors and physical user interface system were attached to an Arduino Uno. A Raspberry Pi computer was attached to the Uno to perform more complex calculations and record a log of performed actions for later reference. A Python program was used on the Raspberry Pi to interface with the Arduino program. The two programs working together are capable of rotating the analyzer and condenser to specified angles, removing or inserting the analyzer into the microscope, calibrating these rotations and translations, and testing the calibration. A third post-processing program implemented in MATLAB allows the combination of images collected at all polarization angles into a single image.

Simple gearing systems were attached to the stepper motors in order to drive rotation of the analyzer and condenser, as well as translation of the analyzer in and out of the machine. A 16 character LCD screen informs the user of the current positions of the motors and any ongoing special actions, while a set of five back-lit buttons allow operation even in low-light conditions necessary for polarization microscopy. If the backlights of the system are too bright, a switch toggles the lights on or off at any point during operation.

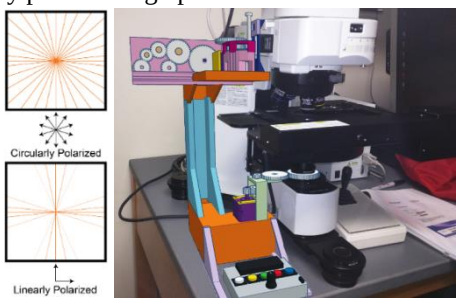

Figure 1: (left) Representative images of the same set of collagen fibers with circular vs linear polarization. **(right)** Photo mockup of final microscope setup.

CONCLUSIONS

The microscope addition was constructed with mostly off-the-shelf consumer parts for <$500 and adds the functionality of a $300k+ polarization microscope to an existing slide scanning microscope. This method can be easily modified to fit any microscope with manually rotatable analyzer and condenser attachments to add multiple-angle linearly polarized functionality.

REFERENCES

1. Matcher, S. J., Winlove, C. P. & Gangnus, S. V. Phys. Med. Biol. 49, 1295–1306 (2004).

Virginia Tech
Wake Forest University
School of Biomedical Engineering and Sciences
15th Annual Graduate Student Research Symposium, May 11, 2016

OPERATIONAL CONSISTENCY OF MEDICAL LINEAR ACCELERATOR PERFORMANCE PARAMETERS

Callistus M. Nguyen[1,2], Charles M. Able[2], Alan H. Baydush[2], Scott Isom[3], and Michael T. Munley[1,2]
1. Virginia Tech – Wake Forest School of Biomedical Engineering and Sciences, Biomedical Engineering
2. Wake Forest School of Medicine, Radiation Oncology
3. Wake Forest School of Medicine, Biostatistical Sciences
Corresponding Author: Callistus M. Nguyen, Email: canguyen@wakehealth.edu

INTRODUCTION

The purpose of this work is to determine if linacs produced by the same manufacturer exhibit operational consistency within the performance states of subsystems and components.

METHODOLOGY

Seven linacs were monitored by delivering a daily robust quality assurance (QA) treatment. Each QA treatment generated trajectory and text log files that were used to monitor various operational components and subsystem performance. Statistical process control (SPC) analysis of the log files was used to evaluate the performance of the linacs. A total of 525 operational or performance parameters were monitored (35 text log and 490 trajectory log) using individual and moving range (I/MR) charts. The individual (I) grand mean values and control limit ranges of the linac I/MR charts were extracted and compared across all linacs using statistical and graphical analyses. The "I" values were subjected to a ranked analysis of variance (ANOVA) to determine if there were differences between each of their parameter means. Parameters were also graphically compared using their parameter means, deviations from their overall mean, and performance operating windows.

RESULTS

The linacs were found to be statistically and operationally different (**Table I**). The "range" is the minimum and maximum grand mean of that specific performance parameter. The "maximum difference" is the difference between the maximum and minimum grand mean. Each monitored performance parameter was statistically different and operated at a unique, distinct value. The treatment delivery parameters reported here are representative of all the performance parameters being monitored. Graphical analysis provided a greater inspection of this result, further supporting the uniqueness of linear accelerator operation.

Table I. Statistics for Important Performance Parameters in 7 linacs.

Performance Parameter	Range	Maximum Difference	P-Value
Angle Radial Current (A)	-0.063 – 0.111	0.175	< 0.00001
Angle Transverse Current (A)	-0.127 – 0.145	0.272	< 0.00001
Position Angle Current (A)	-1.264 – 0.273	1.536	< 0.00001
Position Transverse Current (A)	-0.476 – 0.759	1.234	< 0.00001
Gantry Speed 2 (Deg/sec)	5.534 – 5.841	0.307	< 0.00001

CONCLUSIONS

Linacs are highly complex machines that consist of many subsystems. Each subsystem was found to function at a unique operating value. Thus, linacs and their components operate at distinct values, statistically and operationally. Yet, accelerators collectively meet all the clinical treatment specifications. SPC can therefore be implemented as a means to identify nonrandom changes in a specific accelerator's parameter performance. The SPC techniques have the potential to be a powerful accelerator evaluation tool.

Poster,B
Atrium, 11:45

Virginia Tech
Wake Forest University
School of Biomedical Engineering and Sciences
15th Annual Graduate Student Research Symposium, May 11, 2016

THE DEVELOPMENT OF A THIN-FILMED, NON-INVASIVE TISSUE PERFUSION SENSOR TO QUANTIFY CAPILLARY PRESSURE OCCLUSION OF EXPLANTED ORGANS

Timothy O'Brien[1, 2], Ali Roghanizad[2], Phillip Jones[2], Charles, Aardema[2], John Robertson[1, 2], Thomas Diller[1, 2]
1. Department of Biomedical Engineering and Mechanics, Virginia Tech
2. Department of Mechanical Engineering, Virginia Tech
Corresponding Author: Timothy O'Brien, Email: tjobrien@vt.edu

INTRODUCTION

According to the Organ Procurement and Transplant Network (OPTN), there are approximately 121,443 people currently in need of a life-saving organ transplant. Typically, fewer than 20% of wait list candidates have received a transplant. Machine perfusion organ preservation systems (hypothermic and normothermic) have affected the future of organ preservation, yet many of these systems are still overlooking the effect of capillary pressure occlusion. Capillary pressure occlusion is the restriction of blood flow to tissue due to some applied pressure. This, of course, becomes critical to organ transplantation when considering the manner in which the organ is resting throughout the transition. In the work reported here, a novel, non-invasive, thin-filmed sensor (CHFT+, patent pending) was designed for measuring tissue perfusion on both the topside and underside of an explanted organ. Smart Perfusion's Vasowave™ (VW) was utilized as the platform to support organ viability and collect vital data of explanted organs. The goal of this effort was to illustrate the need for future organ preservation systems to consider the effects of pressure ischemia during preservation.

METHODOLOGY

The CHFT+ sensor is applied to the tissue and given approximately 10 seconds to acquire steady-state values. Then a thermal event is introduced, creating a steady rise in temperature to the back side of the CHFT+ sensor for approximately 60 seconds. The acquired temperature and heat flux signals are applied to a mathematical model, fundamentally based on the Penne's bioheat equation, to estimate the capillary perfusion, core temperature, and contact resistance between the sensor and tissue. Porcine renal tissue testing was performed with a preservation fluid temperature of both 5 ˚C and 20˚C over a 20 hr. experimental period. The data capture rate was set to 15 minutes.

RESULTS

This work illustrated the manufacture of a novel perfusion sensing technology and exploited its unique qualities to measure and evaluate the capillary perfusion of explanted porcine kidneys from the top- and undersurfaces. Figure 1 illustrates two different CHFT+ sensors being applied to both the topside and underside of an explanted porcine kidney. Also displayed are the estimated perfusion results for the topside and underside at both 5 ˚C and 20˚C.

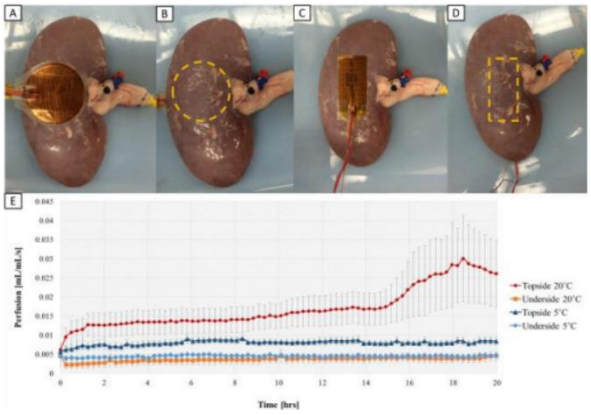

Figure 1: (A-D) CHFT+ sensors on the topside and underside of renal tissue. **(E)** Estimated capillary perfusion of the topside and underside of porcine kidneys perfused at 5 ˚C and 20˚C.

CONCLUSIONS

The results of the live tissue testing indicate that the pressure due to the weight of the organ creates an additional resistance to capillary perfusion on the underside of an explanted organ. This in itself could effectively change the way the organ preservation technologies are designed and potentially lead to pressure occlusion relieving technologies.

Poster,A
Atrium, 11:15

Virginia Tech
Wake Forest University
School of Biomedical Engineering and Sciences
15th Annual Graduate Student Research Symposium, May 11, 2016

DEVELOPMENT AND VALIDATION OF A BRAIN PHANTOM FOR THERAPEUTIC COOLING DEVICES

Ryan D. M. Packett[1], Philip J. Brown[1], Gautam S. Popli[2], and F. Scott Gayzik[1]
1. Department of Biomedical Engineering, Wake Forest University School of Medicine
2. Department of Neurology, Wake Forest University School of Medicine
Corresponding Author: F. Scott Gayzik, Email: sgayzik@wakehealth.edu

INTRODUCTION

Individuals with medically refractory epilepsy seek relief through resection of the epileptogenic portion of the brain. However, this treatment method has limited success due to the difficult nature of correctly identifying the exact scope and location of the zone of seizure onset. Cooling the brain tissue at a depth of 5 mm below the surface by 12 °C has been shown to greatly reduce seizure activity [1][2][3].

The long term aim of the study is to develop a cooling device to achieve this. When cooling is applied to the surface of the brain, a reduction in seizure activity strongly indicates a correct identification of the location of seizure onset, thereby informing the surgical resection procedure and increasing the chances of seizure liberation. To that end, the current study focuses on development of a physical phantom to analyze prototype device performance. Here, a prototype phantom is assessed against a finite difference model prediction.

METHODOLOGY

Two approaches were used to suggest the feasibility of cooling the brain in the desired way. The first method utilized a mathematical model which calculates the temperature over time for various depths into a one-dimensional body of uniform properties [4]. The second method centers around developing a physical brain phantom for use as a device test bed, in which the goal is to mimic the temperature drop observed in the model. One component of the phantom models the human brain and consists of pumping 37 °C water through absorbent polymer spheres (11 mm diameter). The second component of the test setup includes the cooling device (40 mm^2 face copper cooling block), which circulates cold water and is placed on top of the phantom. Thermocouples embedded at 5, 10 and 15 mm deep obtain temperature information which is plotted over time. This test setup is depicted in Figure 1 below.

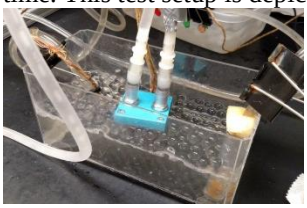

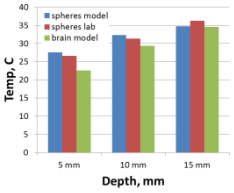

Figure 1 (Left): Bench top setup using water block to cool SAP spheres. **Figure 2 (Right):** Comparison of steady state lab results to finite difference solver [4].

RESULTS

Steady states of the computational and experimental models suggest that cooling brain tissue 5 mm deep by 12 C is viable. The temperature results from the benchtop test loop are shown below in Figure 2.

CONCLUSIONS

Given the viability of achieving the desired temperature reduction as a goal for seizure, this data warrants further exploration. Next we will assess the transient response of the polymer spheres and phantoms that utilize a finer polymer or hydrogel. Ultimately, once reasonable transient characteristics are demonstrated, prototypes of cooling devices will be assessed.

ACKNOWLEDGMENTS
Pilot funding was provided by Wake Forest Innovations and Wake Forest University School of Medicine Department of Biomedical Engineering.

REFERENCES
1. Kwan, P. and M.J. Brodie, N Engl J Med, 2000.
2. Rothman, S.M., et al., Epilepsy Behav, 2005.
3. Fujii, M., et al., Neurol Med Chir (Tokyo), 2010.
4. Gayzik, F.S., et al., J Biomech Eng, 2006.

Poster,B
Atrium, 11:45

DEVELOPMENT AND VALIDATION OF A 95TH PERCENTILE MALE PEDESTRIAN FINITE ELEMENT MODEL

Wansoo Pak[1] and Costin D. Untaroiu[1]
1. Virginia Tech, School of Biomedical Engineering and Sciences
Corresponding Author: Wansoo Pak, Email: wspak@vt.edu

INTRODUCTION

Pedestrian represents one of the most vulnerable road users and comprise nearly 22 percent of the road crash related fatalities in the world [1]. Therefore, protection of pedestrians in the car-to-pedestrian collisions (CPC) has recently generated increased attention.

High biofidelity computational human models could predict both pedestrian kinematics and risks of injuries during a CPC, and therefore could be useful in the development of new pedestrian-friendly vehicles. The primary goal of this study was to develop and validate a Finite Element (FE) model corresponding to a 95th percentile male (M95) anthropometry in standing posture.

METHODOLOGY

The model mesh was developed by morphing the Global Human Body Models Consortium (GHBMC) 50th percentile male pedestrian (M50) model to the reconstructed geometry of a human subject having 194 cm height and 103 kg weight. The material properties of the M95 pedestrian model were assigned based on GHBMC M50 occupant model. The knee joint and upper torso of the FE model were preliminarily validated against Post Mortem Human Surrogate (PMHS) test data recorded in four-point knee bending tests and upper body blunt lateral impact tests [2, 3]. Then, pedestrian-to-vehicle impact simulations were performed using the whole pedestrian model (Fig. 1) and the results were compared to corresponding pedestrian PMHS tests [4].

Figure 1. Vehicle-to-M95 pedestrian FE simulation

RESULTS

Due to the lack of M95 PMHS test data, the impact responses of the pedestrian model were compared to existing test corridors scaled to M50 anthropometry. The kinematic trajectory of head's centre of gravity (CG), obtained from the CPC simulation, was close to the trajectories recorded on tall PMHS (Fig 2). Similarly, the results of the knee and upper torso FE simulations predicted higher responses than that PMHS test data.

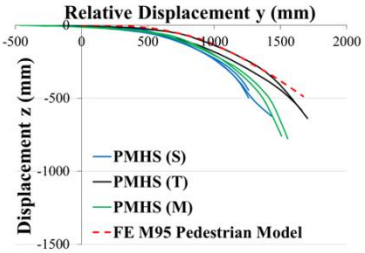

Figure 2: The M95 pedestrian kinematic head CG marker trajectories relative to the car

CONCLUSIONS

Overall, the model showed promising results and a good capability to predict the injury risk of pedestrian during lateral vehicle impact.

ACKNOWLEDGMENTS

The authors are grateful for help received from WFU and GHBMC.

REFERENCES

[1] W. H. Organization, "Global status report on road safety," 2013.
[2] D. Bose, et al., "Injury tolerance and moment response of the knee joint to combined valgus bending and shear loading," *Journal of biomechanical engineering*, vol. 130, p. 031008, 2008.
[3] D. C. Viano, "Biomechanical responses and injuries in blunt lateral impact," SAE Technical Paper 0148-7191, 1989.
[4] J. R. Kerrigan, et al., "Pedestrian kinematic response to mid-sized vehicle impact," *International journal of vehicle safety*, vol. 2, pp. 221-240, 2007.

INVESTIGATION OF THORACOLUMBAR FRACTURES IN MOTORSPORT DRIVERS DURING FRONTAL IMPACTS

John Patalak[1], Joel Stitzel[1]
1. Wake Forest, Center for Injury Biomechanics
Corresponding Author: John Patalak, Email: jpatalak@wakehealth.edu

INTRODUCTION

Following a frontal on-track incident in 2015 a NASCAR® (National Association for Stock Car Auto Racing, Inc) driver was diagnosed with L1 and L2 superior endplate vertebral body wedge compression fractures without neurologic symptoms. The driver received medical clearance to return to racing activities approximately seven weeks following the incident.

The driver was utilizing a helmet, HANS® head & neck restraint, nine point seat belt restraint system and full containment seat. The details of this restraint system have been described in other publications. Each NASCAR vehicle is equipped with an onboard incident data recorder (IDR) which records tri-axial vehicle acceleration from the left mid frame rail.

A post impact vehicle and equipment inspection did not identify any equipment or system abnormalities which could be attributed to the driver's injuries. Investigation focus was shifted to the seat pan geometry and the driver's abdominopelvic orientation in the seat.

METHODOLOGY

The injury investigation consists of two primary elements. First magnetic resonance imaging (MRI) of the driver and a surrogate where conducted in standing and seated positions. Figure one shows a seated surrogate in the upright MRI. The purpose of the MRI imaging is to quantify the orientation of the pelvis and spine in two different seated motorsport driving positions. In the second element of the investigation this quantitative pelvis and spine geometry will be used to confirm the positioning of the Toyota Total Human Model for Safety (THUMS). Impact simulations will be conducted varying the fore-aft pelvis orientation in the seat, the seat pan ramp angle, the preload on the seat belt restraint system, and the crash pulse severity and direction.

Figure 1: Seated surrogate in upright MRI

RESULTS

Initial MRI scans have been completed with a surrogate in a standing and two seated positions. Improvements will be made to the MRI coil placement and seating configuration before attempting subsequent scans.

CONCLUSIONS

This research is ongoing and will begin THUMS simulations in the summer of 2016.

ACKNOWLEDGMENTS

The author would like to thank Dr. Joel Stitzel, Dr. Jerry Petty, Byran Harmon, Dr. John Greenhalgh and the many other people from NASCAR, Carolina NeuroSurgery & Spine, FONAR and Wake Forest CIB who have helped and provided guidance on this project.

NON-VIRAL GENE DELIVERY UTILIZING IMIDAZOLIUM-CONTAINING POLYESTERS

Allison M. Pekkanen[1], Ashley M. Nelson[2], Ryan J. Mondschein[2], and Timothy E. Long[1,2]
1. School of Biomedical Engineering and Sciences, Virginia Tech, Blacksburg, VA 24061
2. Department of Chemistry, Macromolecules Innovation Institute, Virginia Tech, Blacksburg, VA 24061
Corresponding Author: Name, Email: apekk@vt.edu

INTRODUCTION

Gene delivery is a promising therapeutic option for the treatment of a wide variety of diseases involving mutated or missing genes, and therapeutic options to treat these diseases must be improved. The most common non-viral gene delivery vehicles are positively charged polymers, dendrimers, and micelles, but many are plagued with cytotoxicity due to the high concentration of positive charge. In this work, a novel imidazolium diol is synthesized and utilized to create a series of polyesters of varying charge content and varying charge density.

METHODOLOGY

Melt polycondensation of imidazolium diol, neopentyl glycol, and adipic acid is performed with a temperature ramp of 150 °C for 12 h, 200 °C for 12 h, and finally 200 °C plus 0.2 mbar vacuum for 6 h. The polymers are analyzed for thermal transitions via differential scanning calorimetry. Cell studies utilizing HeLa human cervical cancer cells are performed via CellTiter Glo® assay to measure cell viability and a luminescence assay to evaluate transfection efficiency.

RESULTS

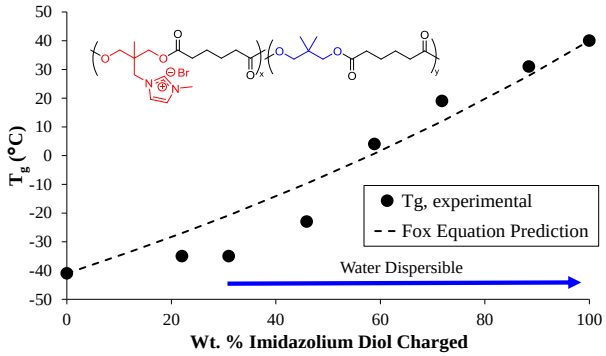

Figure 1. The T_g of imidazolium-containing copolyesters increasing with increasing charge content.

As the content of imidazolium diol is increased, the polymers exhibit and increase in the T_g as well as imparted water solubility above 30 wt % imidazolium diol, as shown in Figure 1. Following confirmation of cell compatibility, transfection efficiency was measured with HeLa cells, the results of which are shown in Figure 2. While the imidazolium copolyesters fall short of commercial standards in terms of transfection efficiency, they still exhibit successful transfection at low N/P ratios.

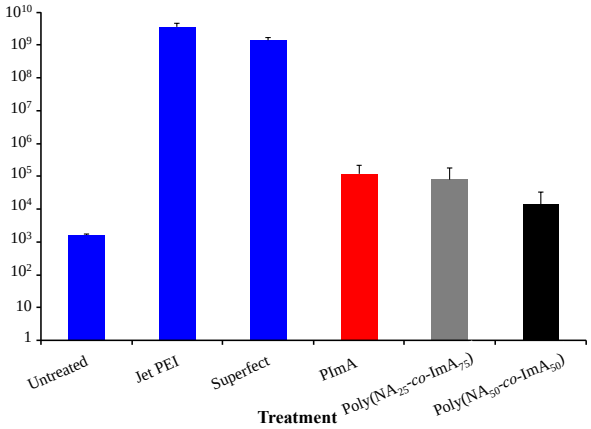

Figure 2. Imidazolium copolyesters show significant increase in luciferase as compared to untreated controls.

CONCLUSIONS

A novel imidazolium diol was used to create charged polyesters that successfully transfect HeLa cells. These polyesters have the ability to improve dramatically on the gold standard gene delivery vectors through their enhanced colloidal stability and their lack of cytotoxicity.

REFERENCES

Kabanov, A. V.; Felgner, P. L.; Seymour, L. W. *Self-Assembling Complexes for Gene Delivery: From Laboratory to Clinical Trial*; Wiley, 1998.

EFFECTIVE ATOMIC NUMBER AND ELECTRON DENSITY OF THE IODINE-BASED CONTRACT AGENT COMPOUNDS OF THE VARYING CONCENTRATION IN THE DIAGNOSTIC X-RAY RANGE

Authors: Olga V. Pen[1], Guohua Cao[1]
1. Virginia Polytechnic Institute and State University, School of Biomedical Engineering and Sciences
Corresponding Author: Olga V. Pen, Email: olgapen@vt.edu

INTRODUCTION

The Z_{eff} (effective atomic number) and ρ_{el} (electron density) of the material are important parameters that describe the materials' physical properties and its X-ray and gamma interaction and might aid in materials' differentiation when the traditional attenuation-based imaging does not provide enough contrast. However, a single number is not sufficient to fully characterize Z_{eff} and ρ_{el} of the material. A curve that describes the changes in the Z_{eff} for a particular chemical mixture over a certain range of x-ray energies, particularly the energies used for diagnostic purposes (20-120 keV), might be more helpful in identifying the material or compound.

With the recent emergence of the energy-discriminative detectors, a single scan with a readily available polychromatic x-ray beam is sufficient in order to obtain a necessary number of comparison points.

Iodine, as the commonly used contrast agent, has been chosen as an object of the study for the purposes of more precise measurement of the variation of the iodine concentration in the blood pool of the small animals.

METHODOLOGY

After obtaining the mass attenuation coefficient $\frac{\mu}{\rho}$ via the experimental measurements, we can calculate the atomic cross-section σ_i of each i-th element of the compound of interest [2]:

$$\sigma_i = \frac{A_i}{N_A}\left(\frac{\mu}{\rho}\right)_i \quad (1)$$

Where A_i is the atomic mass, and N_A is Avogadro number.

The effective atomic number Z_{eff} can be calculated as:

$$Z_{eff} = \frac{\sum_i n_i A_i \left(\frac{\mu}{\rho}\right)_i}{\sum_j n_j \frac{A_i}{Z_j}\left(\frac{\mu}{\rho}\right)_j} = \frac{\sum_i n_i \sigma_i}{\sum_j n_j \frac{(\sigma)_j}{Z_j}} \quad (2)$$

And the electron density ρ_{el} then is calculated as:

$$\rho_{el} = N_A \frac{nZ_{eff}}{\sum_i n_i A_i} \quad (3)$$

The series of Z_{eff} for different energies are acquired and the resulting curve is then compared to the theoretical database [2] until the match is found.

RESULTS AND CONCLUSION

The theoretical calculation of Z_{eff} dependency on the energy in the x-ray diagnostic energy range results in the curve of a shape specific to the material or compound. The number stabilizes at higher energies as the Compton Effect becomes prevalent.

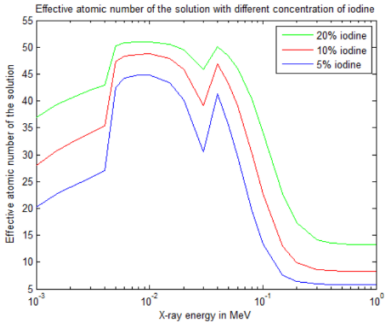

Figure 1: Z_{eff} of iodine-water solutions of different concentrations over 1 KeV – 1 MeV range

Further study will provide the experimental Z_{eff} values for the iodine contrast agents of varying concentration, allowing matching of the experimentally obtained results to the particular curve.

REFERENCES

1) Manohara, S. R., et al. (2008):
2) NIST XCOM Database

Poster,B
Atrium, 11:45

Virginia Tech
Wake Forest University
School of Biomedical Engineering and Sciences
15th Annual Graduate Student Research Symposium, May 11, 2016

RHEOLOGICAL DIFFERENCES BETWEEN BUFFER DIALYZED AND WATER DIALYZED KERATOSE FILMS

Nils A. Potter[1], Mark Van Dyke[1]
1. Virginia Tech Department of Biomedical Engineering and Mechanics
Corresponding Author: Nils Potter, Email: npotter2@vt.edu

INTRODUCTION

Keratin proteins are instrumental in the structural integrity of hair follicles by providing strength and shape, and have been used as structural proteins for biomaterials. Hair keratins are often extracted through oxidation or reduction of hair fibers, which results in solubilization of Keratose (KOS) or Kerateine (KTN), respectively [1]. Purifying keratins includes a dialysis step, and it was recently determined that excessive aggregation confounds this process and that certain buffer solutions may be better suited for keratin purification than water. Keratin sample purity is therefore effected, which has implications for network formation and mechanical properties of hydrogels. Therefore, the rheological properties of KOS prepared by these purification methods was investigated.

METHODOLOGY

20 wt% KOS hydrogels were created using buffer dialyzed and MQ water dialyzed KOS. Both samples were hydrated in MQ water and crosslinked with 1,4-butanediol diglycidyl ether (BDDE) at 20 wt% relative to the KOS. Samples were pipetted into silicone molds and allowed to cure for 72 hours at 25°C. The ARG2 Rheometer (TA Instruments) was used to obtain shear properties by using a 25 mm diameter parallel plate geometry. Stress sweep tests from 0.1-600 Pa at 1 Hz were to obtain a stress value within the linear viscoelastic region (LVER) and used for frequency sweep tests.

RESULTS

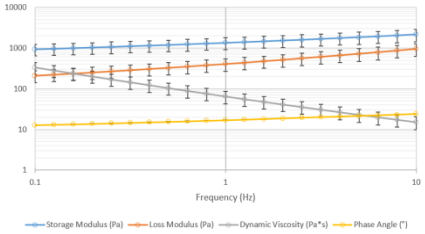

Figure 1: Frequency Sweep of MQ Water Dialyzed KOS

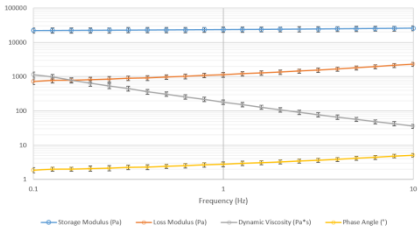

Figure 2: Frequency Sweep of Buffer Dialyzed KOS

Stress values of 25 Pa were used for both frequency sweep tests as they resided on both hydrogels' LVER.

CONCLUSIONS

The collected data reveals that the buffer dialyzed KOS samples result in storage moduli (G') 20x greater than that of MQ dialyzed KOS. Similar trends are observed with loss moduli (G") and dynamic viscosity (η') at a scale of 3x. Phase angle (δ) differences suggest buffer dialyzed hydrogels have a more robust structure since the stress stimulus and strain response are nearly synced with each other whereas the MQ water dialyzed hydrogels introduce a slipping factor.

ACKNOWLEDGMENTS

The authors acknowledge Dr. Rick Davis for generously allowing the use of the ARG2 Rheometer. Funding was provided by BEAM departmental and overhead funds.

REFERENCES

[1] Hill P, Brantley H, Van Dyke M. Some properties of keratin biomaterials: kerateines. Biomaterials 2010;31(4):585-93.

Virginia Tech
Wake Forest University
School of Biomedical Engineering and Sciences
15th Annual Graduate Student Research Symposium, May 11, 2016

TUMOR ORGANOIDS IN AN ULTRA-THIN MICROFLUIDIC SYSTEM FOR *IN SITU* DRUG RESPONSE TESTING

Shiny Amala Priya Rajan[1], Parker Hambright[2], Aleksander Skardal[1,3, 4], Adam, R Hall[1,2,3, 4]
1. Virginia Tech –Wake Forest School of Biomedical Engineering and Sciences, 2. Wake Forest University, 3. Wake Forest Institute for Regenerative Medicine, 4. Comprehensive Cancer Center of Wake Forest
Corresponding Author: Adam R. Hall, Email: arhall@wakehealth.edu

INTRODUCTION

Realizing effective treatments for cancer is dependent on understanding the mechanisms of disease initiation and progression as well as the effect of various chemotherapeutic drugs. Animal models are complex and may not translate to humans, and so *in vitro* models are attractive. However, conventional 2D cell culture models have had only limited capacity to recapitulate the tumor microenvironment and have failed to accurately replicate patient physiology[1]. 3D cell cultures can overcome many of these challenges by mimicking the *in vivo* system more accurately[2]. These models can closely imitate the 3D mechanics of tissue[1], reproduce oxygen gradient-inducing hypoxia in tumors[2], and replicate cell proliferation rates in primary tumor growth[3]. Two major challenges, are reproducing the complexities of multi-domain *in vivo* tumors and parallel testing of these models with chemotherapeutic drugs.To address these challenges, we have developed a microfluidic platform in which multi-domain 3D cellularized constructs can be formed *in situ* to study the effects of drug treatment.

METHODOLOGY

Our devices are fabricated using a low-cost approach[4] by layering thin, patterned adhesive membranes between microscope slides with ports for fluid delivery. Tumor models are produced simultaneously in multiple, parallel chambers by patterning a mixture containing UV photopolymerizable hydrogel, extracellular matrix extract, and target cells directly in the device using a photo-mask. After flushing with clean buffer, discrete 3D cell cultures of defined shape and size are left in the chamber. .

RESULTS

In our preliminary experiments, we demonstrate an ability to form 3D tumor organoid of diameter 800µm and thickness of 100 um. Live-dead staining provides an initial metric for *in vitro* drug effects. We observe an increase in dead human colon carcinoma (HCT116) cells concomitant with the concentration of a chemotherapeutic drug, 5-Fluorouracil (5-FU). Cell cultures are viable for at least 7 days and we are also able investigate cell motility. These results demonstrate the efficacy of our system to probe target cells quantitatively in parallel 3D culture.

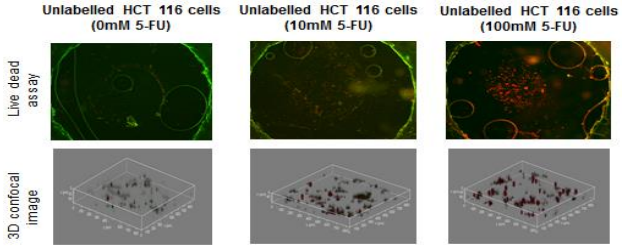

Figure 1: Top: Live-dead analysis on HCT116 cancer cells exposed to indicated 5–FU concentrations on day 7. Green are live cells and red are dead. Bottom: 3D confocal stack reconstructions of corresponding images.

CONCLUSIONS

We have developed a microfluidic platform containing ultra-thin tumor organoids that can be used for parallel testing of multiple tumor constructs in a single device. We can study the motility and viability of tumor cells under the influence of chemotherapeutic drug. As long-term goal, this tool will be expanded to a patient-specific test module for in situ assessment of drug dosing to improve treatment design.

ACKNOWLEDGMENTS

We thank Steve Forsythe, Mahesh Devarasetty and Dr. Philip Brown for their contributions to this project.

REFERENCES

1. Loessner, et al. Biomaterials 31(32):8494-506, (2010).
2. Imamura, et al. Oncol Rep 33(4):1837-43, (2015).
3. Lee, et al. Lab Invest 93(5):528-42, (2013).
4. Cooksey, et al. Lab Chip14(10):1665-1668, (2014)

Poster,B
Atrium, 11:45

EFFECT OF HYALURONAN SYNTHASE KNOCKOUTS ON QUASI-LINEAR VISCOELASTIC PROPERTIES OF MOUSE ACHILLES TENDON

Kristen Renner[1], Katie Trella[2], Anna Plaas[2], Vincent M. Wang[1]
1. Virginia Tech, SBES
2. Rush University Medical Center, Chicago, IL
Corresponding Author: Kristen Renner, Email: hulbertk@vt.edu

INTRODUCTION

Hyaluronic acid (HA) has several biological functions such as the prevention of cellular damage and the regulation of proliferation and migration[1]. Exogenously applied HA has been shown to promote tendon healing and decrease adhesion formation following acute injury[2]. HA synthesis *in vivo* is catalyzed by a group of transmembrane proteins, the hyaluronan synthases (Has), of which there are three isoforms in mammalian cells. The current study examines the effect of Has1, Has3, and Has1/3 deletion on the viscoelastic properties of the Achilles tendon.

METHODOLOGY

Achilles tendons were harvested from 4 genotypes of male 12-week C57BL/6 mice. The genotypes included wild type (WT), HAS1-KO, HAS3-KO, and HAS1/3-DKO. Tensile testing was conducted using an MTS Insight 5 Materials Testing System **(Figure 1)** under a stress relaxation protocol. Each tendon was preloaded to 0.05N for 2 minutes before being loaded to 5% strain at 0.3 mm/sec for 10 minutes.

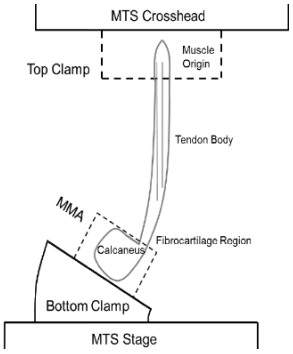

Figure 1: Side view of the testing setup[6]

Tensile stress relaxation was modeled using Fung's quasi-linear viscoelastic (QLV) formulation[3]. This model yields coefficients A (elastic stress constant) and B (elastic exponential power constant); C is the relaxation index, τ_1 is the short relaxation time constant and, τ_2 is the long relaxation constant. To facilitate determination of τ_2 the stress relaxation data was extrapolated to equilibrium using an equation validated by Huang et al[5].

RESULTS

There was no significant difference across genotypes for any of the parameters, although there was a strong trend (p=0.054) towards increased *C* in HAS1/3-DKO relative to wild type tendons. Values for A, C, τ_1 and τ_2 are similar to those reported for mouse tail and rat Achilles tendons[4,6].

Table 7: Summary of QLV Fitting for Achilles Tendon

Genotype	A	B	C	τ_1	τ_2
HAS1KO	3.22±0.71	8.63±0.98	0.23±0.17	0.17±0.08	595.90±5.83
HAS3KO	3.09±1.16	8.41±2.10	0.16±0.05	0.21±0.12	578.50±55.96
HAS1/3DKO	2.72±1.31	8.31±2.28	0.22±0.08	0.13±0.11	565.60±51.53
WT	3.12±1.22	9.47±2.10	0.14±0.05	0.18±0.14	593.80±10.50

CONCLUSIONS

Prior studies have shown that deletion of Has1 or Has3 significantly reduced maximum stress (as determined from load to failure experiments) relative to WT Achilles tendons[7]. However, at 12 weeks of age the tendons do not show statistical differences in QLV parameters across the four genotypes. Future research will include the evaluation of mice at 4 and 8-weeks of age to determine if growth and development impacts the elastic and viscoelastic properties of tendons.

REFERENCES

[1] Liang, J-I, et al., *J Mater Sci: Mater Med* (2014) 25:217-227. [2]Tanaka T, et al., J Hand Surg Am 2007;32(6):876–81 [3] Fung YCB. Biomechanics: Its foundations and objectives. 1972. pp. 181–208.[4]Elliott, DM et al., *Ann Biomed Eng* (2003) 31:599-605. [5]Huang, C et al., *J Biomech* (2005) 38(4): 799-809. [6]Plate, J et al., *J Biomech* (2013) 46:450-455. [7]Trella KJ et al., Podium presentation at International Society for Hyaluronan Sciences, 2015.

ACKOWLEDGEMENTS: NIH R01 AR63144 (VMW)

Virginia Tech
Wake Forest University
School of Biomedical Engineering and Sciences
15th Annual Graduate Student Research Symposium, May 11, 2016

HYALURONIC ACID CHARACTERIZATION USING SOLID STATE NANOPORES

Felipe Rivas[1], Adam R. Hall[1], Elaheh Rahbar[1]
1. Virginia Tech-Wake Forest School of Biomedical Engineering, Wake Forest University School of Medicine
Corresponding Author: Elaheh Rahbar, Email: erahbar@wakehealth.edu

INTRODUCTION

Hyaluronic Acid (HA), has emerged as a reliable biomarker for early diagnosis of osteoarthritis[1], as well as an indicator of wound healing[1] and repair mechanism. HA is a polysaccharide, composed of the disaccharide repeated unit of N-acetylglucosamine and D-glucuronic acid. It is highly hydrophilic and has a predominantly negative charge at physiological pH. HA has different physiological functions based on its size. Current methods to measure HA are costly and time consuming. Given HA's role as a biomarker with diagnostic potential, there is a need for quick and effective detection and quantification method. In this study, we propose a novel method to detect both High molecular weight-HA and Low molecular weight -HA based on its electrophoretic movement across the nanometer-scale opening of a SiN solid-state (SS-) nanopore.

METHODOLOGY

A single nanopore SS-membrane with a 5 nm diameter, as described by Hall et. al[2] was used to separate two electrically isolated chambers denoted as cis- and trans-chambers. 3 M LiCl and 10mM EDTA buffer solution was added to the trans-chamber while the same solution with 2μM of purified monodisperse HA of 100 kDa was added to the cis-chamber. A 200 mV was applied across these two chambers generating an electric field gradient capable of translocating the HA molecules. Temporary interruptions ("events") in the electrical current signal (due to HA translocation) were recorded using custom software. Similar current readings were obtained at 400 and 600 mV at a bandwidth of 100 kHz rate with a low-pass filter of 30 kHz. Event rate at each voltage reading was obtained as well as average event duration. Events were defined as changes in conductance (nS) $\geq 5*\sigma$ from baseline, with dwell times ranging from $10 \leq t \leq 2000$ μs.

RESULTS

Our initial goal is to determine the event rate and dwell time for varying sizes of HA, for which we have purified monodisperse samples. Preliminary results with 100kDa HA show that there is a positive correlation in the number of events, with an increased applied voltage, as a higher driving EMF causes molecules to translocate more frequently. This verifies the ability of SS-nanopores to detect HA for the first time. However, average dwell time is not significantly different across voltage steps.

Table 1: Electrical Event Rate and average Dwell time of HA-B 100K Da, at different voltages (200mV, 400mV and 600mV).

Voltage (V)	Event Rate (Hz)	Std. Dev Event Rate (Hz)	Dwell Time (μs)	Std. Dev Dwell Time (μs)
0.2	0.008	0.022	35	0
0.4	0.040	0.026	51	42
0.6	0.227	0.032	47	81

CONCLUSIONS

Event rate scales with voltage, similar to measurements with DNA[3]. However, event dwell time is not significantly different across voltages. Optimal HA concentration in buffer solution is being tested for higher rate event occurance detection. The unchanging dwell time indicates most HA may translocate too fast to be resolved. Therefore, future approaches will be developed to reduce translocation speed to provide better read-out accuracy[3].

ACKNOWLEDGMENTS
Dr. Elaheh Rahbar and Dr. Adam Hall and their funding sources that support this project.

REFERENCES

1. Necas, J. Veterinarni Medicina.2008, 53, 397–411.
2. Yang, J., et al. Nanotechnology.2011, 22, 285310.
3. Kowalczyk, S. W., et al. Nano Lett. 2012, 12, 1038–1044

Poster,B
Atrium, 11:45

IRREVERSIBLE ELECTROPORATION AND HIGH-FREQUENCY IRREVERSIBLE ELECTROPORATION FOR THE TREATMENT OF OVARIAN CANCER

Andrea Rolong[1], Eva M. Schmelz[2], and Rafael V. Davalos[1]
1. Virginia Tech – Wake Forest University School of Biomedical Engineering and Sciences
2. Virginia Tech, Department of Human Nutrition, Foods, and Exercise
Corresponding Author: Andrea Rolong, Email: andrear2@vt.edu

INTRODUCTION

Ovarian cancer is the fifth leading cause of cancer-related deaths in women in the United States. An estimated 22,280 women will receive a new diagnosis of ovarian cancer and approximately 14,240 patients will die from the disease in 2016, according to the American Cancer Society. Irreversible electroporation (IRE) is a non-thermal ablation technique with the capability to treat otherwise inoperable tumors. One of the main characteristics that sets IRE apart from the more commonly used ablation modalities such as cryoablation, radiofrequency, high intensity focused ultrasound, microwave, and laser, is its non-thermal mechanism for inducing cell death; IRE uses a series of short (≈100μs), high-intensity pulsed electric fields (PEFs) to destabilize the cellular membrane, which in turn disrupts homeostasis and leads to cell death [1]. Recently, the next generation platform known as high frequency irreversible electroporation (H-FIRE) has emerged with the potential to target cancerous cells over healthy ones [2].
Even though IRE has been gaining attention due to its success in treating tumors with intricate morphologies such as cancers of the pancreas, liver, kidney, and prostate, the potential of this technique to treat ovarian cancer has not been fully investigated. The work presented here used a syngeneic murine ovarian cancer model representative of different stages of the disease [3] and comprises the first study to evaluate the use of H-FIRE to treat ovarian cancer.

METHODOLOGY

Three dimensional tumor models in collagen I were used to determine cell death threshold from IRE and H-FIRE. The death region was imaged by fluorescent microscopy where live cells express enhanced green fluorescent protein (eGFP) and dead cells do not. Lesion sizes were measured and compared to numerical models developed in COMSOL Multiphysics 4.3a to correlate the lesion size to the electric field induced in that region as described by Arena et al [4].

RESULTS

Both IRE and H-FIRE successfully killed ovarian cancer cells in the 3D tumor constructs which showed no recurrence of cancer cells within the death region for more than 7 days post-IRE treatment while maintained in proper cell culture conditions. It was also shown that the highly aggressive tumor-initiating cells (TICs), which have been found to be resistant to chemotherapy and other more commonly used treatment options, have similar susceptibility to IRE and H-FIRE as malignant tumor cells.

CONCLUSIONS

IRE, and particularly H-FIRE, comprise a new treatment modality that offers great potential to successfully treat ovarian cancer as they use short, high-intensity electric pulses to kill cells without damaging neighboring vital structures. Results showing the ability of IRE and H-FIRE to kill highly resilient TICs indicate the potential to completely eradicate both local disease and micrometastases thus preventing the need for complete organ resection which would render the patient sterile.

ACKNOWLEDGMENTS

This work was supported by the NSF IGERT DGE-0966125 (MultiSTEPS, now BIOTRANS)

REFERENCES

1. Davalos, R.V., et al., Ann Biomed Eng, 2005.
2. Ivey, J.W., et al., Sci Rep, 2015.
3. Roberts, P.C., et al., Neoplasia, 2005.
4. Arena, C.B., et al., Biophys J, 2012.

MULTI-CENTER ANALYSIS OF CIREN OCCUPANT LUMBAR BONE MINERAL DENSITY AND CORRELATION WITH AGE AND FRACTURE INCIDENCE

Mona Saffarzadeh [1,2], R. Caresse Hightower [1,2], Anna N. Miller, MD [3], Joel D. Stitzel, PhD [1,2]; Ashley A. Weaver, PhD[1,2]
1. Biomedical Engineering Wake Forest University School of Medicine Winston-Salem, NC, United States
2. Wake Forest School of Medicine, Medical Center Blvd, Winston-Salem, NC, 27157, USA
3. Orthopaedic Surgery Wake Forest University School of Medicine, Winston-Salem, NC, United States
Corresponding Author: Mona Saffarzadeh, Email: msaffarz@wakehealth.edu

INTRODUCTION

Quantification of bone mineral density (BMD) is important in injury causation analysis. This study aimed to quantify bone mineral density (BMD) for 873 seriously injured Crash Injury Research and Engineering Network (CIREN) occupants from 8 centers using phantom-less CT scans and to correlate BMD to age, fracture incidence, and osteopenia/osteoporosis diagnoses.

METHODOLOGY

A validated phantom-less CT calibration method that uses patient-specific fat and muscle measurements was applied on 873 occupants. CT-measured lumbar BMD <145 mg/cc is indicative of osteopenia using a published threshold [1]. CIREN occupant lumbar BMD in mg/cc was correlated with age, osteopenia/osteoporosis comorbidities, height, weight, body mass index (BMI), and the incidence of vertebral and rib/sternum fractures.

RESULTS

Among the 873 occupants, 134 occupants were classified as osteopenic in BMD analysis. Of these 134 occupants, 60% were not classified as osteopenic in CIREN suggesting undiagnosed osteopenia, and 40% were correctly classified in CIREN. Age was negatively correlated with BMD ($p<0.0001$) and occupants with <145 mg/cc BMD sustained an average 2.1 additional rib/sternum fractures (2.3 versus 4.4 rib/sternum fractures, $p<0.0001$). Vertebral fracture analysis revealed that a greater proportion of occupants with <145 mg/cc BMD, sustained thoracolumbar (24% versus 17%), lumbar (16% versus 13%), and thoracic (10% versus 6%) vertebral body fractures (Figure 1).

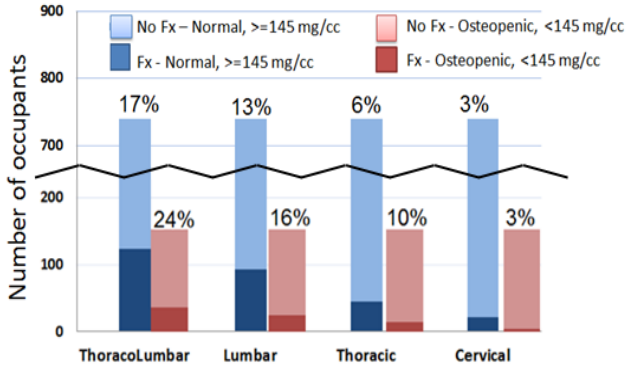

Figure 1. Proportions of vertebral fractures compared between the occupants with >=145 mg/cc and <145 mg/cc lumbar BMD values shown in blue and red bars respectively.

CONCLUSIONS

Low bone quality is associated with an increased number of rib/sternum fractures and a greater incidence of thoracolumbar, thoracic, and lumbar vertebral fractures in this study. The phantom-less technique could potentially be used in place of DXA in the future, resulting in decreased healthcare costs.

ACKNOWLEDGMENTS

Funding was provided by the National Highway Traffic Safety Administration under Cooperative Agreement Number DTN22-10-H-00294.

REFERENCES

[1] Weaver, A.A. et al., J Traffic Inj. Prevention, 16:S153-60, 2015.

Virginia Tech
Wake Forest University
School of Biomedical Engineering and Sciences
15th Annual Graduate Student Research Symposium, May 11, 2016

CHARACTERISTICS OF CHILD FATALITIES IN US MOTOR VEHICLE CRASHES FROM 1995-2013

Lianne M. Sandberg[1], H. C. Gabler[1]
1. Virginia Tech (SBES, BEAM)
Corresponding Author: Lianne M. Sandberg, Email: sandberg@vt.edu

INTRODUCTION

Motor vehicle crashes remain a leading cause of injury and death among children in the United States. While the motor vehicle fatalities among children aged 12 and under have decreased considerably since 1995, traffic related incidents are responsible for approximately 1,000 children continue to die in the US each year. During the 19 year period between 1995 and 2013 children 12 and younger accounted for an average of 4% of the total fatalities yearly. While this is a small percentage overall, these fatalities are preventable and child fatalities carry a very large social and economic burden on society.

The objective of this study is to investigate the epidemiology of child fatalities which resulted from MVCs in the US from 1995 – 2013 in order to identify specific crash characteristics that lead to child fatalities. Specifically, this study analyzes the distribution of child fatalities as a function of crash mode, seating position, age, restraint, and vehicle type.

METHODOLOGY

The study is based upon the analysis of 29,172 US crashes which involved fatally injured children 12 and under from 1995-2013. Fatality records were extracted from the Fatality Analysis Reporting System (FARS) database. FARS is a census of all traffic fatalities which occur in the US. Included were child passengers, pedestrians, bicyclists and drivers. The dataset included a total of 19,608 children who were occupants of cars or light trucks and vans (LTV) only.

RESULTS

From 1995-2013 child fatalities decreased by 57% overall. Frontal and rollover crashes were the most common fatal crash modes accounting for 32% and 34% of fatally injured children in 2013. While child fatalities decreased overall, the proportion of child fatalities in rollover accidents increased from 28% in 1995 to 34% in 2013. The proportion of child fatalities in the front seat declined from 1995 (38%) to 2013 (18%). During this same time period, the proportion of fatalities in the back seat increased from 52% to 74%. This shift in the fatality distribution from the front seat to the back seat may have resulted from child-friendly advanced airbags being installed in increasing numbers in the fleet or simply because children were more likely to be seated in the back seat in 2013 than in 1995. Restraint usage was an important factor associated with child fatalities. The majority of fatally injured children (43%) were unbelted. It is encouraging that the fraction of child fatalities occurring while unrestrained has decreased over time. Infants regardless of seating position comprised the highest fraction of all fatally-injured children (10%).

CONCLUSIONS

Overall child fatalities have decreased despite the fact that adult fatalities have remained nearly constant over the 19 year period. Efforts to reduce child front seat fatalities appear to have been effective however children remain at risk in a number of areas. Rollovers account for an increasing fraction of fatally injured children. Children riding unrestrained are at considerable risk of fatality. Fatally injured children were most likely to be infants. This downward trend in child deaths is encouraging, but the socio-economic burden of child fatalities as a result of an MVC is still large and in many cases may be preventable.

Poster,A
Atrium, 11:15

Virginia Tech
Wake Forest University
School of Biomedical Engineering and Sciences
15th Annual Graduate Student Research Symposium, May 11, 2016

THE DESIGN OF IN VITRO TRANSITIONAL LIVER MODELS

Scott-Eugene Saverot[1], Padmavathy Rajagopalan[2, 3]
1. School of Biomedical Engineering and Sciences, Virginia Tech, Blacksburg, VA 24061, United States
2. Department of Chemical Engineering, Virginia Tech, Blacksburg, VA 24061, United States
3. ICTAS Center for Systems Biology of Engineered Tissues, Virginia Tech, Blacksburg, VA 24061, United States
Corresponding Author: Scott-Eugene Saverot, Email: ssaverot@vt.edu

INTRODUCTION

Hepatic fibrosis is the result of excessive extracellular matrix (ECM) accumulation in response to chronic liver injury.[1] The sustained wound healing response alters cellular phenotypes and leads to the increased production of ECM proteins. Continued perturbation leads to stiffer tissues, the distortion of hepatic architecture, increased blood flow resistance, and ultimately organ dysfunction.

The Space of Disse (SoD) is a protein enriched region which separates layers of cells in the liver. During fibrosis, up to a ten-fold increase of ECM proteins are deposited within the SoD, directly impacting the mechanical and chemical properties of the region.[1] In a positive feedback manner, cells respond to the altered matrix, become activated, and continue the inflammatory response.

Fibrosis occurs in multiple stages over the period of a few years, making it difficult to study *in vivo*. Over its course, many populations of healthy and fibrotic cells exist which can initiate, advance, or reverse these conditions. The interactions between these populations and the altered environment directly regulate fibrotic progression.

Using tunable polymeric biomaterials, the mechanical and chemical properties can be adjusted to match the properties of the cellular environment throughout fibrosis. Integrating these gradient materials with *in vitro* liver models will simulate different degrees of the transformed fibrotic environment.

METHODOLOGY

Detachable polyelectrolyte multilayers (PEMs) will be made through a layer-by-layer deposition of hyaluronic acid and type 1 collagen on poly-tetrafluoroethylene substrates. PEM thickness and Young's modulus will be modulated through the deposition conditions and degree of polymer crosslinking. A gradient of ECM proteins will be incorporated into PEMs.

Following my group's previously reported approach, primary hepatocytes will be cultured as a monolayer upon which a SoD mimicking PEM will be placed.[2] Thereafter, non-parenchymal cell types including: liver sinusoidal endothelial cells (LSEC), hepatic stellate cells (HSC), and Kupffer cells (KC) will be cultured upon the PEM to recapitulate the liver tissue structure (Figure 1).

Within transitional models, the response of each cell type will be investigated along the gradient of transformation. Hepatocyte response will be assessed through the production of urea and albumin. The expression of well-known pro-fibrotic markers and inflammatory cytokines will be monitored as well as the production and deposition of excess ECM proteins.

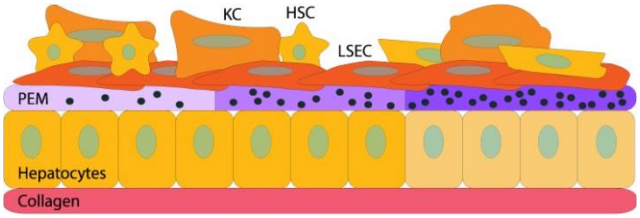

Figure 1: Schematic of a transitional liver model simulating three degrees of fibrotic transformation.

CONCLUSIONS

Transitional models permit the exploration of the complex cell-cell and cell-matrix interactions throughout hepatic fibrosis.

REFERENCES

1. Arias, I.M., et al., *The Liver: Biology and Pathology*, 5th Edition, 2009.
2. Larkin, A.L., et al., Tissue Engineering Part C: Methods, 2013.

Poster,B
Atrium, 11:45

THE POTENTIAL OF INTERSECTION DRIVER ASSISTANCE SYSTEMS TO PREVENT U.S. STRAIGHT CROSSING PATH INTERSECTION CRASHES

John M. Scanlon[1], Hampton C. Gabler[1]
[1.]Biomedical Engineering and Mechanics, Virginia Tech, Blacksburg, VA
Corresponding Author: John Scanlon, Email: john91@vt.edu

INTRODUCTION

Intersection crashes are among the most frequent and lethal crash modes in the U.S. each year [1,2]. One way to potentially prevent these crashes or mitigate associated injuries is through the use of an Intersection Advanced Driver Assistance System (I-ADAS). These systems can detect oncoming vehicles using onboard sensors and during crash imminent scenarios can alert the driver of a potential threat. Given that I-ADAS is only beginning to penetrate the U.S. market, there is a need to evaluate the potential effectiveness of these systems for designers, regulatory agencies, and consumers. The objective of this study was to estimate the number of straight crossing path (SCP) intersection crashes that could be prevented if every vehicle in the U.S. was equipped with I-ADAS.

METHODOLOGY

There were three main steps to this study's methods. The first step was to extract a simulation case set of real-world SCP intersection crashes from a U.S. national crash database. The second step was to reconstruct each vehicle's most likely kinematics, including impact speed, crash avoidance actions, intersection traversal, and intersection approach. The third step was to simulate these crashes as if the vehicle was equipped with an I-ADAS that alerts the driver of an imminent crash 2.0 s, 2.5 s, and 3.0 s prior to the impact.

RESULTS

This study used a simulation case set of 459 real-world, SCP intersection crashes. The results indicate that warning thresholds of 2.0 s, 2.5 s, and 3.0 s could prevent 19.1%, 32.3%, and 34.6% of U.S. SCP crashes, respectively. For about one-half of the crashes (45.1%), neither vehicle stopped prior to entering the intersection. Figure 1 shows how many crashes could be prevented for crashes where (a) no vehicle stopped and (b) at least one vehicle stopped.

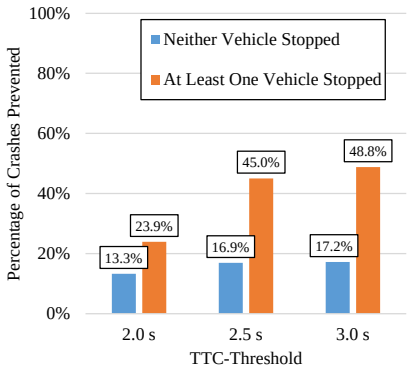

Figure 1: Crash prevention estimates by the pre-crash movements.

CONCLUSIONS

The crash prevention capabilities of I-ADAS were found to be strongly dependent on when the I-ADAS alert was delivered. The effectiveness of these systems is expected to depend on the stopping behavior of these vehicles prior to entering the intersection.

ACKNOWLEDGMENTS

This research was supported by Toyota Collaborative Safety Research Center (CSRC) and Toyota Motor Corporation.

REFERENCES

[1] K. D. Kusano and H. C. Gabler, "Target Population for Intersection Advanced Driver Assistance Systems in the US," *SAE International Journal of Transportation Safety*, vol. 3, pp. 1-16, 2015.
[2] K. D. Kusano and H. C. Gabler, "Comprehensive target populations for current active safety systems using national crash databases," *Traffic injury prevention*, vol. 15, pp. 753-761, 2013.

Virginia Tech
Wake Forest University
School of Biomedical Engineering and Sciences
15th Annual Graduate Student Research Symposium, May 11, 2016

DEVELOPMENT OF SUBJECT-SPECIFIC PROXIMAL FEMUR AND LUMBAR SPINE FINITE ELEMENT MODELS OF OBESE, OLDER ADULTS

Samantha L. Schoell[1], Ashley A. Weaver[1], Joel D. Stitzel[1], and Kristen M. Beavers[2]
1. Virginia Tech- Wake Forest Center for Injury Biomechanics
2. Wake Forest University, Department of Health and Exercise Science
Corresponding Author: Samantha L. Schoell, Email: sschoell@wakehealth.edu

INTRODUCTION

Advanced age and obesity are well-characterized risk factors for chronic disease and disability which can result in increases in individual and societal health burden associated with these conditions [1]. Recommendation of intentional weight loss in older adults remain controversial, due in part to loss of bone density known to accompany weight loss, and potential exacerbation of fracture risk [2]. The purpose of this study is to develop subject-specific finite element (FE) models of the proximal femur and lumbar spine and study the effect of intentional weight loss over 18 months in obese, older adults on bone strength and structure.

METHODOLOGY

Clinical computed tomography (CT) scans of the femur and lumbar spine of 55 obese, older adults undergoing an 18 month weight loss intervention were administered at baseline. 34 of those patients were administered CT scans post-intervention. Quantitative measures of vBMD of the total hip, femoral neck, and lumbar spine were obtained using N-vivo software (Image Analysis, Columbia, KY). High resolution cortical bone thickness measurements from the femur and the lumbar spine were obtained by segmenting each bone and then applying a validated algorithm that assumes a constant density for cortical bone to accurately estimate cortical thickness [3].

Model development of the subject-specific FE models involved homologous landmark collection and model morphing techniques to accelerate the development of the models. Homologous landmark collection involves image segmentation, atlas development, and image registration techniques to derive atlas and subject point clouds. The atlas models used include the GHBMC M50-O v4.4 femur and the Total HUman Model for Safety (THUMS) AM50 v4.01 lumbar spine. Model morphing was performed using thin-plate spline interpolation to accurately capture the subject-specific geometry. A cortical thickness mapping algorithm was developed to apply the cortical thickness measurements directly to the subject-specific FE models. Material properties were assigned based on empirical relations to vBMD for both the femur and lumbar spine. Bone strength will be estimated through simulation of boundary conditions such as one-legged stance and sideways fall configurations for the femur and uniaxial compression for the spine.

RESULTS

Example results of the morphing process and cortical thickness mapping are provided in Fig. 1.

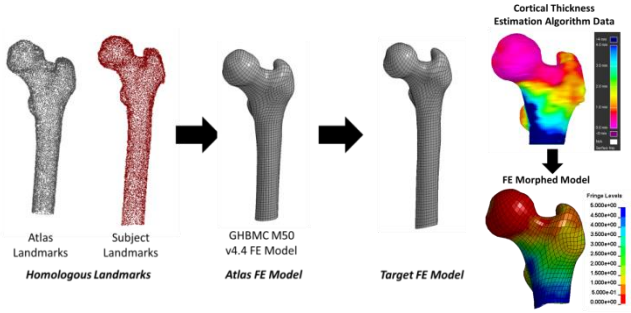

Figure 1: Morphing and cortical thickness results.

CONCLUSIONS

The development of subject-specific FE models of obese, older adults will lead to an improved understanding of the complex relationship between structural, compositional, and mechanical properties, and injury risk. Such models could be used clinically to improve the assessment of osteoporosis and fracture risk.

REFERENCES

[1] Wang YC et al., *The Lancet*, 378(9793), 2011.
[2] Waters DL et al., *Exp. Gerontology*, 48(10), 2013.
[3] Treece GM et al., *Med Image Anal*, 14(3), 2010.

Poster,B
Atrium, 11:45

LEADER CELL MIGRATION ON STEP NANOFIBERS

Puja Sharma[1], Amrinder S Nain[2, 1]
1. Virginia Tech, School of Biomedical Engineering and Sciences
2. Virginia Tech, Mechanical Engineering Department
Corresponding Author: Amrinder S Nain, Email: nain@vt.edu

INTRODUCTION

Single and collective cell migration are relevant to a myriad physiological events including embryogenesis, morphogenesis and diseased phenomenon like cancer metastasis[1,2]. The surrounding microenvironment composed of fibrous proteins and polysaccharides not only serve as sites for cell adhesion, but also provide biophysical and biochemical cues to facilitate cell migration processes. To obtain a better understanding of how the microenvironment dictates cell behavior, it is imperative that we investigate not just the biochemical, but also the biophysical components of the microenvironment. In this study, we utilize a previously used Spinneret based Tunable Engineered Parameters (STEP) technique to investigate the leader cell migration dynamics from monolayer and spheroid structures.

METHODOLOGY

Highly aligned polystyrene fibers of varying diameters (300-1000nm) were manufactured using the STEP technique. NIH3T3 fibroblasts were cultured using American Type Culture Collection (ATCC) recommended protocol and seeded onto raised platforms to form monolayers. As the cells interacted with the suspended fibers, time lapse videos were taken using Zeiss AxioObserver Z1 and analyzed using AxioVision software.

RESULTS

Cells from the monolayer started sensing the nanofibers and eventually migrated onto the fibers. Cells migrated in recoiling (Fig. 1A), chain and collective modes away from the monolayer. Recoiling cells exhibited an almost elastic behavior where their speed was proportional to change in cell length before and after detachment. Cells would initially protrude back and forth onto the fibers, extend their cell body, and detach like an elastic rubber band after severing cell-cell junctions with other cells in the monolayer or spheroid. On an average cells spend 120 minutes exploring the fibers before detachment. Average migration speeds of 428μm/hr and 111μm/hr were recorded for leader cells migrating away from the monolayer and spheroid (Fig. 1B) respectively. Cells spent less time protruding and exhibited higher detachment speeds when they migrated onto higher diameter fibers.

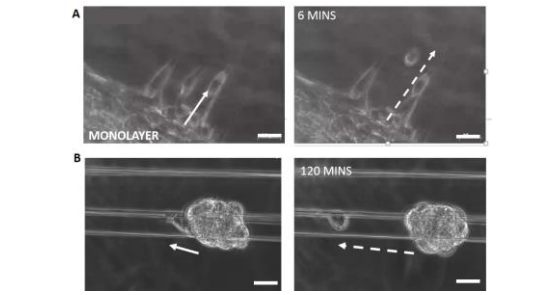

Figure 1. Time lapse video of a leader cell detaching from a monolayer (A), and a spheroid

CONCLUSIONS

Our results suggest that cells respond to changes in fiber curvature. In particular, we show that cells are more prone to detachment when interacting with micron diameter fibers when compared to nanoscale fibers. In future, the platform could be incorporated in microfluidic devices to probe the influence of biophysical and biochemical cues on cell detachment.

REFERENCES

1.Friedl, P. & Gilmour, D. Collective cell migration in morphogenesis, regeneration and cancer. Nat. Rev. Mol. Cell Biol. 10, 445–57 (2009).
2.Friedl, P. & Alexander, S. Cancer invasion and the microenvironment: plasticity and reciprocity. Cell 147, 992–1009 (2011).

DIFFUSION MODEL ACROSS A BLOOD-BRAIN BARRIER (BBB) MIMIC FOR THE TREATMENT OF AUTISM SPECTRUM DISORDER (ASD)

Jamelle Simmons[1], Luke Achenie[2,3], and Yong W. Lee[1,3]
1. Virginia Tech-Wake Forest, School of Biomedical Engineering and Sciences (SBES)
2. Virginia Tech, Department of Chemical Engineering
3. Virginia Tech Center for Autism Research (VTCAR)
Corresponding Author: Jamelle Simmons, Email: jmsimm13@vt.edu

INTRODUCTION

Autism Spectrum Disorder (ASD) is a neurodevelopmental disability defined by deficits in social interaction, communications, and restricted and repetitive interests. With the prevalence rates for ASD rising from 1 in 150 children and 2000 to 1 in 68 children in 2010 accompanied by healthcare costs in the billions the economic burden of the disorder and its prevalence are only expected to rise [1-5].

There is no single cause for ASD and factors such as environment, biology, and genetics can increase the risk for children making this a multifactorial problem [1]. One product of the intersection of these factors are documented increases in oxidative stress levels in brain tissue leading to neuronal loss. Previous work in our lab has documented elevated levels of reactive oxygen species (ROS), microglial activation, and neuronal loss in 3 week old male autism mice. The enzyme Xanthine Oxidase (XO) was found to be elevated in autism mice compared to controls. We hypothesize that the inhibition of XO in the brain will lead to a reduction in brain damage and improvements in behavior. The creation of computation models of drug diffusion across endothelial cells will enable us to predict how much drug to use in future animal studies.

METHODOLOGY

Human brain microvascular endothelial cells (HBMECs) were cultured in multi-well dishes until confluent. Monolayers were incubated with fluorescein isothiocyanate (FITC) for varying time durations and uptake quantified by fluorescence measurements. Partial Differential Equation (PDE) models were created and simulated to reproduce experimental results. The final model variables were extracted and used to predict future scenarios which are checked with validation data.

RESULTS

We have found that the coupling of the diffusion constant and depth of tracer penetration in our PDE model leads to a variety of solution scenarios.

CONCLUSIONS

With FITC serving as a model substitute for our non-fluorescent drug of similar molecular weight we are able to track and quantify the rate of diffusion into HBMEC cells. While running our PDE simulations we have to assume the cell thickness; the diffusion coefficient is obtained through parameter estimation using experimental data. We need to do additional validation studies of the estimated diffusion coefficient with new experimental data. The modeling assumes that the mode of transport is passive diffusion. Therefor if further validation studies fail we may need to revise the hypothesis to allow other mode of transport. For our model to have application in future work, we need to precisely measure the cell thickness the drug would have to diffuse across. Subsequently we would be able to simulate the length of time necessary to travel across the cell barrier as well as the concentration profile. The diffusion model would eventually all us to eliminate drug dosages that would not reach therapeutic levels in the brain and rule out dosage levels, which may be toxic.

REFERENCES

[1] http://www.cdc.gov/ncbddd/autism/facts.html [2] Lord, C., Cook, E., Leventhal, B., & Amaral, D. *Neuron, 28*, 355-363. [3] Levy, S., Giarelli, E., Lee, L., Schieve, L., Kirby, R., Cunniff, C., Rice, C. *Journal of Developmental & Behavioral Pediatrics, 31*(4), 267-275. [4] http://www.cdc.gov/ncbddd/autism/data.html[5] Lavelle, T., Weinstein, M., Newhouse, J., Munir, K., Kuhlthau, K., & Prosser, L. (2014). *Pediactrics*, E520-9.

Poster,B
Atrium, 11:45

Virginia Tech
Wake Forest University
School of Biomedical Engineering and Sciences
15th Annual Graduate Student Research Symposium, May 11, 2016

HEMOLYSIS-INDUCED PLATELET ACTIVATION OVER STORAGE TIME.

Kelli N. Simms[1], Martin Guthold[2] , Daniel Kim-Shapiro[2], and Elaheh Rahbar[1]
1. Wake Forest University, Biomedical Engineering
2. Wake Forest University, Physics Department
Corresponding Author: Kelli Simms, Email: ksimms@wakehealth.edu

INTRODUCTION

Storage of transfusion blood components has evolved, allowing packed red blood cells (RBCs) to be stored for 42 days and apheresis platelets up to 5 days.[1] Despite improvements, there is controversy over the use of "fresh" vs. "old" blood products. Previous studies have revealed a decline in morphology and function through hemolysis, storage lesions, contamination, and apoptosis.[2] Hemolysis of RBCs is a major contributor and has serious consequences through ADP-induced platelet activation. Recent findings from Kim-Shapiro's lab have reported that platelet activation may be caused by the adenosine diphosphate (ADP) bound to free hemoglobin (Hb).[3] ADP is a potent activator of platelets, activating three platelet receptors.[4] The effect of hemolysis-induced activation is important in the case when both stored RBCs and bagged platelets are transfused, since 1% hemolysis can potentially render a unit of platelets dysfunctional.[3] In this study we investigated the effect of hemolysis-induced platelet activation over the allotted 5 days of storage.

METHODOLOGY

Platelet rich plasma (PRP) was obtained from venous blood in citrated tubes and centrifuged at 110g for 15 min. 5µL was added to phosphate-buffered saline (PBS) and warmed at 37°C for 10 min. ADP or Hb was added (0.5 and 1mM concentrates) and warmed for 10 min. Platelets were labeled with Pac-1 (BD340507) and CD61 (BD340506) antibodies. The reaction was stopped using 1% formaldehyde. Platelet activation was determined using flow cytometry (BD FACS Calibur). PRP was stored at room temperature on a rocker for up to 5 days.

RESULTS

We observed a large decline in platelet function and activation over the 5 days. Hemolysis-induced platelet activation was significant compared to normal platelet function, and decreased steadily over time. These values were significant, with p-values less than 3%.

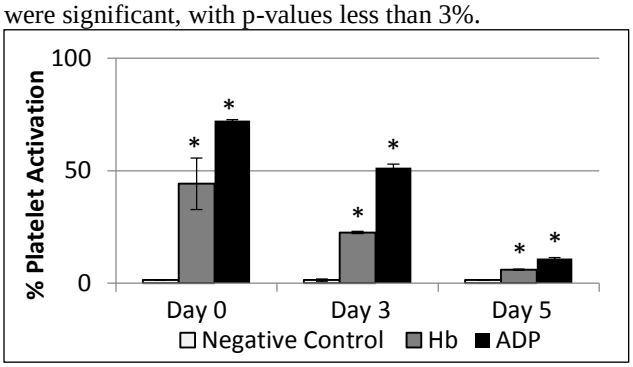

Figure 1: Days 0-5 platelet activation.

CONCLUSIONS

Most notable, there is a large decrease in platelet function over 5 days. In addition, hemolysis contributes to a significant amount of platelet activation, even at days 3 and 5. This is a potential concern as blood transfusions are often administered simultaneously and could render a unit of platelets useless. This data suggests that novel methods are needed to remove hemolysis from packed RBC bags. Future studies will aim to develop magnetic microparticles that can trap free-Hb from RBC bags.

ACKNOWLEDGMENTS

I would like to thank Dr. Elaheh Rahbar, Dr. Daniel Kim-Shapiro, and Dr. Martin Guthold for their contributions to this project. Funding was provided from Dr. Rahbar's start-up funds and grants from Dr. Kim-Shapiro.

REFERENCES

1. Centers for Disease Control and Prevention, 2011. 2. Tuo, WW et al. PLoS ONE. 2014. 3. Helms CC et al. J Thromb Haemo. 2013; 11: 2148-54. 4. Murugappa S, et al. Front Biosci. 2006; 11:1977-86.

Virginia Tech
Wake Forest University
School of Biomedical Engineering and Sciences
15th Annual Graduate Student Research Symposium, May 11, 2016

BIOMECHANICAL COMPARISON OF YOUTH AND ADULT FOOTBALL HELMETS

David W. Sproule[1] and Steven Rowson[1]
1. Virginia Tech, Biomedical Engineering and Mechanics
Corresponding Author: David Sproule, Email: dsproule@vt.edu

INTRODUCTION

Currently, youth football helmets, which are intended for players younger than 14 years old, undergo an identical impact testing protocol and are held to the same performance criteria as adult helmets in the NOCSAE safety standard. Although NOCSAE is in the process of developing a test standard specific to youth helmets,[1] there are many challenges in determining how a youth helmet standard should differ from an adult standard given the differences in head impact exposure, anthropometry, and physiology. This study aims to evaluate the relative impact performance of youth and adult helmets and relate it to on-field head exposure.

METHODOLOGY

Head impact data was collected for the Virginia Tech team and two youth football teams between the ages of 8-10 using the Head Impact Telemetry (HIT) System. These data were mapped to NOCSAE certification impact locations $\pm 15^0$ in the azimuth and elevation planes.[1] These on-field data was then compared to a series of drop tests utilizing a youth and adult Riddell Speed helmet. Each helmet underwent three rounds of drop tests at six impact locations (front, front boss, side, rear boss, rear, and top) and four drop heights (24, 36, 48, and 60 in.). Differences in the relative performance of the youth and adult helmets were also analyzed using a two-way ANOVA for helmet and location by height.

RESULTS

The distribution of the on-field HITS data at NOCSAE locations was similar for youth and adult (Figure 1). The only significant difference in the drop test comparison was in the front location at the 24 in. drop height. All the drop tests yielded high percentile (>90%) impacts, at all location and drop heights, in comparison to the on-field data for both youth and adult (Table 1). Only the front location is presented here.

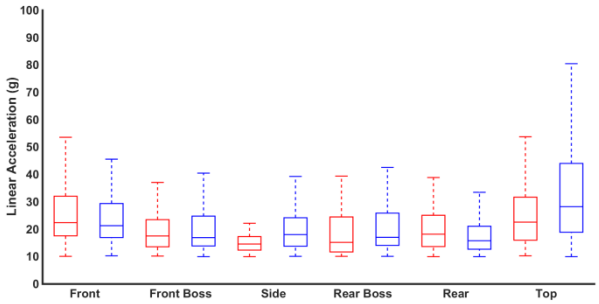

Figure 1: Distribution of on-field data for youth (red) and adult (blue) for NOCSAE locations

Table 8: Lab testing compared to on-field data as percentile of impact for the front location

Front	Acceleration (g)		Percentile	
	Youth	Adult	Youth	Adult
24 in.	53 ± 2	61 ± 5	*93.1%*	*97.5%*
36 in.	63 ± 4	72 ± 4	*97.5%*	*98.8%*
48 in.	88 ± 4	95 ± 2	*99.3%*	*99.7%*
60 in.	114 ± 2	123 ± 2	*99.9%*	*99.8%*

CONCLUSIONS

The on-field distributions were similar for the youth and adult data. Current standards involve impacts in the top 10% of on-field impacts. The youth and adult Riddell Speed helmets performed similarly in drop tests. These data have direct applications to future youth specific football helmet standards.

REFERENCES

1. NOCSAE. DRAFT-Standard Perfomance Specification for Newly Manufactured Youth Football Helmets. 2011.

Poster,B
Atrium, 11:45

NUMERICAL SIMULATION METHOD FOR INJURY PREDICTION IN AUTOMOTIVE CRASHES

Jeffrey Suhey[1], Derek Jones[1], Ashley Weaver[1], Joel D. Stitzel[1]
1. Virginia Tech-Wake Forest, Biomedical Engineering, Center for Injury Biomechanics
Jeffrey Suhey, Jsuhey@wakehealth.edu

INTRODUCTION

In order to capture crash-induced injury mechanisms on automotive drivers, computational finite element (FE) modeling of real world motor vehicle crashes (MVCs) was used in conjunction with crash reconstruction data. Results show that this methodology is robust and can be semi-automated.

METHODOLOGY

The parameters used to modify the SVM were the anthropomorphic test device position data, deceleration crash pulses from a specific New Car Assessment Program (NCAP) crash test, and vehicle interior property ranges. Once positioned, a simulation with an applied crash test pulse was generated. A nine variable Latin hypercube sample space with 120 simulations was created to change occupant safety and restraint properties. In order to choose the optimal set of restraint parameters, Sprague and Geers magnitude and phase error factors helped to reconstruct the Hybrid III's (HIII) kinematic and kinetic responses. With the vehicle tuned, the HIII was replaced with the Total HUman Model for Safety, and event data recorder pulses were applied in the simulation. Injury mechanisms were then assessed for the rib, sternum, and vertebrae of the occupant.

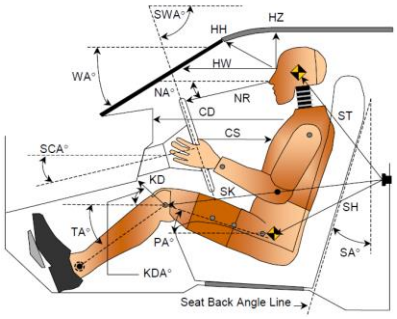

Figure 1: New Car Assessment Program (NCAP) Positioning Measurements.

RESULTS

The ATD responses in the NCAP test compared favorably to the simulation responses. The Sprague and Geers error factors were favorable and THUMS results showed variation of vertebral forces and moments (Figure 2) with adjusted seat parameters.

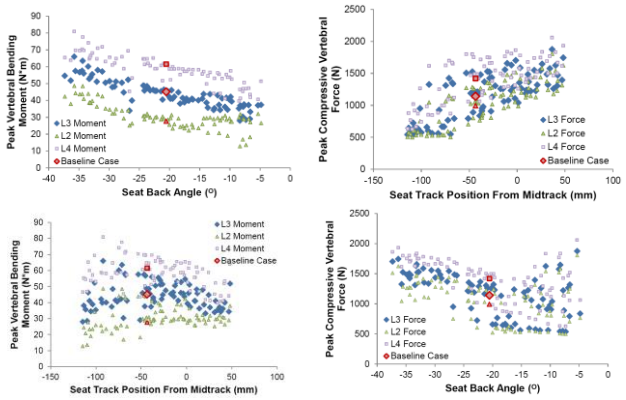

Figure 2: Vertebral Force and Moment with Varying Vehicle Parameters.

CONCLUSIONS

This numerical simulation method provides a useful, robust, and semi-automated approach to assessing injury prediction in automotive crashes. Predicting and understanding injury mechanisms aids in evaluating automotive safety and mitigating driver injury.

ACKNOWLEDGMENTS

Derek Jones, James Gaewsky, Dr. Ashley Weaver, and Dr. Joel Stitzel.

REFERENCES

Jones, D. : A Semi-Automated Approach to Real World Motor Vehicle Crash Reconstruction Using a Generic Simplified Vehicle Buck Model, Virginia Tech, Blacksburg VA, 2002.

HF-IRE TREATMENT INDUCES SYMMETRICAL ELECTROPERMEABILIZATION IN VITRO

Daniel C. Sweeney[1], Matej Reberšek[2], Janja Dermol[2], Lea Rems[2], Damijan Miklavčič[2], and Rafael V Davalos[1]
1. Department of Biomedical Engineering and Mechanics, Virginia Tech
2. Faculty of Electrical Engineering, University of Ljubljana
Corresponding Author: Daniel Sweeney, Email: sweeneyd@vt.edu

INTRODUCTION

High frequency irreversible elctroporation (H-FIRE) has been shown to mitigate undesirable muscle contraction during clinical treatments based on irreversible electroporation (IRE) [1]. We calculate the time course of the effective permeability of an electroporated cell based on real-time imaging of propidium transport. We conclude that bipolar pulses could be used for increasing molecular uptake into cells as efficiently as conventional monopolar pulses at the expense of higher applied voltages.

METHODOLOGY

Cells were seeded and incubated for two hours to adhere yet remain spherical. Platinum-iridium wire electrodes were used to apply electric fields to cells in a solution of low-conductivity buffer containing 10% propidium iodide.

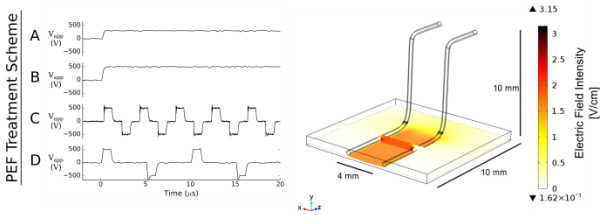

Figure 1: Electrical signals (left) were applied to the electrodes (right) to create generate electric fields

RESULTS

We performed real-time imaging of PI uptake to evaluate the effecacy of electroporation treatments. IRE-like treatments (A and B) generated asymmetric PI fluorescence between the anodic and cathodic poles. Cells exposed to high-frequency IRE-like treatment (C and D) experienced symmetric PI polar uptake, though to a lesser degree than treatments A and B. Treatment B resulted in a rapid uptake of PI that was not limited by membrane resealing, but rather diffusive equilibrium of PI to the intracellular binding sites (Figure 2).

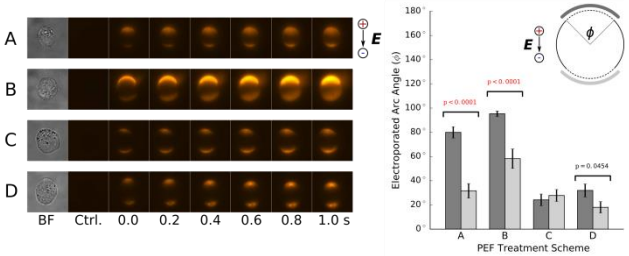

Figure 2: Cells show symmetric, lower level PI uptake at each pole under HF-IRE treatment compared to IRE.

CONCLUSIONS

HF-IRE waveforms may be utilized to permeabilize cells, though at the cost of significantly increased applied voltages because the electric field across the membrane does not reach steady state, as it does in conventional IRE [2]. This incomplete charging/assisted discharge mechanism that mitigates muscle contractions may similarly result in the increased threshold observed. At this expense, HF-IRE repeatably electroporates cells more evenly between the anodic and cathodic poles. [3]

ACKNOWLEDGMENTS

We would like to acknowledge NSF IGERT DGE-0966125 (MultiSTEPS), ARRS, and COST Action TD1104 for their support with these research efforts.

REFERENCES

[1] Arena et al., Biomed Eng Online. 2011 Nov 21;10:102.
[2] Arena et al., IEEE Trans Biomed Eng. 2011 May; 58(5):1474-82.
[3] Sweeney et al., 2016 (*in preparation*)

Poster,B
Atrium, 11:45

Virginia Tech
Wake Forest University
School of Biomedical Engineering and Sciences
15th Annual Graduate Student Research Symposium, May 11, 2016

THE EFFECT OF ROADSIDE BARRIER TYPE ON OCCUPANT INJURY SEVERITY IN MOTORCYCLE-TO-BARRIER COLLISIONS

Whitney M. Tatem[1], Ada H. Tsoi[1], Allison L. Daniello[1], and H. Clay Gabler[1]
1. Virginia Tech, School of Biomedical Engineering and Sciences, Blacksburg, VA
Corresponding Author: Whitney M. Tatem, Email: whitmt2@vt.edu

INTRODUCTION

The impact of roadside barrier type on the injury severity of motorcyclists has been hotly debated over the past few years. It is known that motorcycle collisions with roadside barriers yield more fatalities than accidents involving other vehicle collisions with the same barriers (1). Of particular interest within the motorcyclist community are cable barriers, which many believe to pose a higher risk of injury. However, to date, there has been little definitive evidence to either support or deny these suspicions. This ongoing study aims to both determine if motorcycle collisions with cable barriers do indeed pose a higher risk of injury than those with W-beam guardrails or concrete barriers and to define other significant crash characteristics in such motorcycle-barrier collisions.

METHODOLOGY

Crash sites and barrier type for each crash were located using either the police reported crash latitude and longitude or reported milepost in conjunction with Google Earth and Street View. Crashes were excluded if no barrier was observed, the barrier type was indeterminate, or no Street View images were available.

To date, this study has analyzed 4,031 motorcycle-barrier crashes involving 4,439 riders from 2002-2013 in AZ, FL, IL, MI, NC, OH, TX, and WA. There have been 2,625 W-beam guardrail collisions, 1,259 concrete barrier collisions, and 147 cable barrier collisions observed. In addition to differences between barrier types, the effects of number of passengers, rider age, road alignment, and crash speed were also investigated.

RESULTS

Of the riders involved in W-beam, concrete, and cable barrier collisions with known injury severity, 42.1%, 38.8%, and 36.0% sustained fatal or incapacitating injuries, respectively. The odds of severe injury in cable barrier crashes to W-beam crashes were 0.860 (95% CI: 0.591-1.250) for all riders involved in the barrier crashes analyzed. The odds of severe injury in cable barrier crashes to concrete barrier crashes were 1.274 (95% CI: 0.868-1.870). Neither of these results are significant at the 0.05 level. However, the odds of severe injury in a concrete barrier collision to a W-beam collision were 0.675 (95% CI: 0.570-0.799), which is significant. Finally, although the number of passengers present proved to be insignificant, road alignment, rider age, and crash speed all proved significant factors when considering injury outcomes.

CONCLUSIONS

For all riders in this study, collisions with concrete barriers were found to be significantly less likely to cause severe injury than collisions with W-beam guardrails. There was no significant difference in the odds of severe injury between the cable barrier collisions and the W-beam or concrete barrier collisions. Motorcycle crashes on curved roads posed a higher injury risk than those on straight roads, and elderly riders (age >65) were more likely to be seriously injured. Finally, crashes at high speeds (>40 mph) implied a higher injury risk than those that occurred at lower speeds.

ACKNOWLEDGMENTS

The authors gratefully acknowledge the National Academies of Science for their sponsorship of this research. The authors would also like to thank Wake Forest University and the included states' departments of transportation for the use of their data.

REFERENCES

1. Gabler, HC. The Risk of Fatality in Motorcycle Crashes with Roadside Barriers. Twentieth International Conference on Enhanced Safety of Vehicles, Lyons, France, Paper No. 07-0474, 2007.

Poster,A
Atrium, 11:15

INHIBITORY EFFECTS OF CINNAMON OIL AND MAIN COMPONENT TRANS-CINNAMALDEHYDE IN THE PROGRESSION AND AGGRESSION OF BREAST CANCER CELLS

Marc Thompson[1], Dr. Eva Schmelz[2], Dr. Lissett Bickford[1]
1. Department of Biomedical Engineering and Mechanics, Virginia Tech, Blacksburg, VA, United States
2. Department of Human Nutrition, Foods and Exercise, Virginia Tech, Blacksburg, VA, United States
Corresponding Author: Marc Thompson, Email: Marct@vt.edu

INTRODUCTION

Bioactive dietary agents (ie. neutraceuticals) have been shown to slow or eliminate cancer growth, with marked effects when applied directly to cancer cells. We hypothesize that select agents can be used to reduce or eliminate the aggressiveness of cancer cells while minimizing systemic toxicity. Here, we have examined the effects of trans-cinnamaldehyde (TC), the active ingredient in cinnamon oil and a documented anti-inflammatory and anti-cancer agent, on *in vitro* models of breast cancer. Specifically, we investigated the influence on viability and migratory capabilities, noted hallmarks of cancer progression. Our goal is to elucidate the influence of this agent on cancer cell phenotype and to develop strategies for direct delivery to cancer cells *in vivo*.

METHODOLOGY

The triple-negative breast cancer cell line MDA-MB-231 was treated with documented botanical anti-cancer agents frankincense oil (Böswellness, VT), garlic oil and cinnamon oil (Sigma Aldrich). Cytotoxicity was determined by an MTT assay. Cinnamon oil conferred the greatest immediate cytotoxicity and was further analyzed using Gas Chromatography-Mass Spectrometry (GC-MS). TC was subsequently confirmed as the key active component with cytotoxicity validated *in vitro*. Immediate and long-term effects of agent exposure were examined on a progressive breast cancer model. Cell migratory capabilities were assesed in 2D and 3D environments with wound-healing and transwell migration assays. Migration was observed and quantified using ImageJ.

RESULTS

Cinnamon oil elicited the most immediate cytotoxic effect on MDA-MB-231 cells compared to other agents. Subsequent GC-MS analyses confirmed TC was the key compound, comprising ~75% of the cinnamon oil formulation, its cytotoxicity was later validated *in vitro*. TC-induced apoptosis on the progressive model of breast cancer was evident in a dose-dependent fashion. Dose-dependency was variable in more aggressive cells, but was substantial after 48 hours, reducing viability in all cell lines by 50-80%. TC significantly reduced migratory capabilities in cells in both 2D and 3D environments at minimal treatment concentrations of 25µg/mL (Figure 1).

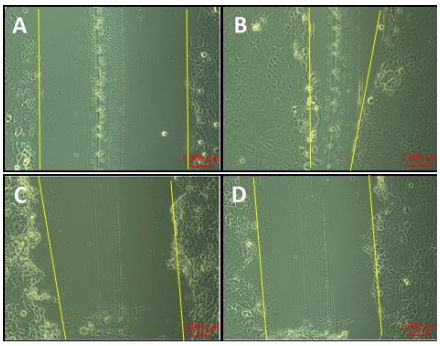

Figure 1. Cell migration to close gap is significantly reduced when comparing controls at t=0 hours (A) to t= 24 hours (B) to cells treated with 25 µg/mL TC at t= 0 hours (C) to t= 24 hours (D).

CONCLUSIONS

Trans-cinnamaldehyde's marked cytotoxic effects and proficiency in inhibiting migration suggests value as a potential bioactive agent in the treatment of both highly invasive and aggressive breast cancer cells. In current and future studies, we will examine the mechanisms responsible for inhibiting biological processes and apply treatment to more physiologically-relevant models.

REFERENCES

[1] Gosslau et al. Nutrition 20.1 (Jan 2004): 95-102.

Virginia Tech
Wake Forest University
School of Biomedical Engineering and Sciences
15th Annual Graduate Student Research Symposium, May 11, 2016

COMPARING THE ABILITY TO MODULATE BRAIN NETWORKS IN ADHD AND HEALTHY SUBJECTS

Tuteja A.[1], Lisinski J.[2], McKinnon A.[2], LaConte S.[2,3]
1. Virginia Tech Carilion School of Medicine
2. Virginia Tech Carilion Research Institute
3. Virginia Tech/Wake Forest School of Biomedical Engineering and Sciences
Corresponding Author: Alisha Tuteja, Email: atuteja@carilionclinic.org

INTRODUCTION

The neurophysiology of attention-deficit hyperactive disorder (ADHD) is not well understood, and stimulant medications, the main line of treatment, are easily abused. A real-time fMRI research design with biofeedback may provide a means to better understand neural changes in ADHD while offering a potential therapeutic benefit. In this study, we compared the ability of healthy and ADHD subjects to modulate activity in the default-mode network (DMN) using a real-time fMRI task. Based on previous studies, we hypothesized that ADHD subjects will not be able to modulate DMN activity as well as controls.

METHODOLOGY

Control and ADHD subjects ages 18-23 performed a resting-state fMRI scan, followed by two "focus vs. wander" tasks – one with feedback, and one without. The resting-state scan was used to model the subject's DMN, and subsequent data gathered during the "focus vs. wander" tasks were compared to the DMN model to provide the subject feedback on their performance. The correlation of actual DMN activity compared to expected DMN activity was calculated as a measure of task performance. The difference between "high" and "low" DMN activity during the "wander" vs. "focus" tasks was interpreted as the ability to modulate DMN.

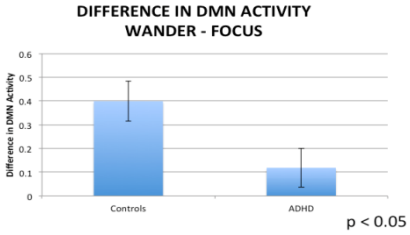

Figure 1: Difference in DMN activity between "wander" and "focus" tasks during "no feedback" trials. Error bars represent standard error of the mean.

RESULTS

As shown in Fig. 1, the DMN modulation performance was better in control than ADHD subjects. With our limited sample size, we were not able to obtain statistical significance in DMN maps between the two groups.

CONCLUSIONS

This study provides proof of concept that real-time fMRI can be used to depict DMN modulation to improve the understanding of ADHD and offer potential therapeutic strategies. We observed a statistically significant difference in the ability of controls to modulate DMN without feedback compared to ADHD subjects. We are currently exploring the role of feedback (or its absence) as subjects learn to control their DMN brain activity.

ACKNOWLEDGMENTS

This study was partially funded by funds provided by both the VTCRI and VTCSOM.

REFERENCES

Konrad K. et al. (2010). Is the ADHD Brain Wired Differently? A Review on Structural and Functional Connectivity in Attention Deficit Hyperactivity Disorder, *Hum Brain Mapp*., 31:904-916.
LaConte S.M. et al. (2007). Real-Time fMRI Using Brain-State Classification, *Hum Brain Mapp*., 28:1033-1044.
Smith S.M. et al. (2009). Correspondence of the brain's functional architecture during activation and rest, *PNAS*, 106 (31):13040-13045.

Poster,A
Atrium, 11:15

HIGHLY SPECIFIC AND MODULAR AFFINITY LABELING OF EPIGENETIC MODIFICATIONS

Fanny Wang[1], Osama K. Zahid[1], and Adam R. Hall[1,2]
1. Virginia Tech-Wake Forest School of Biomedical Engineering and Sciences
2. Wake Forest University School of Medicine, Comprehensive Cancer Center
Corresponding Author: Adam R. Hall, Email: arhall@wakehealth.edu

INTRODUCTION

DNA epigenetics play an important role in the development and progression of a variety of diseases. These base modifications are dynamic, occurring in response to chemical exposure and other environmental cues, but do not result in a change in the genetic sequence, and thus can be difficult to assess. Here, we present a modular affinity labeling method for epigenetic modifications based on the DNA repair mechanisms found in normal cells. With this procedure, it is possible to tag specific epigenetic modifications with an affinity label at single base resolution for enrichment or detection.

METHODOLOGY

Synthetic double-stranded DNA oligos containing a single modified base and end-labeled with a fluorescent tag (FAM) were used. For these experiments, three different modifications were targeted: uracil, 8-oxoguanine, and thymine-guanine mismatch. Each construct was incubated for 1 hour at 37°C in the presence of modification-specific glycosylase and an endonuclease to excise the epigenetic modification. Subsequently, molecules were incubated for 30 minutes at room temperature in the presence of DNA polymerase and a single type of biotinylated nucleotide appropriate for the modification. Labeled molecules were then incubated in the presence of monovalent streptavidin for 10 minutes at room temperature to induce specific binding. Solid-state (SS-) nanopore measurements were performed using a 8 nm diameter nanopore and across a range of applied voltages.

RESULTS

The ability of the DNA repair enzymes to replace epigenetic modifications with a biotinylated nucleotide was demonstrated with the three modifications being studied (Figure 1). SS-nanopore measurements showed selective detection of labeled molecules due to steric hindrance with the pore and demonstrated direct quantification and high sensitivity.

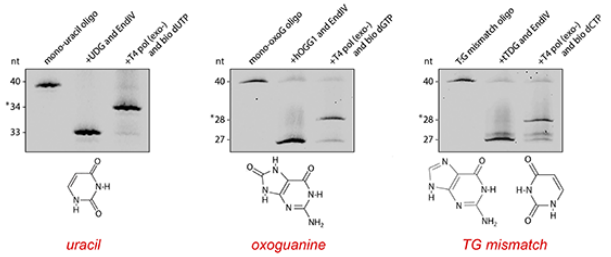

Figure 1: Denaturing gels demonstrating biotin labeling of three epigenetic distinct modifications. The first column in each set is the initial material, the second the material after incubation with glycosylase, and the third the material after incubation with DNA polymerase. Asterix indicates biotinylation.

CONCLUSIONS

This research demonstrates the viability of using DNA repair enzymes to label epigenetic modifications in DNA. Our approach can be extended to a wide variety of additional modification types based on enzyme specificity. In addition to SS-nanopore analysis, labeled material could also be isolated/enriched with streptavidin beads for quantification, sequencing, and other analysis.

ACKNOWLEDGMENTS

We thank M. Howarth (Oxford) for providing materials and J. Ruzicka (High Point University) for contributions to this project.

REFERENCES

1. Ashkenazi R., doi:10.1593/neo.08572
2. Ciccia A., doi:10.1016/j.molcel.2010.09.019
3. Dekker C., doi:10.1038/nnano.2007.27, 2007

Poster,B
Atrium, 11:45

Virginia Tech
Wake Forest University
School of Biomedical Engineering and Sciences
15th Annual Graduate Student Research Symposium, May 11, 2016

FABRICATION OF A NOVEL ELASTOMERIC SUBSTITUTE FOR AUTOLOGOUS VEINS IN CORONARY ARTERY BYPASS SURGERY

Harleigh J. Warner[1,2], William D. Wagner[1,2]
1. Department of Plastic and Reconstructive Surgery, Wake Forest Baptist Medical Center
2. School of Biomedical Engineering and Sciences, Virginia Tech and Wake Forest University
Corresponding Author: Harleigh J. Warner, Email: hwarner@wakehealth.edu

INTRODUCTION

Autologous saphenous vein is the standard material for bypassing small diameter (<6mm) coronary arteries, but is subject to intimal hyperplasia, thrombosis, and accelerated atherosclerosis. To date, no biomaterial functions as a substitute for vein graft.

We have recently developed an endovascular biomaterial, PFC, composed of electrospun poly-(glycerol sebacate), silk fibroin, and type 1 collagen. The biomaterial has tensile, non-thrombogenic, and endothelial cell adhesive properties ideal for use as an artery graft material

The goal of this project is to create a conduit from PFC, fine tune the material with cell derived extracellular matrix (ECM), and evaluate cell growth and mechanical properties of the conduit. We hypothesize that adding ECM components onto the PFC material will strengthen the material and deposit molecules that may facilitate cellular adhesion and proliferation.

METHODOLOGY

Sparse PFC mats composed of nanofibers were fabricated by electrospinning 0.2 mls of PFC onto tissue culture plastic treated slides, resulting in a sparse network of PFC fibers. NIH 3T3 mouse fibroblasts were cultured on the PFC material for 6 days and decellularized using Trypsin/Triton X-100

Dense PFC mats were fabricated by electrospinning 4.4 mls of PFC onto a 9 by 10cm rectangle of aluminum foil. NIH 3T3 mouse fibroblasts were seeded on material for 10 days and either immediately fixed (n=3) or decellularized (n=3) and fixed.

Porous PFC mats were fabricated by electrospinning equal volumes of PFC and PEO. Material was subsequently gluteraldehyde crosslinked, PEO was leached, and material was heat treated.

RESULTS

Fibroblasts deposited a nanofibrous ECM on the surface of sparsely electrospun PFC as shown by crystal violet staining. The ECM was apparent on sparce ECM after decellularization with Triton X-100. The PFC facilitated the ability for the ECM to remain on the material compared to tissue culture plastic slides without PFC. Fibroblasts formed a dense monolayer on the surface of PFC but did not infiltrate the material. A porous PFC material was fabricated to support cellular infiltration.

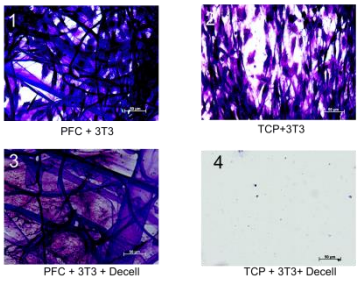

Figure 1. Light micrographs of fibroblasts on PFC fibers (1,3) and tissue culture plastic (TCP) (2,4) with (3,4) and without (1,2) decellularization.

CONCLUSIONS

These studies show 1) we can fabricate a graft material composed of PFC, 2) it is possible to effectively decellularize PFC seeded with fibroblasts and maintain ECM material, 3) the ability to potentially tune the properties of the material.

ACKNOWLEDGMENTS

The authors would like to thank Harold S. Geneen Charitable Trust Awards Program for Coronary Heart Disease Research for support.

Poster,A
Atrium, 11:15

KERATIN BIOMATERIALS AUGMENT ANTI-INFLAMMATORY MACROPHAGE PHENOTYPE IN-VITRO

Michele Waters[1], Pamela VandeVord[1], Mark Van Dyke[1]
1. Virginia Tech, Biomedical Engineering and Mechanics (BEAM)
Corresponding Author: Michele Waters, Email: mwaters1@vt.edu

INTRODUCTION

Macrophage phenotype and dynamics play complex roles in wound healing and the resolution of many inflammatory diseases. Tissue remodeling can become complicated in disease states when an imbalance of pro-inflammatory macrophages (M1) and anti-inflammatory macrophages (M2a/M2c) occurs. Promoting macrophage polarization from the M1 to the M2 phenotype may be a potential avenue of treatment for these disease states. Keratin biomaterials have been used for a variety of tissue engineering applications (e.g. bone/skin/nerve regeneration, drug delivery), in the form of coatings, gels, and scaffolds. Human hair-derived keratins have also demonstrated their ability to shift macrophages towards an M2 phenotype in a previous study using a human monocytic cell line.[1] In the present study, the ability of keratin biomaterials to promote M2 polarization of human primary monocytes is assessed by evaluating changes in morphology, surface receptor expression, and phagocytic function.

METHODOLOGY

Keratin (KOS) proteins were isolated from human hair using an established method of oxidation, solubilization, and tangential flow filtration (TFF); specific fractions of extracted keratins were created during TFF by using nominal low molecular weight cutoff (NLMWCO) cartridges. The high molecular weight keratin fraction (KOS^H) represents extracted keratins greater than 100K Da while the peptide-containing fraction (KOS^P) represents keratins between 30K Da and 5K Da. Primary monocytes (isolated from human blood using Ficoll density gradient separation and immunomagnetic positive selection of $CD14^+$ cells) were differentiated over a period of seven days on keratin coatings or with a cytokine cocktail of M-CSF and either LPS/IFN-γ (M1), IL-4/IL-13 (M2a), or IL-10 (M2c). Cells were then harvested, stained for the presence of CD86, CD206, and CD163 receptors (M1, M2a, and M2c markers respectively), and analyzed via flow cytometry.

RESULTS

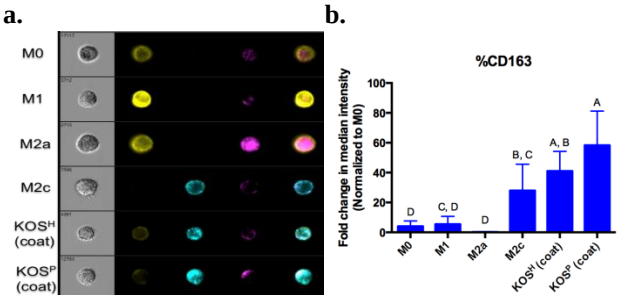

Figure 1: a) Receptor Expression of Differentiated Macrophages and **b)** Mean Fold Change in % $CD163^+$ Population after Flow Cytometric Analysis ($N=6$)

CONCLUSIONS

Cells plated on keratin coatings expressed high amounts of the M2c marker, CD163; this was more pronounced in the KOS^P (coat) group. These findings have important implications for evaluating mechanisms for promoting wound healing and the resolution of inflammation in disease and regenerative processes. Future work will involve exploring the mechanism behind keratin-induced differentiation and evaluating macrophage recruitment following keratin treatment in *in-vivo* rat injury models.

REFERENCES

1. Fearing et al. Acta Biomater, 2014. **10**(7): p. 3136-44.

ACKNOWLEDGMENTS

I would like to thank the Errett Fisher Foundation for supporting this research.

PELVIC RESPONSE OF A TOTAL HUMAN BODY FINITE ELEMENT (FE) MODEL TO LATERAL IMPACT USING CROSS-SECTIONAL FORCE AS A METRIC

Caitlin M. Weaver[1,2] and Joel D. Stitzel[1]
1. Virginia Tech-Wake Forest University, Center for Injury Biomechanics
2. US Army Research Laboratory, Soldier Protection Sciences Branch
Corresponding Author: Caitlin M. Weaver, Email: cweaver@wakehealth.edu

INTRODUCTION

Pelvic fracture is a very serious injury resulting in a high risk of mortality and resulting morbidity. This injury can be caused by low energy trauma or high energy trauma. Low energy trauma pelvic fracture is commonly caused by slips and falls while high energy trauma is caused by MVCs, pedestrian collisions, and falls from height.[1] MVCs are consistently the leading cause of pelvic fracture, accounting for 44 to 64% of these injuries.[2] Lateral MVCs are more likely to result in pelvic fracture due to the compressive nature of this injury. This type of MVC results in more than 15,000 pelvic fractures in the US annually.[3]

The purpose of this study is to develop injury risk prediction curves for specific regions of the pelvis by comparing the presence of fracture in these regions in experimental testing to the cross-sectional force response in these regions in a total human body FE model.

METHODOLOGY

The total human body FE model used for this study was Global Human Body Models Consortium (GHBMC) 50th percentile detailed male FE model (v4.3). Lateral impact FE simulations were performed using input data from lateral impact tests performed by Bouquet et al. on post mortem human subjects (PMHS).[4,5] Simulations were performed using the same impactor geometry, mass, initial velocity, and impact energy target as the corresponding experimental test. Logistic regressions were performed on the experimental test data and the simulation test data to generate injury risk prediction curves for total pelvic injury and regional pelvic injury.

RESULTS

The results show good correlation for total pelvic injury risk prediction between the experimental and simulation data. The injury risk prediction curve generated from the simulation data shows slight under prediction of injury in comparison to the experimental data curve. The difference in specimen size between the experimental testing and the simulation testing can account for this difference in injury prediction. A scaling analysis will be performed to account for specimen size difference between tests in order to reduce the discrepancy in injury prediction between the experimental and simulation results.

CONCLUSIONS

Pelvic injuries are often debilitating, resulting in increased healthcare expenses and a reduced post-injury quality of life. Fractures to certain regions of the pelvis can result in high risk of blood loss as well as pelvic instability. This research can be used to analyze the effects of risk mitigation techniques on specific regions of the pelvis that are more life threatening and debilitating than others.

ACKNOWLEDGMENTS

The authors would like to acknowledge the US Army Research Lab, the US Army WIAMan project, the John Hopkins University Applied Physics Laboratory, and the Science, Mathematics And Research for Transformation (SMART) Scholarship for Service Program for their support and collaboration.

REFERENCES

1. Balogh, Z. et al. The Journal of Trauma Injury, Infection, and Critical Care. 2007;63(5):1066-1073.
2. Inaba, K. et al. Injury, International Journal of the Case of the Injured. 2004;35:759-765.
3. Schiff, M. A. et al. Accident Analysis and Prevention. 2008;40:387-391.
4. Bouquet et al. Paper No. 94-S1-O-03.
5. Bouquet et al. Paper No. 98-S7-S-16.

DEVELOPMENT OF A GÖTTINGEN MINIATURE PIG FINITE ELEMENT MODEL FOR INVESTIGATION OF INJURY SCALING TECHNIQUES

Keegan M. Yates[1], Elizabeth M. Fievisohn[1], Warren N. Hardy[1], and Costin D. Untaroiu[1]
1. Virginia Tech, Center for Injury Biomechanics
Corresponding Author: Keegan Yates, Email: kmyates@vt.edu

INTRODUCTION

Traumatic brain injuries (TBIs) cause roughly 50,000 deaths per year in America. In order to lessen the severity or prevent TBIs, accurate dummy models, simulations, and injury risk metrics must be used. Human data is ideal to develop models, but injury conditions are often complex, e.g. primary and secondary impacts, and tissue level response can often only be studied via an autopsy, but death usually only occurs as the result of severe TBI. To develop better graded injury risk metrics, animal study data must be applied to the human brain. The ultimate objective of our study was to develop a better method to scale injury data by using finite element (FE) analysis.

METHODOLOGY

In this study, an FE model of a Göttingen miniature pig brain and skull was created from MRI and CT images. These pigs' brains have several characteristics in common with human brains that that make them suitable for testing such as shape and material properties. The regions of the brain were divided into white/gray matter, and the ventricles each with viscoelastic material properties. To validate this model, tests were conducted using Göttingen pigs in a translation/rotation injury device subjecting the pig skull to a linear acceleration from 40-96 g's and an angular acceleration from 1,000-3,800 rad/s2 [1]. Four of these pigs' brains were embedded with neutral density radio-opaque markers to track the motion of the brain with a biplanar X-ray system. Fifteen pigs were also tested without markers to allow for injury data to be taken with MRI scans and immunohistochemistry. The impact was then simulated in LS-Dyna, and the motion of nodes closest to the marker locations was recorded.

RESULTS

The displacement histories of the node marker pairings were compared (Fig. 1). The magnitude and phase of the nodal displacements matches the experimental test results.

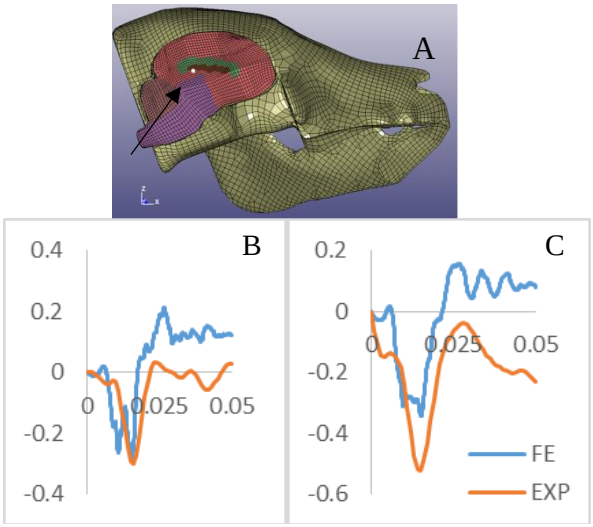

Figure 1. Skull and brain mesh with location of one of the markers (A) and experimental and finite element displacement (mm) time (s) histories in the horizontal (B) and vertical (C) directions.

CONCLUSIONS

When used in tandem with a human model this will allow for a more accurate transfer function to scale injury data from a pig study to be relevant to humans. While the loading conditions in this study simulate a small range of possible injuries, the scaling methods involved may be applicable to a wide variety of injuries from sports injuries to blasts.

ACKNOWLEDGMENTS
This work was sponsored by the Takata Corporation.

REFERENCES
1. Fievisohn, E.M., et al., *Evaluation of impact-induced traumatic brain injury in the Göttingen Minipig using two input modes*. Traffic injury prevention, 2014. 15(sup1): p. S81-S87.

AUTOMATED ANALYSIS OF DRIVER RESPONSE IN A FINITE ELEMENT CRASH TEST RECONSTRUCTION

Xin Ye[1, 2], James P. Gaewsky[1, 2], Bharath Koya[1, 2], Derek A. Jones[1, 2],
Ryan Barnard[1, 2], Ashley A. Weaver[1, 2], Joel D. Stitzel[1, 2]
1. Wake Forest School of Medicine
2. Virginia Tech - Wake Forest University Center for Injury Biomechanics
Corresponding Author: Xin Ye, Email: xye@wakehealth.edu

INTRODUCTION

Motor vehicle crashes (MVCs) resulted in an estimated 32,675 fatalities in 2014 across the United States [1].This study aims to develop an automated algorithm of optimizing a simplified vehicle model (SVM) to mimic the driver response in frontal crash test reconstructions. The vehicle-specific parameters of the model will be optimized and tailored to reproduce the occupant response from crash test data.

METHODOLOGY

Previously, a finite element simplified vehicle model (SVM) was developed as an aggregate of laser scans from 14 different vehicle interior models [2]. The current SVM incorporated several vehicle restraint systems, including seatbelt with pre-tensioner and load-limiting retractor, frontal airbag and knee airbag models. The New Car Assessment Program (NCAP) database was queried and a full-frontal 2010 Toyota Camry NCAP test was selected as the sample case. A fully-automated method was developed to tune the SVM to mimic the crash response from the NCAP frontal crash test. A total of 240 independent simulations were performed to optimize the SVM structural properties and restraint systems using a Latin Hypercube design of experiments sampling method.

RESULTS

From the dummy positioning procedure, the automatically positioned ATD closely matched the anthropometric measurements from the NCAP crash test (Figure 1). The corresponding vehicle parameters of the best simulation were picked as the best set that matched closest with the chosen NCAP test, and were applied to the optimized SVM.

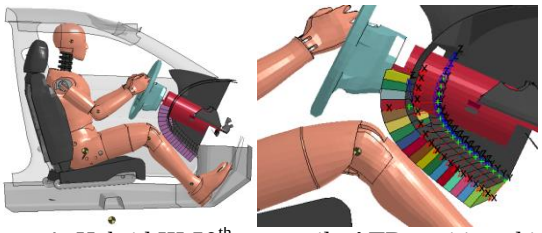

Figure 1: Hybrid III 50th percentile ATD positioned in the SVM (Left) Knee airbag model (Right)

For the best simulation, thoracic vertebrae T6 acceleration was accurately predicted. Right femur force reached a peak value of 3513.0N from the simulation (Figure 2).

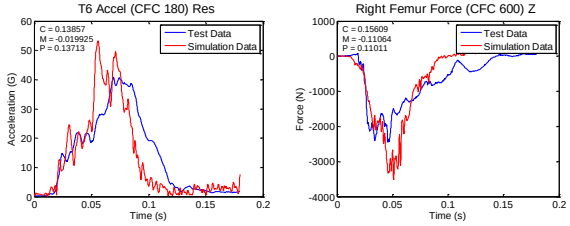

Figure 2: Comparison of best simulation with crash test data for the T6 accel. (Left) and right femur force (Right)

CONCLUSIONS

This study investigated the kinematic and kinetic responses of the driver as a function of vehicle properties and restraint systems from crash test reconstruction.

ACKNOWLEDGMENTS

Toyota's Collaborative Safety Research Center.

REFERENCES

[1] Ntl. Ctr. for Stats. Anlys, No. DOT HS 812 160, 2014.
[2] Iraeus et al. TIP.2014; 15 (sup1):S88-S95.

Virginia Tech
Wake Forest University
School of Biomedical Engineering and Sciences
15th Annual Graduate Student Research Symposium, May 11, 2016

A NOVEL SOLID-STATE NANOPORE ASSAY FOR THE DETECTION OF DNA EPIGENETIC MODIFICATIONS

Osama K. Zahid[1], Fanny Wang[1], and Adam R. Hall[1,2]
1. Wake Forest University School of Medicine, Department of Biomedical Engineering
2. Wake Forest University School of Medicine, Comprehensive Cancer Center
Corresponding Author: Adam R. Hall, Email: arhall@wakehealth.edu

INTRODUCTION

Increasing evidence implicates DNA epigenetic modifications and modified DNA as important biomarkers for both development and disease susceptibility. Two such modifications have been widely studied: 5-methylcytosine (5-mC) and 5-hydroxymethylcytosine (5-hmC), both with significant links to cancer. Conventional assays to differentiate and quantify these modifications are laborious, require sophisticated equipment, and demand large amounts of starting material. Therefore a detection technique that is inexpensive, rapid, and sensitive is desirable. Solid-state (SS-) nanopores are an ideal candidate for this purpose. Briefly, two reservoirs of electrolyte solution are attached through a single nanoscale pore drilled in an insulating membrane. An applied voltage facilitates molecular translocation through the pore, which can be detected with resistive pulse sensing.

METHODOLOGY

We have developed a novel SS-nanopore assay[1] that is capable of selectively detecting short biotinylated dsDNA oligonucleotides. Here, monovalent streptavidin (MS, Howarth Group, Oxford U.) is used as a highly charged, high affinity tag for biotinylated DNA. Free MS is translocated through the pore too rapidly to be detected by our electronics. However, when attached to a DNA molecule, the biomoelcular complex interacts with pore walls and reduces the speed to a resolvable level. Since translocation events occur almost exclusively due to DNA-MS binding, we can accurately quantify biotinylated DNA within a mixed sample.

RESULTS

By converting or tagging specific epigenetic modifications with a biotin, we use our assay to selectively detect and quantify those target modifications. Our initial measurements utilize an enzymatic approach[2] in which DNA glucosyltransferase attaches an azide glucose moiety to 5hmC selectively. Click chemistry can then be used to covalently link biotin to this glucose, enabling SS- nanopore detection to be performed (Fig. 1).

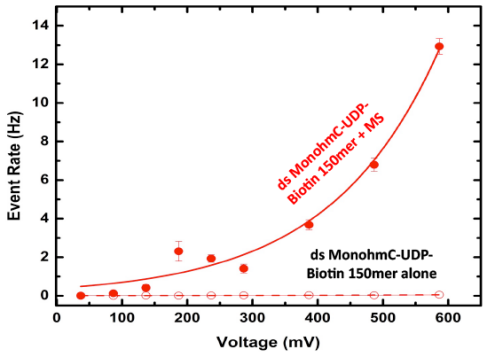

Figure 1: Event rate vs voltage for dsDNA with a single 5hmC nucleotide selectively labeled with biotin and measured alone (dashed red line) and with MS (solid red line). Significant events are caused only by MS binding.

CONCLUSIONS

A biotin labeling approach enables highly selective detection of 5hmC DNA. We demonstrate quantification of 5hmC content in mouse genomic DNA and find our results comparable to conventional techniques like Mass spectrometry.

ACKNOWLEDGMENTS

We thank J. Ruzicka and E. W. Taylor at UNCG for contributions.

REFERENCES

1. Carlsen, A., doi: 10.1021/nl501340d, 2014
2. Song, C.-X., doi:10.1038/nbt.1732, 2010

Poster,B
Atrium, 11:45

Virginia Tech
Wake Forest University
School of Biomedical Engineering and Sciences
15th Annual Graduate Student Research Symposium, May 11, 2016

MORPHOLOGICAL AND FUNCTIONAL VALIDATION OF INDUCED PERICYTES

Huaning Zhao[1], John C. Chappell[2]
1. School of Biomedical Engineering 2. Center for Heart and Regenerative Medicine Research, VTCRI
Corresponding Author: John C. Chappell[2], Email: JChappell@vtc.vt.edu

INTRODUCTION

Pericytes are cells which tightly wrap around endothelial cells of microvessels. Pericytes maintain the stable structure and homeostasis of microvessels. Also pericytes play an important role in angiogenesis under both healthy and disease conditions (Figure 1).

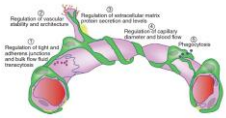

Figure 1: Functions of Pericytes. [1]

Recent studies suggest pericyte dysfunction as a key mechanism in pathological angiogenesis. For example, in diabetic retinopathy, loss of pericytes is considered as a first step in disease progression, and this event may cause abnormal angiogenesis and finally result in vision loss. [2] However, it is difficult to determine how pericytes act in pathology and how re-introducing viable pericytes may help to cure or slow down the disease progression. In the current study, we have designed experiments to explore how isolated pericytes may contribute to normal blood vessel development.

METHODOLOGY

Neural Glial Antigen-2 (NG2) is a biomarker of pericytes. We isolated NG2:DsRed-positive cells and tested their morphological and functional characteristics in both in vitro and ex vivo blood vessel formation.

Briefly, NG2:DsRed-positive cells were isolated from NG2:DsRed transgenic mouse embryos at embryonic day 14.5 (E14.5), using Fluorescence Activated Cell Sorting (FACS). While sorted cells may have included small amounts of fibroblasts, astrocytes and other cells, we enriched for pericytes. These cells were then introduced into developing vessels of day 7 embryoid bodies and explanted back skin of E14.5 embryos.

RESULTS

Isolated NG2-positive cells display morphological and functional characteristics similar to endogenous pericytes. Figure 2 demonstrates NG2:DsRed-positive cells with morphology, location and attachment along endothelial cells that are similar to endogenous pericytes. We are currently testing our isolated pericytes in skin explants from E14.5 embryos, and we anticipate that these isolated pericytes will have a similar function as endogenous pericytes in blood vessel development. By re-introducing healthy pericytes into pathological tissue, we may help re-establish normal angiogenesis.

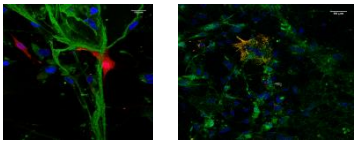

Figure 2: Induced NG-2 DsRed cells with embryo body (left); Original pericytes in embryo body (right). eGFP is endothelial cells and cell nucleus is stained with DAPI.

CONCLUSIONS

The introduced NG2:DsRed-positive cells display similar morphology and function in embryoid body blood vessel development as endogenous pericytes. Future goals include establishing whether isolated pericytes have morphological and functional similarity in other tissues. In addition, we will ablate pericytes in mice to determine the deleterious effects after programmed pericyte apoptosis, and how re-introduced pericytes might rescue any adverse conditions.

REFERENCES

[1] Winkler, E. A., Bell, R. D., & Zlokovic, B. V. (2011). Central nervous system pericytes in health and disease. Nature neuroscience, 14(11), 1398-1405.